University of Salerno

Department of Chemistry and Biology "Adolfo Zambelli"

Ph.D. School in Chemistry

XXXI Cycle

An ecological approach to the integrated monitoring of freshwater ecosystems

Dr. Alessandro Bellino

Supervisor
Prof. Daniela Baldantoni

Head of the Ph.D. School
Prof. Gaetano Guerra

A.Y. 2017-2018

Contents

List of Figures

List of Tables

Chapter 1

Introduction

Diffuse environmental pollution is considered one of the key evidences of Earth system transition into a novel geologic era, defined as "Anthropocene" from the pervasive effects of human activities on the whole ecosphere (Malhi, 2017). This is the outcome of the large auxiliary energy inputs and the introduction of novel materials, determining a massive outbreak of human population during the last centuries, with a shift from internally controlled (density dependent) logistic to exponential dynamics (Cohen, 2003). Undoubtedly welcomed from sociological and welfare points of view, the changes in human population dynamics and the associated ever growing demand for energy and resources, is nonetheless steadily impairing global equilibria, with dramatic consequences on millions of species, human inclusive. Indeed, the current biodiversity crisis, sometimes considered the 6th mass extinction event in Earth history (Barnosky et al., 2011), is primarily caused by anthropogenic activities both directly (through harvesting, habitat loss, introduction of invasive species. . .) and indirectly (through climate change, pollution, disease spreading. . .). The causes of species extinction are regularly multiple and interwined, with dynamics usually too complex to be coped with (Barnosky et al., 2011). A chilling example is provided by the near extinction of the Mediterranean endemic and iconic bivalve *Pinna nobilis* L., already threatened by pollution, harvesting, trawling and anchoring, which is currently brought to extinction by a novel parasite favoured by climate warming and possibly spreaded by human transports with unprecedented speed (Vázquez-Luis et al., 2017).

Generally, habitat degradation and loss is considered the single most important determinant of biodiversity decline (Segan et al., 2016), and the institution of protected areas where species can persist is often proposed to locally counteract the process (Le Saout et al., 2013). However, protected areas may serve multple purposes, involving the conservation of peculiar geological structures and even the preservation of cultural or social aspects (Geneletti and Van Duren, 2008). An example of a multi-purpose protected area is the "Cilento, Vallo di Diano e Alburni" National Park (PNCVDA), awarded of four UNESCO World Heritage designations for its biodiversity, geodiversity, cultural landscape and mediterranean diet. Irrespective of the purpose, environmental monitoring is pivotal in the management of protected areas, allowing to gather information on current environmental criticalities and evaluate the effects of policies and actions (Arthington, 2015). The process, known as "adaptive management", forms the backbone of ecosystem management and promotes the adaptation of environmental policies based on monitoring results (Valavanidis, 2018). At the European level, the Water Framework Directive (WFD) provides an exceptional example of adaptive ecosystem management (Spencer, 2017) not confined to protected areas. Indeed, the directive introduced an experimentalist approach to water governance through a recursive strategy based on setting provisional goals and revising them in the light of monitoring outcomes. On monitoring itself, the WFD also constitutes a leap forward, encouraging the use of biomonitoring and integrated approaches (Besse et al., 2012).

Monitoring of water ecosystems, especially rivers, represents an exceptionally complex task, due to the continuous water movements and the consequent need to consider the temporal fluctuations in the parameters analysed (Besse et al., 2012; Szczerbińska and Galczyńska, 2015). For physical parameters like conductivity or temperature, field installation of probes and dataloggers allows reconstructing continuous-like dynamics (Mueller et al., 2013). Field probes made up by ion-sensitive electrodes are also available for some chemicals but, with the exception of a few selected ions, they are used as "watch-dogs" for anomalous events rather than for accurate parameter measurements. Therefore, monitoring of dissolved chemical pollutants is mostly accomplished by periodically analysing water, the time required for the analyses setting the maximum achievable temporal sampling frequency (Bartram and Ballance, 1996). This approach provides information on the real temporal variations in pollutant concentrations, but has major drawbacks in the costs associated with and the coarse reconstruction of pollutant dynamics (Baldantoni et al., 2018). Indeed, pollution peak events are easily missed with monthly or even weekly samplings, which already constitute a challenging task (Besse et al., 2012). Moreover, the associated costs usually impose a trade-off between temporal and spatial density of samplings: the wider the monitored area the lesser the achievable sampling frequency (Besse et al., 2012). High spatial sampling densities are still necessary to reconstruct accurate spatial pollution gradients, which is one of the main goals of most monitoring programs. In this context, working with average concentrations per site rather than dynamics would be even more straightforward and would provide clearer, but less informative, scenarios.

For chemicals with high affinity for sediments like non-polar organics and several metals, sediments act as pollutant reservoirs and their analysis may fulfill these goals (Kilunga et al., 2017), providing information on the mean temporal concentrations per sampling site. Sediments are often readily available in large quantities, store pollutants over long times and, considering their stratigraphy, may be even used for retrospective reconstruction of historical pollution events (Blais et al., 2015; Schillereff et al., 2016). The advantages of sediment analysis have drawn considerable attention for environmental monitoring of rivers, lakes, estuaries and marine coastal systems (Spencer, 2017) whenever the study of temporal dynamics is not concerned. Sediment analysis is also pivotal in the estimation of environmental risks associated to the re-mobilization of stored pollutants due to changes in hydrological or chemical processes of the system (Zoumis et al., 2001; Zhang et al., 2015). Indeed, the adsorption/desorption equilibria at the interface between water and sediments are controlled by several factors like sediment mineralogy, temperature, pH, redox potential, conductivity and presence of chelating agents like humic compounds (Matagi et al., 1998). Variations in each of these parameters, even due to the natural hydrological fluctuations, may promote pollutant mobilization from sediments and enhance their availability for biota (Zhang et al., 2015). The dependence of pollutant accumulation in sediments upon environmental conditions and sediment properties (Bartram and Ballance, 1996) is not only of concern for risk evaluation, but constitutes also the main drawback of sediment analysis for pollution gradient reconstruction (Baldantoni et al., 2018). Gradients obtained this way, in fact, mostly reflect the spatial variations in sediment pollutant accumulation potential rather than true pollutant loads (Bartram and Ballance, 1996). To overcome these limitations, systems exhibiting coherent behaviour toward pollutant concentrations over the monitoring area should be employed. The complexity of these systems spans from simple chemical matrices accumulating selected pollutants, as in the case of diffusive gradient thin films, to organisms or communities (Mangal et al., 2016).

The use of biota for environmental monitoring is defined "biomonitoring" and is not only a cheaper and more accurate way to derive spatial pollution gradients (Besse et al., 2012; Bartram and Ballance, 1996; Chapman, 1992), but also the unique way to evaluate the possible transfer of pollutants through food webs and their effects on organisms and higher organization levels (Chapman, 1992). Organism behaviour toward environmental pollutant concentrations set the delimitation between two biomonitor classes (Markert et al., 2003; Czédli et al., 2014): bioaccumulators, exhibiting linear accumulation dynamics over wide ranges without significant damages, and bioindicators, sensitive even to small concentrations of pollutants, determining alterations in their physiology, biochemistry, morphology, behaviour or community structure and composition. These alterations constitute the endpoints employed in evaluating environmental quality using bioindicators (Markert et al., 2003; Czédli et al., 2014). Conversely, pollutant concentrations are directly measured in bioaccumulators and constitute proxies for cumulative environmental concentrations over the exposure time (Markert et al., 2003). Plant roots (Baldantoni and Alfani, 2016) or animal liver (Czédli et al., 2014) are common targets in bioaccumulation studies, since most pollutants tend to accumulate there, but the ultimate sites of pollutant accumulations are species- and pollutant-specific. A clear example is provided by Pb and Cd, both non-essential elements to plants and both commonly present as divalent cations in the environment, but the first accumulating preferentially in roots and the latter in leaves (Greger, 2004). The choice of target organisms, organs and pollutants is thus crucial in any biomonitoring program using bioaccumulator species (Markert et al., 2003). Between plants and animals, the former are usually preferred for bioaccumulation studies because they absorb pollutants directly from the environment without any transfer through food webs, because they are non-mobile, ensuring precise georeferentiation of results, and for ethical considerations (Markert et al., 2003; Parmar et al., 2016). Animals on their own, especially those of higher trophic levels, provide information on the actual pollutant transfers through food webs, where plants only provide estimates based on the availability for primary consumers (Markert et al., 2003; Parmar et al., 2016). The data, however, cannot be referenced to precise areas and the analyses are usually unfeasible due to the small and often endangered populations of top predators. Nonetheless, animals are commonly employed as bioindicators, either through the use of behavioural endpoints and biomarkers like enzyme activities or stress-related gene expression, or at the community level by exploiting the differential sensitivity of taxa (Parmar et al., 2016). An example of the latter approach in river monitoring is provided by the macro-invertebrate water quality index (MWQI), based on both relative abundance of taxa and their pollution sensitivity (Parmar et al., 2016). Moreover, sessile animals like some filter feeders (*e.g.* mussels) share several traits with plants in their behaviour as bioaccumulators and can be used alike (Aguirre-Rubí et al., 2019). To fill in the table, bacteria, fungi, algae, mosses and lichens are also used as biomonitors, either as bioindicators (even in commercial ecotoxycological test kits like those with *Vibrio fischeri* or *Raphidocelis subcapitata*), or as bioaccumulators, particularly in the case of mosses and some fungi (Markert et al., 2003). The large surface area of moss phylloids and several algal thalli, and their direct absorption of pollutants like polycyclic aromatic hydrocarbons and metals, make them valued bioaccumulators for these kinds of pollutants (Favas et al., 2018). So far, however, mosses are used primarily for air biomonitoring (Renaudin et al., 2018), with fewer applications in aquatic environments, and only recently (Favas et al., 2018) algae received attention despite some evidences of considerable accumulation potentials for several metals. An unique feature of these organisms, placing them among the most useful tools for field biomonitoring, is the ease of transplanting to areas where they are not originally present. The technique, known as "active biomonitoring" as opposed to "passive biomonitoring" using native organisms, fulfills two primary goals: monitoring areas where no biomonitor naturally occurs and controlling for the exposure time, which are the main limitations of passive biomonitoring (Chmist et al., 2018; Szczerbińska and Galczyńska, 2015). Indeed, exposure time has to be grossly estimated in passive biomonitoring rather than accurately measured (Markert et al., 2003), although the long exposures, usually of several months, partly made up for this by dumping the effects of estimation errors. Most importantly, the spatial covering in passive biomonitoring is constrained by the natural occurrence of biomonitors, which may lead to knowledge gaps in critical areas (Markert et al., 2003; Chmist et al., 2018). Mosses and algae, instead, can be placed almost anywhere in multiple samples, using a variety of containers collectively known as "bags" (Esposito et al., 2018), and allowing to obtain higher spatial sampling densities than those usually achievable through passive biomonitoring.

Whichever approach, the use of multiple biomonitors at the same time is a means to obtain higher confidences on the derived gradients and possibly fill the gaps for some biomonitors based the others, although direct comparisons are only possible among sites with the occurrence of the same species (Markert et al., 2003). The biomonitoring of the Irno river (Baldantoni and Alfani, 2016) and the Sarno river (Baldantoni et al., 2018) are two examples of the advantages of using an ensemble of biomonitors, employed to enhance the confidence on spatial pollution gradients in the former and to monitor two different areas in the latter. It is worth noting that in (Baldantoni et al., 2018), with no overlap in the distribution of the two biomonitors, no direct comparison was possible between the springs and the river course, but clear pollution gradients were still obtained. In fact, here lies the main strength of biomonitoring in respect to water chemical monitoring (Szczerbińska and Galczyńska, 2015): the ability to derive stationary gradients by integrating the temporal fluctuations in pollutant concentrations, although at the expense of no information about the actual pollutant concentrations in the environment (Markert et al., 2003). Most importantly, biomonitors are sensitive and may accumulate only pollutants in bioavailable form, providing information on the actual spatial distribution of pollutant availability for biota (Baldantoni et al., 2018). These points advocate for a change in the perspective by which biomonitoring and chemical water/sediment monitoring are viewed: they are *complementary* rather than alternative solutions for environmental monitoring (Allan et al., 2006). The idea of an *integrated monitoring* is a straightforward consequence of the change and has its foundations in trying to bring together the advantages of both techniques. The drawback is represented by the higher costs and time associated to this approach, but they are worthwhile in areas with peculiar criticalties or vulnerability, like protected areas.

The concept of integrated monitoring may be further expanded to include the gathering of all the information necessary to obtain a comprehensive view of ecosystem status, processes and functionality, involving not only pollution monitoring, but also activities like

Figure 1.1: Sceneries on the Bussento (left) and Calore Salernitano (right) rivers.

biodiversity or geodiversity estimation (Liu et al., 2012). The present research falls in this context by combining passive and active biomonitoring, sediment mineralogy, element total content analysis and partitioning among sediment fractions and water chemical analyses. The approach was applied to the main river systems of the PNCVDA, the Bussento and the Calore Salernitano Figure 1.1, in order to obtain clear scenarios of river quality and of the subtended processes, in an area hosting exceptional biodiversity comprising endangered species like the otter (*Lutra lutra* L.), the freshwater crayfish (*Austrapotamobius pallipes* Lereboullet) and the Apennine wellow-bellied toad (*Bombina pachypus* Bonaparte). A graphical abstract of the main tasks and goals is shown in Figure 1.2.

The project was especially focused on chemical element analysis, either in matrices like sediments and water, or in passive and active biomonitors. Specifically, 19 elements among (according to Farago, 2008) macronutrients (Ca, K, Mg, P, S), micronutrients (Co, Cr, Cu, Fe, Mn, Na, Ni, Si, V, Zn) and non-essential elements (Al, As, Cd, Pb), collectively referred to as Potentially Toxic Elements (PTEs), were analysed. Being persistent, potentially biomagnified and, in some cases, toxic even at low concentrations like As, Cd and Pb, PTEs are pollutants of major concern in aquatic ecosystems (Cardwell et al., 2013). Within the Bussento and the Calore Salernitano rivers, PTEs were monitored using a passive approach for two consecutive years using the roots of two bioaccumulator plants: *Helosciadium nodiflorum* (L.) W.D.J. Koch and *Mentha aquatica* L. They were flanked during the 2nd year by two active bioaccumulators: a moss, *Fontinalis antipyretica* Hedw., and a charophyte alga, *Chara gymnophylla* A. Braun, to expand spatial covering to sites with potential criticalties but without passive biomonitors. Such an experimental setup is a novelty in biomonitoring studies, where passive and active biomonitoring were, to our knowledge, never combined and where one-year studies are the rule. Indeed, by integrating the temporal fluctuations in pollutant concentrations over exposure times often of several months, bioaccumulators are able to provide stationary pollution gradients even after one sampling, mak-

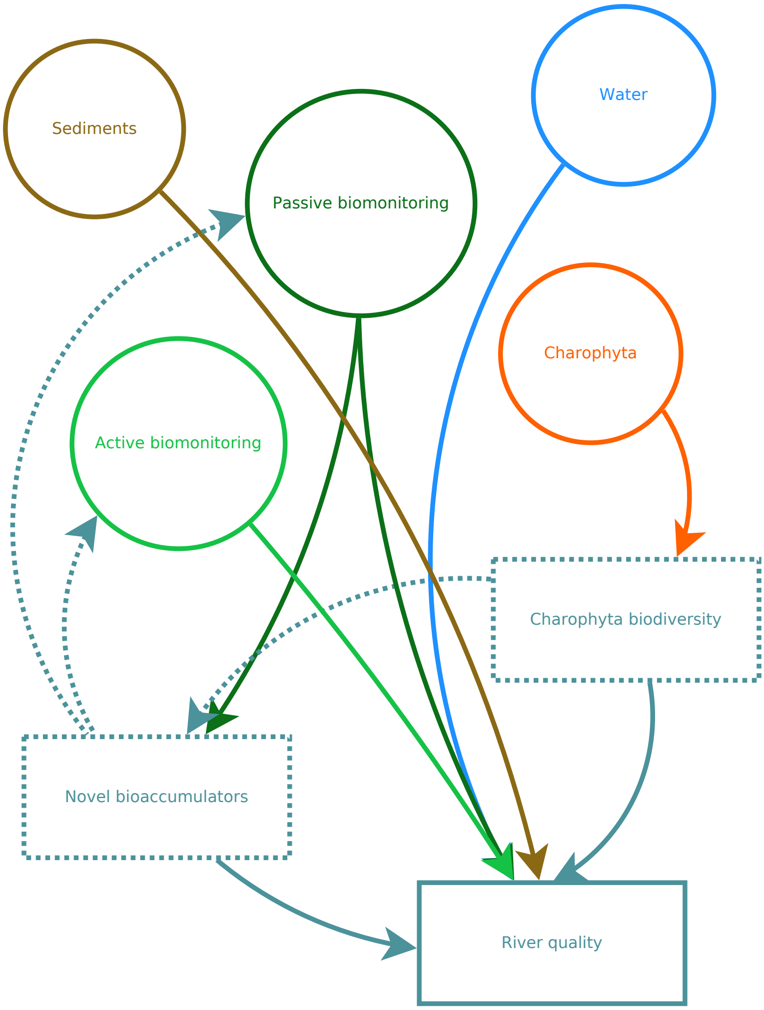

Figure 1.2: Diagram relating the various tasks (circles) and the intermediate (dotted boxes) and principal (solid box) aims of the project.

ing repetitions usually undue (Markert et al., 2003; Szczerbińska and Galczyńska, 2015). Albeit far more expensive in terms of time and resources, the experimental setup chosen for the project fulfilled the need of ascertaining possible variations in PTE concentration gradients over the time in a highly vulnerable area, and to validate the use of novel biomonitors. Indeed, *H. nodiflorum* (Baldantoni et al., 2018; Baldantoni and Alfani, 2016) and *F. antipyretica* (Alam, 2018) are widely recognised as useful biomonitors of PTEs in Mediterranean rivers, but this is not the case of *M. aquatica* and, especially, *Ch. gymnophylla*. *M. aquatica* was already employed as passive bioaccumulator in freshwater ecosystems (Zurayk et al., 2001; Branković et al., 2012), but the use of its roots was never validated, whereas *Ch. gymnophylla* was never employed as biomonitor so far. It is known that some *Chara* spp. are able to accumulate Cd, Cu, Zn and Pb (Srivastava et al., 2008), but nothing is known on the relationship between environmental concentrations and accumulation, and thus on the actual feasibility of these species in biomonitoring studies. Shedding light on these topics, validating the use of *M. aquatica* as a passive biomonitor and *Ch. gymnophylla* as an active biomonitor, is thus one of the primary goals of the present research and an essential step in river quality estimation.

The selection of novel bioaccumulators was obviously constrained to native species, in order to avoid the introduction of allochtonous species, possibly interfering with local communities. *M. aquatica* is widely distributed in Italy (Maffei, 1998) and its choice was straightforward, but notions on the Charophyte flora of the PNCVDA were non-existent and outdated at the regional level. Therefore, the biodiversity of Charophyta within the boundaries of the PNCVDA and in its neighbourhood was investigated, in order to discover which species were present, their distribution and their ecology, allowing also to evaluate the feasibility of transplanting specimens in rivers from the lentic systems usually colonised.

The gradients obtained from passive and active biomonitoring often provide hints on the possible causes of environmental contamination, from the associations among pollutants and the neighbourhood of potential polluting activities. The derived scenarios, however, are usually provisional and additional information from other matrices is needed. To this end, PTEs were also analysed in water and sediments, where, in addition to PTE total concentrations, their partitioning into several fractions (exchangeable, bound to Fe and Mn oxides, bound to organic matter, included in minerals) was also investigated, as well as sediment mineralogy through X-ray diffraction. Indeed, although detailed information on element concentrations in soils (Thiombane et al., 2018) and sediments (Albanese et al., 2007) of the PNCVDA is already available, element actual availability and distribution in different sediment fractions was never investigated, in spite of their importance for biota. PTEs, however, are usually not sufficient to identify certain types of river pollution, like wastewater discharges, and to evaluate their effects at the ecosystem level, including dissolved oxygen depletion, eutrophication and dramatic effects on communities. For this reason, water analysis involved also parameters like anions, photosynthetic pigments, conductivity and dissolved oxygen.

Chapter 2

Materials and Methods

2.1 Study area

The "Cilento, Vallo di Diano e Alburni" National Park is the largest protected area in Campania and one of the largest in Italy (Romano et al., 2013), covering ~ 181.048 hectares and including 80 districts. It lies in the southernmost part of the province of Salerno where it was founded in 1991 to preserve the unique flora and fauna biodiversity of the area Figure 2.1, warranting the park a UNESCO biosphere reserve designation. Several species, mostly endangered, are endemic of the area, like *Primula palinuri* Petagna, which symbolizes the park on its logo, *Minuartia moraldoi* Conti, or *Soldanella sacra* A. & L. Bellino, a novel plant species described by our research group in 2015 on the Gelbison Massif, with unique phylogeography and ecology (Bellino et al., 2015). Numerous other endangered species, often endemic to southern Italy, find in the park isolated refugia, like *Eokochia saxicola* (Guss.) Freitag & G. Kadereit and *Athamanta ramosissima* Port., or constitute large populations in the area, as in the case of *Lepus corsicanus* de Winton and *Lutra lutra* L. (Marcelli and Fusillo, 2009). The outstanding geomorphological diversity of the park (Longobardi et al., 2011), with landscape mosaics of steep mountains, deep ravines, hilly areas and alluvial planes seamless interlacing from the coastline to the inland, partly accounts for its rich biodiversity and justified its recognition as the first geopark in Italy and its inclusion in the European and UNESCO Global Geopark Network in 2010 (Cuomo et al., 2013). According to Santangelo et al. (2005) 263 geosites may be recognised, distributed in 4 geomorphological units: carbonatic mountainous massifs, with summit karst landscapes, deep structural slopes and wide piedmonts areas, ii) terrigenous mountainous massifs, with sharp crests and deeply incised ravines, iii) marly-clayey hills, with gentle slopes and dendritic drainage patterns and iv) intermontane basins, alluvial and coastal plains. Although mostly comprising sites of geomorphological and stratigraphical value, approximately 26% of the geosites are of paleontological and paleoenvironmental importance, comprising also human settlements dating back to paleolithic times. The area has been successively occupied over time during the Neolithic period, by Bronze and Iron Age societies, Etruscans, Greek colonists, Lucanians, Romans, and was pivotal for the ancient road network during the Middle Ages, as evident in the feudal castles and religious establishments built along routes (`http://whc.unesco.org/en/list/842`). In recognition of its outstanding cultural heritage, the "Cilento, Vallo di Diano e Alburni" National Park was included also in the UNESCO World Heritage List in 1998 (`http://whc.unesco.org/en/list/842`), and it was still here that the Mediterranean diet, defined as an intengible heritage by UNESCO (`http://www.unesco.org/culture/ich/index.php?lg=en&pg=00011&RL=00884`), was first described.

The Bussento and Calore Salernitano are among the main river systems of the PNCVDA, and originate both from Mt. Cervati (40° 17′ N, 15° 29′ E; 1899 m a.s.l.), in the Apennines. Accurate descriptions of the drainage basins of the Bussento and Calore Salernitano rivers are reported in Longobardi et al. (2011) and in Maione et al. (2000), respectively. The drainage basin of the Bussento river (37 km long) is characterized by soils and rocks with different hydraulic permeability and a highly hydrogeological conditioning (Longobardi et al., 2011). Consequently, the groundwater circulation is very complex and exchanges between surface water and groundwater usually occur

Figure 2.1: An example of the biodiversity of the "Cilento, Vallo di Diano e Alburni" National Park. From top to bottom and left to right: *Bombina pachypus* Bonaparte, *Austropotamobius pallipes* Lereboullet, *Calopteryx virgo* L., *Chalcolestes viridis* Van der Linden, *Primula palinuri* Petagna, and *Soldanella sacra* A. & L. Bellino. All the photographs from the author.

(Longobardi et al., 2011; Cuomo et al., 2013). The main stream of the Bussento river partly flows in wide alluvial valleys and partly carving steep gorges and rapids, where a number of springs increase progressively the river discharge (Longobardi et al., 2011; Cuomo et al., 2013). Downstream, the river merges with its main tributary, the Bussentino creek, originating from the eastern sector of the drainage basin and flowing along deep canyons and gorges, mainly constituted of limestone and marly limestone (Cuomo et al., 2013). After the confluence with the Sciarapotamo creek, the Bussento river crosses a terraced floodplain and, finally, a coastal plain (Cuomo et al., 2013), flowing into the Tyrrhenian Sea. The drainage basin of the Calore Salernitano (or Calore Lucano) river (63 km long) is characterized by heterogeneous patches: gorges and endorheic areas, with tectonically driven drainage patterns (Maione et al., 2000). This wide range of landforms is mainly due to the heterogeneous lithology characterizing the entire area (Maione et al., 2000). The main course of the Calore Salernitano river flows between high rocky walls and merges with two important tributaries in the middle course: the Fasanella and the Rio Pietra creeks. The Calore Salernitano river is an important left tributary of the Sele river, in which it flows into at a distance of around 10 Km from the Tyrrhenian Sea.

2.2 Field surveys

Extensive field surveys, aimed at defining the spatial sampling grid and at searching for suitable passive biomonitors, were carried out in April-June 2016 on the Bussento-Bussentino and the Calore Salernitano-Rio Pietra-Fasanella river systems. The expeditions focused on sites with potential criticalties, like those in the neighbourhood of roads, rails and wastewater treatment plants, and on sites with peculiar hydrogeomorphological features, like springs, ponors and confluences. Candidate sites for field surveys were selected using a Geographical Information System developed for the project on the Quantum GIS 2.18 platform (QGIS Development Team, 2018), with information obtained from the "Geoportale della Regione Campania" (`https://sit2.regione.campania.it/`), the SINAnet network (`www.sinanet.isprambiente.it/`) and the "Geoportale Nazionale" (`http://pcn.minambiente.it/mattm/`). River networks were extracted from the SINAnet 20 m Digital Elevation Model (DEM), interpolated at 5 m using a regularized spline with tension and smoothing algorithm with the function `r.resamp.rst` of the Quantum GIS GRASS backend. Specifically, drainage basins were extracted from the depressionless DEM, obtained with the function `r.fill.dir`, using the `r.watershed` function and selecting the cells in the log-transformed flow accumulation layer with values > 6. The hydrological networks within the Bussento and the Calore Salernitano drainage basins were then manually cleaned and classified based on the Strahler's order using the function `r.stream.order`. The 1^{th} order stretches contributing directly to high order streams (4^{th} to 6^{th}) were then selected as candidate spring areas for field surveys. Moreover, the ends of the stretches of the second and third to highest order were included in the candidate site list as representative of the principal confluences in the Bussento and Calore Salernitano river systems. Sites with potential criticalties related to vehicular or train traffic, and accessible by car, were then obtained with the intersection of the river networks and the road and rail networks, using the function `intersect` of the basic Quantum GIS function set. Additional sites were also selected based on literature information on the presence of wastewater treatment plants, resurgences along the main river paths and ponors, as well as to enhance spatial resolution of sampling. Overall, 18 Km of the Bussento-Bussentino river system and 14 Km of the Calore Salernitano-Rio Pietra-Fasanella were explored, defining the spatial sampling grid and a set of candidate biomonitors fulfilling the following criteria:

- wide distribution in both the river system;
- wide distribution along the river path from spring to mouth;
- native in the area;

- reliable records as bioaccumulator in literature for at least one species in the set.

The criteria were chosen to ensure accurate biomonitoring of the river systems while possibly validating novel biomonitors, to allow direct comparisons among sites within and between the river systems, and to avoid the use of allochtonous species. The resulting set comprised 2 plant species: *Helosciadium nodiflorum* (L.) W.D.J. Koch and *Mentha aquatica* L.

2.3 Passive biomonitoring

2.3.1 Bioaccumulators

2.3.1.1 *Helosciadium nodiflorum* (L.) W.D.J. Koch

H. nodiflorum, previously known as *Apium nodiflorum* (L.) Lag. (Ronse et al., 2010), is a perennial aquatic plant belonging to the Apiaceae family (Pignatti, 1982). It has stems up to 1 m tall (Zurayk et al., 2001), erect or prostrate, glabrous, rooting at lower nodes, with leaves pinnately compound with up to 4 pairs of leaflets (Pignatti, 1982). The umbels are compound, with up to 20 unequal rays and small flowers with white or greenish white corolla. The flowers are self-compatible but protandrous and insect pollinated, producing schizocarps having 5 slightly raised ridges, and mericarps ovate oblong and brownish (Pignatti, 1982). The species is diploid (Ronse et al., 2010), with a chromosome number $2n = 22$, but an aneuploid count ($2n = 20$) also has been reported. Natural hybrids have been reported between *H. inundatum* × *H. nodiflorum* and between *H. nodiflorum* × *H. repens* (Ronse et al., 2010). *H. nodiflorum* grows in canals, ditches, marshes, springs and along the margins of lakes, ponds, rivers and streams at elevations of up to 350 m, either emersed or submersed at depths < 1 m (Bonanno et al., 2017; Bonanno and Vymazal, 2017). It is particularly common in clear, shallow water along the margins of high order streams, being moderately shade-tolerant and highly tolerant of turbulence, although it occurs most often in sites with moderate flow rates (Baldantoni and Alfani, 2016). This species grows mainly in alkaline waters (pH: 7.7–8.0; alkalinity: 170–250 ppm), which are low in nutrients (3–6 ppm nitrate; <0.3 ppm ammonia nitrogen; <0.3 ppm phosphate phosphorous), but can also grow in eutrophic waters (http://dx.doi.org/10.2305/IUCN.UK.2013-1.RLTS.T164030A13575513.en). The fruits lack a dormancy requirement and are dispersed by the water. They remain afloat for less than 2 days when ripe, but for more than 90 days when dry, retain their germinability (Les, 2017). The seeds germinate on wet substrates or in shallow water. Seedling establishment requires open conditions and they can appear quickly in sites that have been dredged. However, seedling survivorship usually is low and continual disturbance is necessary to alleviate competition with other species. The populations persist principally by means of overwintering shoots rather than as seedlings. The plants are perennial from a persistent root crown. Vegetative propagation occurs by shoot fragments, which develop new roots within a few days. The stems can become fairly persistent when rooting firmly into gravel substrates. The plants tend to be shallowly rooted (22–29 cm) but are fairly tolerant to substrate desiccation if not for prolonged duration, and produce longer roots in drained sites. When growing under hypoxic conditions, this species is also able to oxygenate the substrate. The species is regarded as a weed in Portugal and Spain, where it is native. According to Les (2017), it has not yet been reported as invasive anywhere in North America, where it was introduced (reportedly before 1788), along with Chile (before 1878), Mexico and New Zealand (before 1947). *H. nodiflorum* is recognised as a good bioaccumulator for river biomonitoring of PTEs in the Mediterranean area (Baldantoni et al., 2018; Baldantoni and Alfani, 2016; Zurayk et al., 2001), and its ability to uptake significant concentrations of As, Cd, Cr, Cu, Hg, Mn, Ni, Pb, Sn, U, and Zn, phytostabilising them in the roots, makes this species also a potential candidate for phytoremediation applications (Moreira et al., 2011).

2.3.1.2 *Mentha aquatica* L.

M. aquatica is a perennial aquatic pant belonging to the Lamiaceae family (Pignatti, 1982). It has stems up to 1 m tall, erect, square, glabrous to pubescent, with leaves opposite, elliptic, lanceolate or ovate, shortly petiolate and with serrate margins (Pignatti, 1982). The flowers are bilabiate, in dense verticillate cymes condensed in a terminal globose cluster, with a pink, pubescent, tubular corolla characterised by a 2-lobed upper and 3-lobed lower lip and with 4 stamens, gynobasic style, and 4-lobed ovary (Les, 2017). The flowers are self-compatible but protandrous and mainly insect pollinated, producing a schizocarp dehiscing into 4 smooth nutlets. The species is octaploid, with a chromosome number 2n = 96. The species is keen to hybridise with numerous species of the genus *Mentha*, notably with *M. piperita*, *M. longifolia*, *M. spicata*, and *M. suaveolens* (Les, 2017). *M. aquatica* grows emersed or submersed in shallow water of fens, marshes, meadows, and along lake, pond, river, and stream margins at elevations of up to 1000 m. The plants are adapted to a wide range of pH (4.5–7.8) and tend to occur on sandy substrates or muck. They are not salt-tolerant but can occur along brackish wetland margins or in tidal freshwater sites (`http://dx.doi.org/10.2305/IUCN.UK.2014-2.RLTS.T164509A63304147.en`) They do withstand physical perturbation and tend to increase at sites where disturbance (e.g., trampling by livestock) occurs. This species is regarded as a wetland pioneer and occurs in sunny to partially shaded sites. Mature nutlets, about 200 per plant, are dispersed by water and can represent a large proportion of viable propagules occurring in river drift. Plants growing in a submerged state usually produce lower biomass, but their shoots elongate significantly as an adaptive response. Vegetative reproduction occurs mainly by the diffuse production of rhizomes, but plants also are dispersed by stem or rhizome fragments. The roots normally are colonized by arbuscular mycorrhizae (Les, 2017).

M. aquatica has been demonstrated to accumulate metals, but no information on their distribution in different plant organs is available

(Branković et al., 2010, 2012), and the species was rarely employed in biomonitoring studies so far (Zurayk et al., 2001).

2.3.2 Sampling, sample processing and laboratory analyses

The 2016 sampling campaign encompassed 39 sites, 21 on the Bussento and 18 on the Calore Salernitano river systems, later changed to 24 on the Bussento and 15 on the Calore Salernitano for the 2017 sampling campaign. Overall, 17 and 14 sites overlapped in the two years for the Bussento and Calore Salernitano river systems, respectively (Figure 2.2). Each site was georeferenced using a GPSMAP 62s (Garmin, USA) handheld GPS receiver with a horizontal resolution of 1-3 m. In order to carry out samplings in the least achievable time span and minimize sampling efforts, expeditions were carefully planned using web-based routing services like Google Maps® and IGM 1:25000 charts to allow sampling at 4-8 sites per day. At each site, 6-10 healthy and fully developed *H. nodiflorum* and *M. aquatica* plants were randomly collected from riverbanks over a 20-50 m stretch of the river. For each species, roots were then sampled, washed throughly *in situ* with river water to remove sediments, organisms and other exogenous materials, pooled together to obtain an homogeneous sample, and stored in polyethylene bags.

Back at the laboratory samples were left to dessicate on filter paper sheets at room temperature for one week, then manually pulverised in china mortars using liquid nitrogen and finally dried in an incubator (ISCO 9000, Sil.Mar Instruments, Milano, Italy) at 75 °C until constant weight.

Three subsamples per root sample were acid digested in a microwave oven (Milestone Ethos, Shelton, CT, USA), using 1 mL 50% HF (Sigma-Aldrich, Milano, Italy) and 2 mL 65% HNO_3 (Sigma-Aldrich, Milano, Italy) per 125 mg of sample. The mineralization program is reported in Table 2.1.

After digestion, the solutions were diluted to a final volume of 25 mL in polypropilene flasks, using milli-Q water (Millipore Elix 10,

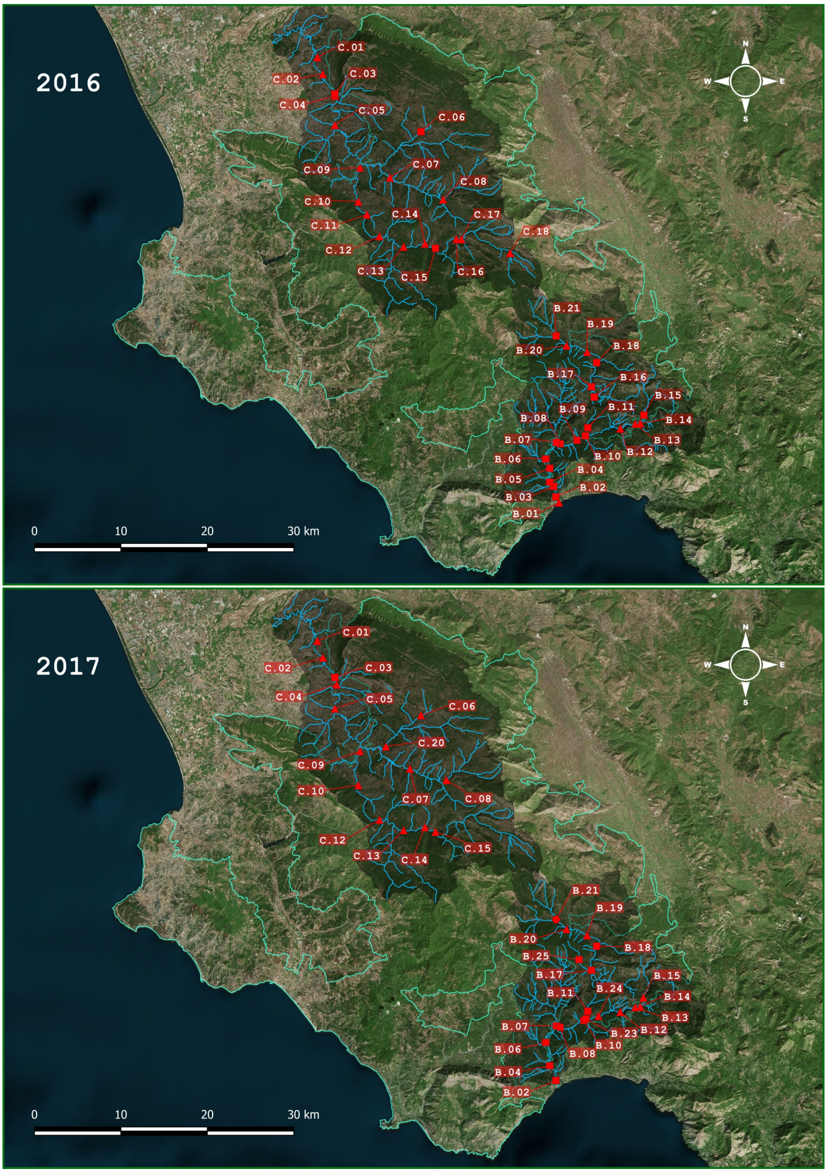

Figure 2.2: Map of the sampling sites, in 2016 and 2017, along the Bussento (B) and Calore Salernitano (C) rivers (image from Bing Maps) indicating where *H. nodiflorum* (■), *M. aquatica* (▲) or both the species (●) were found. Boundaries of the "Cilento, Vallo di Diano e Alburni" National Park (—) and drainage basins (☁) are also shown.

Table 2.1: Microwave oven mineralization program adopted for sample preparation.

	1^{st}	2^{nd}	3^{rd}	4^{th}	5^{th}	6^{th}
Power (W)	250	0	250	400	0	500
Time (min)	2	2	5	5	2	5

Darmstat, Germany) and analysed by means of inductively coupled plasma optical emission spectrometry (PerkinElmer Optima 7000DV, Wellesley, MA, USA) to quantify macronutrient (Ca, K, Mg, P, S), micronutrient (Co, Cr, Cu, Fe, Mn, Na, Ni, Si, V, Zn) and non-essential element (Al, As, Cd, Pb) concentrations. A PTFE Gem-Cone/Cyclonic chamber nebulizer was employed. Method accuracy was estimated through the concurrent analysis of standard reference material (1575a pine needles, Mackey et al. (2004)), using the recovery percentage of each element to correct PTE quantification in root samples. The method precision, calculated as relative standard deviation, based on n = 9 sequential measurements of the same sample for each element, ranged from 2 to 7%, depending on the element.

2.4 Active biomonitoring

2.4.1 Bioaccumulators

2.4.1.1 *Fontinalis antipyretica* Hedw.

F. antipyretica is a large pleurocarpous aquatic moss belonging to the Fontinalaceae family, with shoots 5-8 mm wide and up to 50 cm long (Welch, 2014). The leaves are 4-5 mm long and strongly folded inwards along the midline, with the fold-line forming a prominent keel. The shoots are usually 3-sided, with the keels forming the angles and the overlapping halves of adjacent leaves forming the sides. The leaf lacks a nerve and its tip is bluntly pointed and untoothed. Capsules are uncommon, and almost hidden amongst the leaves, occurring only on thalli which have undergone a period of exposure above the water

(Atherton et al., 2010). The species colonizes various substrates, including rocks, stones, tree roots and branches, always submersed or emersed nearby water, along streams and rivers from the plain to the subalpine belt (Symoens, 2012). It is the moss species most commonly used as bioaccumulator in biomonitoring of freshwater environments, especially in relation to PTEs like As, Cd, Co, Cr, Cu, Fe, Mn, Ni, Pb and Zn (Debén García et al., 2016; Bruns et al., 1997; Phillips and Rainbow, 2013).

2.4.1.2 *Chara gymnophylla* A. Braun

Ch. gymnophylla, a macroscopic algae belonging to the Characeae family (`http://www.algaebase.org`), is closely related to *Ch. vulgaris* L. and sometimes considered a variety of the latter (Bazzichelli and Abdelahad, 2009). However, although intermediate forms between the species are commonly observed, the species in their typical habitus are easily distinguished, even at macroscopic level, with the presence of gametangia on ecorticate (*Ch. gymnophylla*) or corticate (*Ch. vulgaris*) branchlets (Bazzichelli and Abdelahad, 2009). The thalli of *Ch. gymnophylla* are 3–25 cm tall, slender, green to brown, usually with carbonate encrustations and with short globose stipulodes in 2 rows. The internodes are 1-6 times longer than branchlets, corticated, with diplostichous, aulacanthous, thylacanthous or sometimes isostichous cortex. Spine cells are globular, shorter then axis diameter (Bazzichelli and Abdelahad, 2009; Stoyneva and Gärtner, 2004). The branchlets are 6–11 per whorl, ecorticated or with 1–2 corticated segments. In this case, ecorticate cells bring antheridia and archegonia. Branchlet terminal cells are conical or mucronate (Bazzichelli and Abdelahad, 2009; Stoyneva and Gärtner, 2004). The species is monoecious, with gametangia separated or more often geminate or conjoined. Archegonia are usually encrusted by carbonate depositions and are 500–800 x 350–525 μm in size, 1-2 times shorter than bracteoles. Mature oospores are brown to black, smooth or granulated. The antheridia are orange-red, globose, 400-600 μm in diameter (Bazzichelli and Abdelahad, 2009;

Stoyneva and Gärtner, 2004). The species is usually observed in lacustrine environments, where it's able to form large mats (Ahmadi et al., 2012). To our knowledge, *Ch. gymnophylla* has never been employed in biomonitoring studies as a PTE accumulator.

2.4.2 Material selection and bag preparation

The selection of the source populations of *F. antipyretica* and *Ch. gymnophylla* fulfilled two main criteria: i) large population consistency, preventing harms from collection on its viability, and ii) absence of criticalties according to the results of 2016 passive biomonitoring. For *F. antipyretica*, the population located in the middle stretch of the Bussento river around 200 m upstream of a sluice (site B.07), was selected. Due to the lack of *Chara* spp. populations on the Bussento and the Calore Salernitano rivers large enough to provide sufficient material without threatening their conservation, transplants of *Ch. gymnophylla* were collected from a spring pool (40° 16′ 38.82″ N; 14° 59′ 53.00″ E) on the coastal area of the "Cilento, Vallo di Diano e Alburni" National Park. For each species, ~1.5-2.0 Kg f.w. of thalli were collected in one occasion, cleaned *in situ*, and stored in separate pools with original river or spring pool water for 1-7 days until bag preparation and installation.

Figure 2.3: Bag construction from cheese molds.

Bags were built using pairs of cheese molds, coupled and fastened together on 3 points using zip ties with uncutted long ends, favouring bag uncluttering and their tossing around in water (Figure 2.3). The 250 mL "Primavera" mold model (Morgan Line, Firenze, Italy) was choosen for its truncated hemisphere shape, better approximating a spherical shape when joined in pairs than common conical or cylindrical molds. Moreover, the low density of the polyethylene/polypropylene copolimer used for mold construction allows bags to float at the water level, keeping mosses and algae in the euphotic zone and reducing variance associated to bag vertical position in the water column (Figure 2.4).

Figure 2.4: Bags floating in water and bag sampling. Bags containing *F. antipyretica* and *Ch. gymnophylla* can be distinguished from the darker color of the former.

2.4.3 Bag installation, sampling and analysis

Bags were filled with ~20-30 g of *F. antipyretica* or *Ch. gymnophylla* right before field installation and were then washed in EDTA 1M solution for 10′ to reduce PTE initial content and variability among samples (Debén García et al., 2017). In each site, 6 bags were attached to tree roots and branches or stones with floating nylon line to further prevent bag sinking. Specifically, bags were placed in pairs, each constituted by a moss bag and an algae bag, over a 20-50 m stretch of the river, attaching them alternately on both riverbanks, whenever possible. At 2 sites, the 6 bags were attached together, due to local water depth constraints.

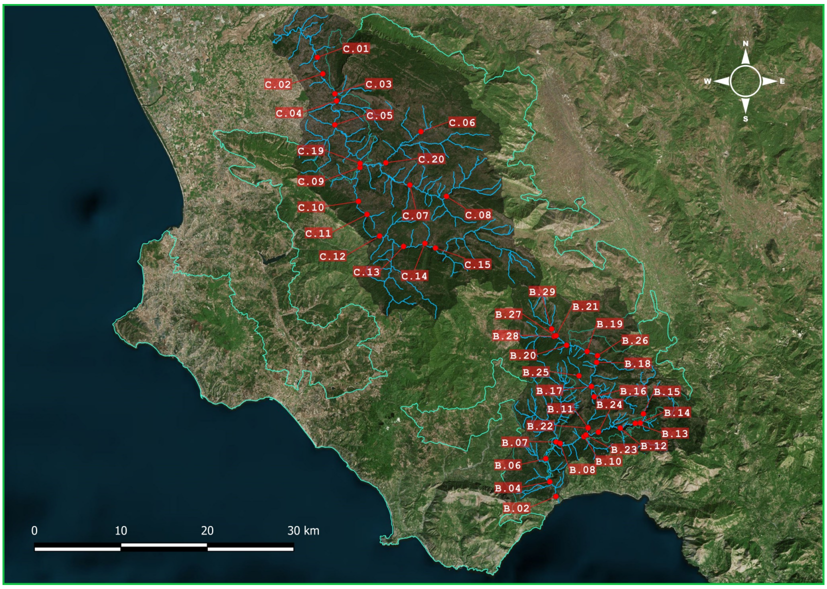

Figure 2.5: Map of the sampling sites, in 2017, along the Bussento (B) and Calore Salernitano (C) rivers (image from Bing Maps) indicating where (●) *F. antipyretica* and *Ch. gymnophylla* bags were placed. Boundaries of the "Cilento, Vallo di Diano e Alburni" National Park (—) and drainage basins (☁) are also shown.

Active biomonitoring allowed extending monitoring to 4 sites missing *H. nodiflorum* and *M. aquatica* populations: 3 sites in the spring area of the Bussento river and one site on the Fasanella river (Figure 2.5). Bags were left to accumulate *in situ* for 3 weeks before collecting and dessicating at room temperature for 1 week. Samples were then manually pulverised in china mortars, using liquid nitrogen in the case of *F. antipyretica*, oven dried at 75 °C until constant weight, and were then mineralized following the acid digestion protocol described for passive biomonitors (subsection 2.3.2). Similarly, PTE analysis was carried out as described in subsection 2.3.2.

2.5 Water

2.5.1 Sampling and sample processing

During the 2016 and 2017 sampling campaigns, water physical and chemical analyses, including electrical conductivity (HI9835, Hanna Instruments), temperature, dissolved oxygen, redox potential and pH (all with a multi-parametric probe (HI9147, Hanna Instruments) were performed *in situ* (Figure 2.6). Moreover, water samples were collected for i) PTE analysis (3 x 50 mL), acidified to pH = 2 in the field with 65% HNO_3, ii) total organic carbon (TOC), inorganic carbon (IC) and total nitrogen (TN) (3 x 50 mL) and iii) photosynthetic pigment and anion analysis (3 x 1.5 L). Samples were kept cold and in the dark during sampling and processed the same day, back in the laboratory, to extract photosynthetic pigments or frozen at -18 °C for all the other analyses. Specifically, water samples for pigment analysis were vacuum-filtered on glass filters, from which pigments were extracted with 100% acetone at -18 °C until the analysis, carried out 1 week later. A 10 mL aliquot of each filtered water sample was further filtered on 0.2 μm cellulose filters for anion analysis.

2.5.2 Laboratory analyses

Water PTE concentration analysis was carried out by means of inductively coupled plasma optical emission spectrometry (PerkinElmer Optima 7000DV, Wellesley, MA, USA), as described in the subsection 2.3.2.

Quantification of Br^-, Cl^-, F^-, NO_2^-, NO_3^-, PO_4^{3-}, and SO_4^{2-} was performed through Ion-Exchange chromatography, using a IonPac AS19 250 mm x 4 μm column (Dionex, USA), with a 50 mm security guard, on a DX120 chromatography system (Dionex, USA). Eluent was con-

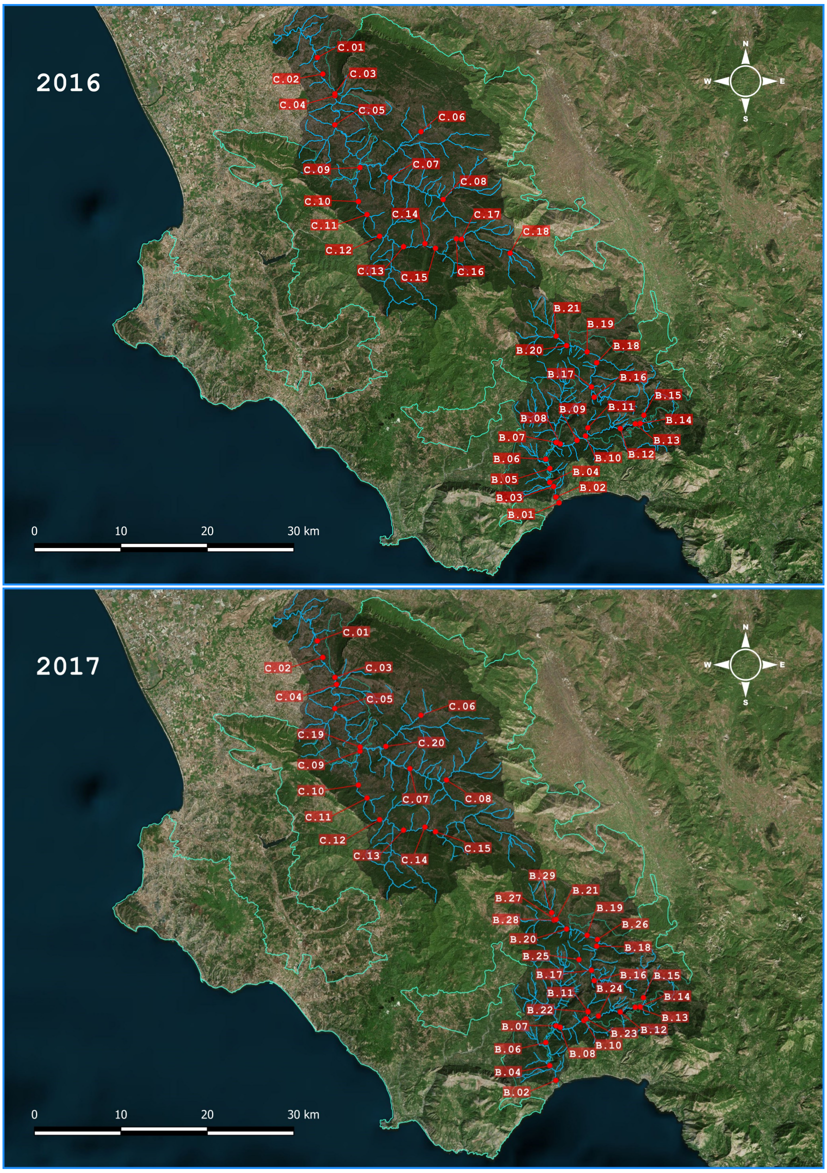

Figure 2.6: Map of the sampling sites, in 2016 and 2017, along the Bussento (B) and Calore Salernitano (C) rivers (image from Bing Maps) indicating where (●) water analyses has been performed. Boundaries of the "Cilento, Vallo di Diano e Alburni" National Park (—) and drainage basins () are also shown.

stituted by a $Na_2CO_3 : NaHCO_3$ solution (3.5 mM : 1.0 mM), flushed at 1.10 mL min^{-1} flow rate and pression < 1400 KPa.

Photosynthetic pigment analysis was performed by means of UV-Vis spectrophotometry, using a UV-Vis 1800 (Shimadzu, Kyoto, Japan) spectrometer, and spectra deconvolution in the range 350-750 nm through Gauss Peak Spectra fitting (Küpper et al., 2007). Equations for Chlorophyta were employed for all the samples with the exception of the one belonging to site C.16 in 2016, for which the equations for Euglenophyta provided a better fit.

TOC, IC and TN analyses were carried out using a TOC-V CSN TOC/TN analyzer (Shimadzu, Kyoto, Japan), measuring TOC as the difference between total carbon and IC.

2.6 Sediments

2.6.1 Sampling and sample processing

Sediment sampling was carried out in April 2018 on a restricted set of sites (Figure 2.7), 10 on the Bussento and 8 on the Calore Salernitano rivers, including all sites exhibiting criticalties according to the 2016 or 2017 monitorings and a few controls. At each site, 1-2 Kg of sediments from the 0-3 cm layer were manually collected using plastic bags, limiting the loss of fine particles and avoiding metal contamination. Back in the laboratory, sediments were placed in boxes built of filter paper, in order to facilitate water loss, dried in an incubator (ISCO 9000, Sil.Mar Instruments, Milano, Italy) at 75 °C until constant weight and sieved through 2 mm mesh size sieves (Retsch GmbH, Haan, Germany) to retrive the granulometric fraction. An aliquot (~50 g) of sieved sediments was pulverised in agata mortars using a PM4 planetary ball mill (Retsch GmbH, Haan, Germany) for PTE total concentration analysis and X-ray diffraction analysis, and the rest was kept for PTE fractionation and particle size distribution analysis.

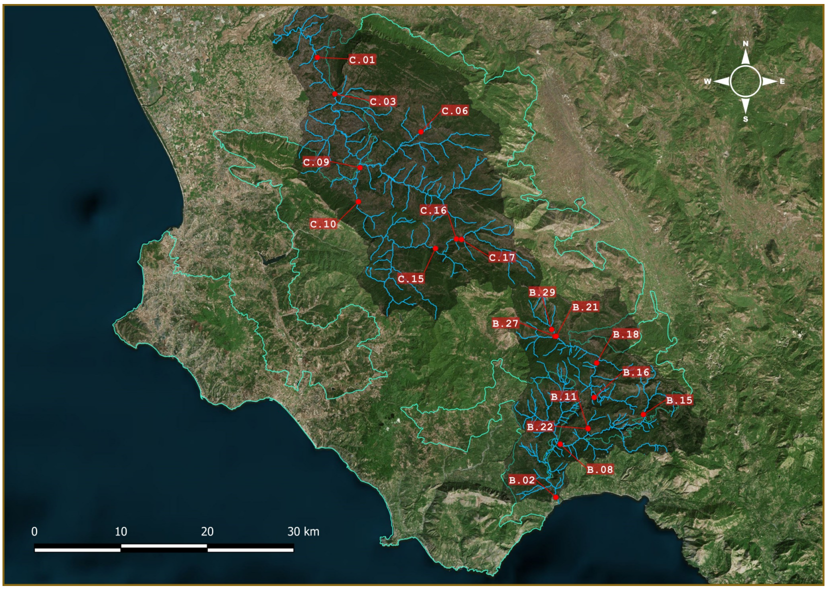

Figure 2.7: Map of the sampling sites, in 2017, along the Bussento (B) and Calore Salernitano (C) rivers (image from Bing Maps) indicating where (●) sediments were collected. Boundaries of the "Cilento, Vallo di Diano e Alburni" National Park (—) and drainage basins (●) are also shown.

2.6.2 Laboratory analyses

Sediment PTE total concentration was analysed on mineralised samples according to the method described in subsection 2.3.2, with slight modifications. In particular, three subsamples of 250 mg per sediment sample were mineralised with 2 mL 50% HF (Sigma-Aldrich, Milano, Italy) and 4 mL 65% HNO_3 (Sigma-Aldrich, Milano, Italy) and diluted to a final volume of 50 mL in polypropilene flasks, using milli-Q water (Millipore Elix 10, Darmstat, Germany). PTE quantification was carried out by means of inductively coupled plasma spectrometry, as described in subsection 2.3.2. Due to the different matrix in respect to plant samples, method accuracy was estimated through the concurrent analysis of NCS DC73321 "China soil" certified reference material from China National Analysis Center for Iron and Steel (Beijing, China), using the recovery percentage of each element to correct

PTE quantification in sediment samples.

PTE fractionation in sediments was carried out according to a modified BCR sequential extraction procedure (Rauret et al., 1999). Specifically, 3 subsamples of 500 mg per each sediment sample were weighted in 40 mL Nalgene™ PTFE centrifuge tubes, along with a blank and 3 subsamples of BCR-701 "Lake sediments" certified reference material from European Community Bureau of Reference (Pueyo et al., 2001). Each sample was then subjected to the following sequential extraction steps (Rauret et al., 1999):

1st Step **Exchangeable PTEs** - 20 mL of an acetic acid (CH_3COOH) 0.11 M solution, shaked head-to-toe for 16 hours at room temperature;

2nd Step **PTEs bund to Fe/Mn oxides** - 20 mL of a hydroxylamine hydrochloride ($NH_2OH{\cdot}HCl$) 0.5 M solution in 50 mM HNO_3, shaked head-to-toe for 16 hours at room temperature;

3rd Step **PTEs bund to organic matter** - 5 mL of a hydrogen peroxide (H_2O_2) 8.8 M solution at pH = 2, for 1 hour at room temperature and then for 1 hour at 85 °C. At the same temperature, the volume was then reduced to ~1.5 mL and additional 5 mL of hydrogen peroxide solution were added, further drying the solution to ~1 mL. 25 mL of an ammonium acetate (CH_3COONH_4) 1.0 M solution at pH = 2.0 were added and the suspension was shaked head-to-toe for 16 hours at room temperature;

4th Step **Residual PTEs** - 24 mL of aqua regia (37% HCl : 65% HNO_3, 3:1 v:v) solution, shaked head-to-toe for 16 hours at room temperature.

After each step, samples were centrifuged at 3000 rpm for 20 minutes to collect and store, in polypropylene bottles, the extracts, and the sediments were washed with milli-Q water and newly centrifuged with the same settings before the subsequent extraction step.

The extracts from the 4th Step were diluted 1:5 with milli-Q water in polypropylene flasks to a final volume of 50 mL, whereas the extracts from the other steps were directly analysed. PTE concentrations were quantified by means of inductively coupled plasma optical emission spectrometry (PerkinElmer Optima 7000DV, Wellesley, MA, USA), correcting concentrations based on the average PTE concentrations in the extracts from the BCR-701 certified reference material.

Mineralogical analysis was performed by means of X-ray diffraction analysis on pulverised samples, using a D2 PHASER (Bruker Corporation, Billerica, USA) benchtop XRD system. In particular, pulverised samples were placed in plastic holders for powder analysis, and the X-ray diffractograms were aquired using the parameters reported in Table 2.2, with continous scanning. The presence and estimated abundances of the major mineralogical components in the sediment samples were then obtained through Rietveld refinement of the diffractograms, using the Profex (Doebelin and Kleeberg, 2015) software and data from the Crystallography Open Database (`http://www.crystallography.net`) and the RUFF (`http://rruff.info/`) databases.

Table 2.2: D2 PHASER XRD system settings for sediment mineralogy analysis.

Timestep	2θ	Step width	PSD opening
0.100 s	5.002° - 65.004°	0.006°	5.002°
Fence height	Anode material	Tension	Current
1 mm	Cu	30.0 kV	10.0 mA

2.7 Charophyte biodiversity

2.7.1 Sampling and sample processing

Each Charophyte population encountered during the 2016 and 2017 sampling campaigns was georeferred using a GPSMAP 62s (Garmin, USA) handheld GPS receiver with a horizontal resolution of 1-3 m and identified at the species or subspecies/variety level using dichotomous keys (Bazzichelli and Abdelahad, 2009). Considering the lack of information on the Charophyte flora of the "Cilento, Vallo di Diano e Alburni" National Park, also populations outside the Bussento and Calore Salernitano drainage basins, and even outside the park boundaries (owing to its involuted perimeter) but in its neighbourhood, were included in the present research. A map showing all the observed populations is provided in Figure 2.8.

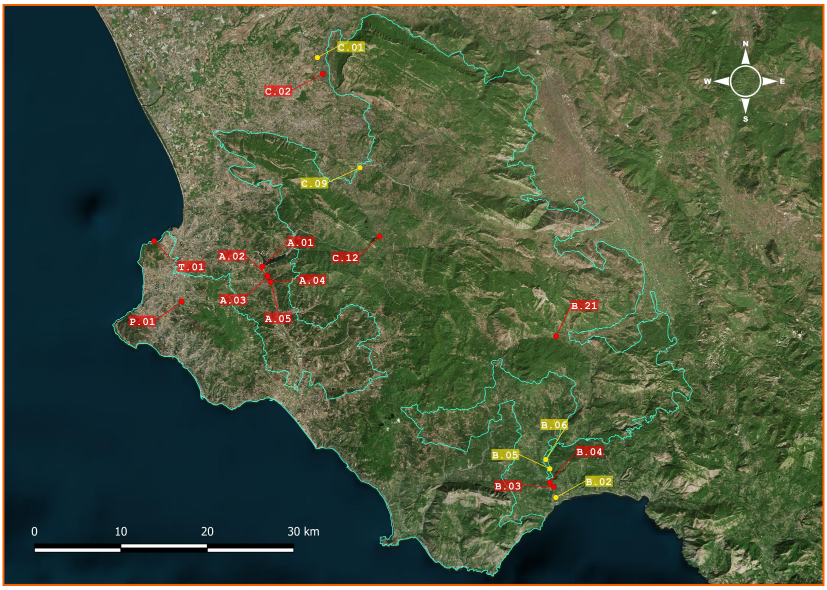

Figure 2.8: Map of Charophyte populations observed along the Bussento (B), the Calore Salernitano (C) and the Alento (A) rivers, and in spring pools within the Perdifumo discrict (P) and Trentova (T) zone (image from Bing Maps). Populations on which morphological, physiological and ecological analyses were carried out (●) and those observed but not analysed due to their disapparence in 2018 (●) are indicated.

In order to further confirm species identification and evaluate the differentiation among populations, several morphological, biochemical and ecological traits of all the populations occurring in 2018 were also analysed. Thalli were collected using polyethylene bags during May 2018, ensuring the presence of reproductive structures for most of the taxa and avoiding the loss of some populations due to Summer drought. In the laboratory, thalli were carefully separated and treated according to the type of traits analysed. Specifically:

- 5 thalli were fixed and preserved in formalin-acetic acid-alcohol (FAA) solution at 4 °C for morphological analyses (Ruzin, 1999);
- 5 thalli were fixed in FAA for epiphyte diatom biomass analysis (Sviben et al., 2018);
- 5 thalli were used for photosynthetic pigment extraction, by means of 3 replicate extractions per sample with 100% acetone at -18 °C for 1 day, and pooling of the fractions (Bellino et al., 2014);
- 3 x ~5 g f.w. of thalli per population were dried in an incubator (ISCO 9000, Sil.Mar Instruments, Milano, Italy) at 75 °C until constant weight for carbonate encrustation analysis (Sviben et al., 2018).

In addition, oospore for Scanning Electron Microscopy (SEM) analysis were retrieved from sediments, manually cleaned under a SMZ445 stereomicroscope (Nikon Instruments, Tokyo, Japan) with pin forceps and placed in 10% aqueous solution of Triton-X100 for 1 hour at 60 °C in 1.5 mL polypropilene microcentrifuge tubes. Oospore were then washed throughly with distilled water, kept in 1N HCl for 60″ at room temperature to remove carbonate encrustations, and then cleaned of the radiate cells using pin forceps under a SMZ445 stereomicroscope. Oospore were finally dehydrated using a graded ethanol series as reported in Table 2.3, placed on SEM stubs, dried under N_2 flux overnight, and sputter coated with a 10 nm Au layer, optimizing the method reported in Urbaniak (2011).

2.7.2 Laboratory analyses

Morphological analyses (Ruzin, 1999) were performed through image analysis using the ImageJ 1.8.0 (Schneider et al., 2012) software, on

Table 2.3: Dehydration steps adopted in *Chara* spp. oospore preparation for SEM analysis.

	1^{st}	2^{nd}	3^{rd}	4^{th}	5^{th}	6^{th}	7^{th}
EtOH	25%	40%	60%	80%	90%	100%	Anhydrous
Time	1 day	1 day	1 day	1 day	1 day	2 days	2 days

images taken either using a D*f* (Nikon Imaging, Tokyo, Japan) camera equipped with a 58 mm f/1.4 (Voigtländer, Tokyo, Japan) lens, for the measurement of internode length, or a CoolSnap K4 (Photometrics, Tucson, USA) camera mounted on a Dialux 20 (Leitz, Wetzlar, Germany) microscope, for all the other parameters. These included cortex and stipuloides types, internode length and diameter, spine length and width, number of branchlets, number, length and width of corticate and ecorticate cells on branchlets, diameter of antheridia, length and width of archegonia, and height and diameter of coronula. Microscope images were taken at 25x, 100x, 250x and 400x magnifications.

Weighted samples for epiphyte diatom biomass analysis (Sviben et al., 2018), placed in 50 mL polyethylene centrifuge tubes, were sonicated in a Labsonic LBS1-3 (FALC, Treviglio, Italy) ultrasonic cleaner in FAA solution for 30 minutes. Thalli were then removed, the FAA solution centrifuged at 4000 rpm for 20 minutes and the supernatant discarded. Samples were treated with 30% hydrogen peroxide for 7 days, in order to remove organic matter and, after a second centrigugation, the supernatant was discarded and the samples were dried in an incubator (ISCO 9000, Sil.Mar Instruments, Milano, Italy) at 75 °C. Epiphyte diatom biomass was then estimated through weighting of the diatom frustules, referring it to each thallus fresh weight.

Gravimetric analyses were employed in measuring carbonate encrustation, according to Sviben et al. (2018). Specifically, the dried samples were weighted and treated with 16% HCl for 15 min, in order to remove carbonates, then washed several times with distilled water, dried in an incubator (ISCO 9000, Sil.Mar Instruments, Milano, Italy) at 75 °C and then weighted again. The mass of carbonates precipitated on the surface of Charophyte samples was then estimated as the difference between the initial and the final weight.

Chlorophylls, pheophytin and carotenoids were quantified on the acetone extracts through UV-Vis spectrophotometry and spectra deconvolution (Bellino et al., 2014) using the Gauss Peak Spectra fitting (Küpper et al., 2007) technique. In particular, the absorbance spectra of the centrifuged (5000 rpm for 10 minutes) samples were recorded in the range 350-750 nm using a UV-Vis 1800 (Shimadzu, Kyoto, Japan) spectrometer and were deconvoluted using the set of equations for Chlorophyta provided by Küpper et al. (2007). Micromolar concentrations were then referred to the fresh weight of thalli. Pigment profile (Bellino et al., 2014), instead, was evaluated by means of reversed phase high performance liquid chromatography (RP-HPLC) with MWD (430 nm and 450 nm) and fluorimetric (ex: 432 nm, em: 660 nm) detection. Specifically, pigments were separated on a Kinetex 5 μm EVO C18 150 x 4.6 (Phenomenex, Torrance, USA) analytical column, equipped with the dedicated security guard column, with a TSP AS3500 (Thermo Scientific, Waltham, USA) chromatography system, using a binary gradient method specifically developed for the task. Details on the RP-HPLC protocol are provided in Table 2.4.

2.8 Data analysis

Data analysis was tailored on each specific aim represented in Figure 1.2: i) investigate Charophyte biodiversity and ensure the use of native active biomonitors, ii) validate *M. aquatica* and *Ch. gymnophylla* as novel PTE biomonitors and iii) evaluate river quality, with special emphasis on spatial PTE concentration patterns.

2.8.1 Charophyte biodiversity

Length and width of internodes, spines, corticate and ecorticate cells on branchlets, archegonia and coronulas were employed in calculating

Table 2.4: RP-HPLC settings adopted for Charophyta photosynthetic pigment profiling.

Column	Kinetex 5 μm EVO C18 150 x 4.6			
Loop	20 μL			
Sample matrix	Acetone:water 7:3 v:v			
Elution type	Gradient			
Eluent A	250 mM Pyridin in water (30%) : MeOH (70%)			
Eluent B	Ethyl acetate (30%) : MeOH (70%)			
Temperature	30 °C			
Detection	UV-Vis spectrometry: 430 nm and 450 nm / Fluorimetry - ex: 432 nm, em: 660 nm			
	Time (min)	**A (%)**	**B (%)**	**Flow rate (mL/min)**
Gradient profile	0	58	42	1.00
	6	45	55	1.00
	10	15	85	1.00
	20	0	100	1.00
	24	0	100	1.00
	25	58	42	1.00

the sizes (as the product length × width) and proportions (as the ratio length × width) of each thallus part. Sizes and proportions were the used as morphological traits in multivariate analyses, with the addition of the ratio of corticate cells on the total branchlet cell number, of the presence/absence of reproductive structures on corticate cells, and of the cortex type. The assignment of each thallus to one of the three species observed was performed using fuzzy partitioning into 3 clusters, choosing an exponential membership coefficient equal to 1.4, in order to provide an optimal compromise between partitioning crispness and fuzziness. The analyses were performed using the functions `daisy` and `fanny` of the "cluster" (Maechler et al., 2018) package, visualizing membership probabilities through a ternary diagram drawn with the function `ggterm` of the "ggterm" (**?**) package. The differentiation among Charophyte populations (Figure 2.8) in respect to the morphological traits was evaluated through a Non-metric Multidimensional Scaling (NMDS), based on 2 axes and on the Gower distance metric, with the superimposition of confidence ellipses (for $\alpha = 0.05$) for the species. The choice of the Gower distance metric was forced by the need to calculate distances with mixed type variables: binary, multinomial, and numeric. The analyses were performed within the R 3.5.1 (R Core Team, 2018), using functions `metaMDS` and `ordiellipse` of the "vegan" package (Oksanen et al., 2018). The contribution of each morphological trait to the differentiation of populations was then evaluated by fitting murphometric variables onto the NMDS space, with the function `envfit` of the "vegan" package. The same techniques were adopted also in evaluating population differentiation, and variable contribution in determining it, based on the abundance of chlorophyll *a*, chlorophyll *b*, pheophytin *a*, pheophytin *b*, and total carotenoids.

The differences in carbonate encrustation and epiphyte diatom biomass among species and populations were analysed through one-way analyses of variance using either the population or the species identifier as fixed factors. Pairwise comparisons over estimated marginal means, using the Tukey multiplicity correction were carried out following rejection of the ANOVA null hypothesis. The analyses were performed within the R 3.5.1 programming environment, with the functions `aov` of the "stats" (R Core Team, 2018) package and `emmeans` of the "emmeans" (Lenth, 2018) package.

2.8.2 Biomonitor validation

The validation of *M. aquatica* and *Ch. gymnophylla* relied on the similarities between their PTE accumulation behaviour and those of *H. nodiflorum* and *F. antipyretica*, respectively. To this aim, distance based multivariate techniques, involving NMDS/confidence ellipses superimposition and Mantel correlation test, were employed. In particular, the differentiation in PTE accumulation behaviour was estimated by analysing the possible overlap of confidence ellipses (for $\alpha = 0.05$)

relative to the biomonitors in NMDS spaces, based on 3 axes and on a Manhattan distance metric. As previously described in subsection 2.8.1, different distance metrics were tested, choosing the one providing the best stress figure. To separately evaluate the similarities between the couples of passive and active biomonitors in relation to the absolute PTE concentrations or in relation to the spatial accumulation patterns only, the analyses were performed either on the raw data or on data scaled in the $[0, 1]$ interval for each biomonitor. Details on the functions employed are provided in subsection 2.8.1. Moreover, the overall similarities in PTE accumulation behaviour between *M. aquatica* and *H. nodiflorum* and between *Ch. gymnophylla* and *F. antipyretica* was also evaluated through the Mantel correlation test, using the same distance matrices employed in NMDS analyses and $1 \cdot 10^5$ permutations, with the function `mantel` of the "vegan" package.

2.8.3 River quality

The evaluation of river quality, in relation to PTEs, focused primarily on extracting the spatial scales of variations in PTE concentrations in biomonitors, sediments, and water, on estimating the spatial extent of local alterations in PTE concentrations and on identifying critical locations. The same approach was adopted also in analysing the spatial patterns of organic or nutrient loads from soil leaching, through several indicators measured in water, like TOC, TC, photosynthetic pigments and anions.

The extraction of the spatial scales relied on Moran's Eigenvector Maps (MEMs), coupled with Redundancy Analysis (RDA). Specifically, shapefile layers containing the average PTE concentrations per site in *Ch. gymnophylla* and *F. antipyretica*, and in *H. nodiflorum* and *M. aquatica* in both 2016 and 2017 were created using the Quantum GIS 3.2 software (QGIS Development Team, 2018), and imported as "SpatialPointDataFrame" within the R 3.5.1 programming environment using the function `readOGR` of the "rgdal" (Bivand et al., 2018) package. Lists of candidate spatial weighting matrices for sampling points on the Bussento and Calore Salernitano rivers, based on Delanunay triangulation, Gabriel's graph, Relative neighbourhood graph and Minimum spanning tree connectivity topologies, were then built and individually weighted according to 4 different weighting shemes: "binary" - without weights, "flin" - linear weighting function, "fdown" - concave-down weighting function, and "fup" - concave-up weighting function. The 0.2, 0.4, 0.6, 0.8 set of coefficients was employed for both the "fdown" and "fup" functions. Separate lists for each of the "W", "B", "C", "U", "minmax", and "S" weighting styles were produced, summing up to 240 individual spatial weighting matrices evaluated for each dataset of passive biomonitors, active biomonitors, sediments and water. Since the dataset of *Ch. gymnophylla* and *F. antipyretica*, and those of *H. nodiflorum* and *M. aquatica* were jointly analysed, a normally distributed random jitter, with ($\mu = 0;\ \sigma = 2$) was added to the site coordinates in order to avoid duplicates. The lists of spatial weighting matrices were built using the function `listw.candidates` of the (Dray et al., 2018) (Dray et al., 2018) package.

The MEM variables (*i.e.*, eigenvectors of a doubly centered spatial weighting matrix) were then computed for each candidate spatial weighting matrix and both the selection of the best spatial weighting matrix and of a subset of significant positive MEMs were carried out using the function `listw.select` of the "adespatial" package. The selection of the spatial weighting matrices was performed by maximizing the adjusted r^2, using a Sidak correction for multiple tests to the P-value of the global test for each spatial weighting matrix, whereas the selection of the best MEM subsets was performed through forward selection. The final covariance-based RDAs, with MEMs as predictors and PTE concentrations in biomonitors and environmental matrices as response variables, were then computed using the function `rda` of the "vegan" package.

The extent at which local alterations propagated in space was estimated through the analysis of Mantel correlograms, calculated using the function `mantel.correlog` of the "vegan" package.

The identification of spatial outliers was performed using the functions map.plot and uni.plot of the "mvoutlier" (Filzmoser and Gschwandtner, 2018) package, to identify sites with peculiar criticalities using the approach of Filzmoser (2005). In particular, multivariate outliers were identified separately in relation to macronutrients, micronutrients, and non essential elements in passive and active biomonitors, and water, and in relation to TOC, TC, photosynthetic pigments and anions in water.

The analysis of PTE fractionation data on sediments, aimed at evaluating differences among sites in their pattern of PTE distribution among the exchangeble, bound to Fe-Mn oxides, bound to organic matter, and residual fractions, required the development of a novel machine learning approach. BCR data can be represented, in fact, by 3-mode compositional tensors, in which a matrix containing the proportion of each PTE in the 4 different fractions is associated to each site. The analysis of this data structure poses two main challenges: i) the use of Compositional Data Analysis (CoDA) approaches, and ii) an extension of classic multivariate techniques to 3-mode tensors. The proposed approach couples log-ratio transformation, commonly employed in opening closed compositional data, and Principal Tensor Analysis on 3-modes (PTA-3) for the truncated Singular Value Decomposition of compositional tensors.

Compositional matrices relative to the distribution of each PTE in the exchangeble, bound to Fe-Mn oxides, bound to organic matter, and residual fractions in each site were coded as "acomp-class" objects using function acomp of the "compositions" (van den Boogaart et al., 2018) package within the R 3.5.1 programming environment. The resulting 19 matrices were organised in a list and subjected to an isometric log-ratio transformation using the function ilr of the "compositions" package. The resulting matrices were then stacked and organised in an array using the function sapply of the "base" (R Core Team, 2018) package, which was then subjected to a PTA-3 decomposition, using the function PTA3 of the "PTAk" (Leibovici, 2010) package. The maximum number of Principal Tensors was set to 2 (nbPT = 2), computing all the solutions for 2-mode tensors (nbPT2 =

1), and selecting tensors explaining a percentage of the total variance $> 1\%$.

Object loadings onto the selected tensors (mode n. 1) were then employed as descriptors of the pattern of PTE distribution in the BCR fractions for each site and used to build a dendrogram representing the distances among sites. The dendrogram was computed using functions `agnes` and `as.dendrogram`, from the "cluster" and "dendextend" packages, respectively, starting from an Euclidean distance matrix produced using the function `daisy` of the "cluster" package. Biplot of the element loadings (mode n. 3) and ilr-transformed variables (mode n. 2) were then produced to evaluate the distribution of elements in relation to their characteristic distribution pattern into the exchangeble, bound to Fe-Mn oxides, bound to organic matter, and residual fractions.

Site differentiation in relation to the total PTE concentrations in sediments, and in relation to the PTE concentrations in each of the BCR fractions was also evaluated through NMDSs, based on 2 axes and on the Manhattan distance metric, with the superimposition of the confidence ellipses (for $\alpha = 0.05$) relarive to the sites. The analysis was performed using the functions `metaMDS` and `ordiellipse` of the "vegan" package.

The estimated abundance of quartz, Calcite, and dolomite, obtained through Rietvield's refinement of XRD diffractograms, was employed in evaluating site differentiation based on mineralogical composition and to evaluate possible relationships between the mineralogical composition and the total and exchangeable PTE concentrations. To these ends, a ternary diagram, with the superimposition of confidence ellipses for 1σ, 2σ, and 3σ, was firstly produced using the function `plot.acomp` of the "compositions" package. The compositional variables representing the abundance of quartz, calcite, and dolomite were then subjected to an isometric log-ratio transformation and employed as predictors in RDAs using the total PTE concentrations and the loadings of the mode n.1 compositional tensor upon the selected tensors as response variables. Confidence ellipses (for

α = 0.05) relative to the Bussento and the Calore Salernitano rivers were also superimposed on the RDA triplots to evaluate possible differentiations between the two rivers.

The analysis of the spatial outliers based on the concentrations in water of macronutrients, micronutrients, non-essential elements, anions, photosynthetic pigments, TOC, and TN was carried out according to Filzmoser (2005), as described for the computing of the outlier maps based on PTE concentrations in passive and active biomonitors. The functions `map.plot` and `uni.plot` of the "mvoutlier" package were employed.

Chapter 3

Results

3.1 Charophyte biodiversity

Overall, 4 Charophyceae taxa were observed within the "Cilento, Vallo di Diano e Alburni" National Park and in its neighbourhood, all belonging to the *Chara* genus: *Ch. globularis* Thuillier, *Ch. gymnophylla* A. Braun, *Ch. vulgaris* L., and *Ch. vulgaris* var *papillata* K. Wallroth. Pure populations were invariably observed in all the studied area.

According to the classification based on dichotomous keys, *Ch. vulgaris* was the most widely distributed taxon, constituting 7 out of 17 populations, followed by *Ch. gymnophylla*, with 6 populations, and *Ch. globularis*, with 3 populations, whereas only 1 population of *Ch. vulgaris* var *papillata* was observed (Figure 3.1). *Ch. gymnophylla* and *Ch. vulgaris* colonised a wider range of environments than *Ch. globularis*, being observed in spring ponds, small lakes, and riverbanks, whereas the latter was observed only in small lakes.

Unfortunately, population traits were investigated on 3 of the observed taxa, due to the disappearance of the *Ch. vulgaris* var *papillata* population (B.06, Figure 2.8) in 2018. In addition, due to insufficient amount of thalli, photosynthetic pigments were not analysed in population A.05 and carbonate encrustation was not analysed in populations A.05 and B.03.

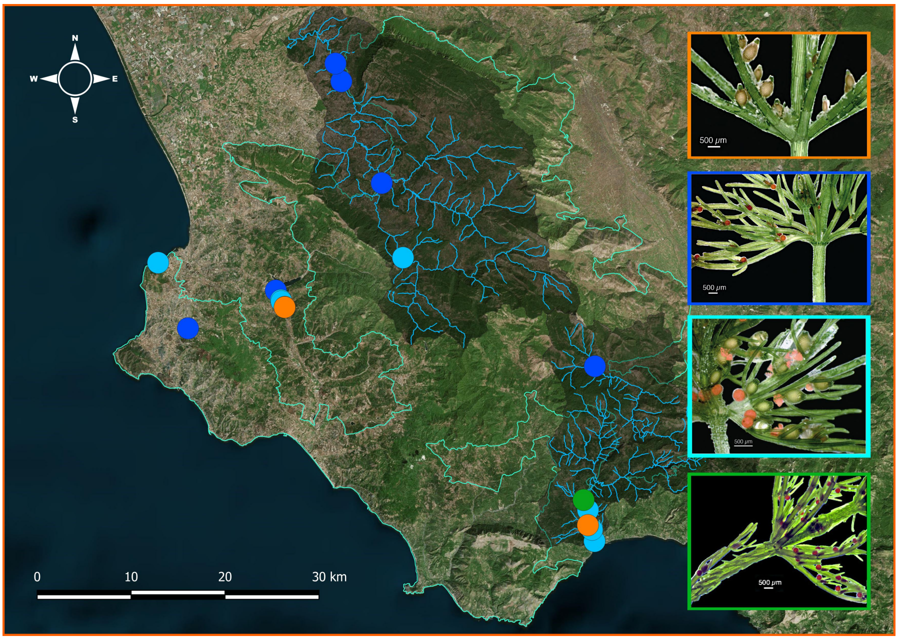

Figure 3.1: Charophyte populations observed during the project, with indication of the species they belong to: *Ch. globularis* Thuillier (🟠), *Ch. gymnophylla* A. Braun (🔵), *Ch. vulgaris* L. (🔵), and *Ch. vulgaris* var *papillata* K. Wallroth (🟢).

The main morphological traits (Table 3.1) of the 12 populations from the Alento, the Bussento, and the Calore Salernitano rivers, and from the spring ponds in the Perdifumo and Trentova districts are reported in Tables 3.2 and 3.3. SEM images of *Ch. globularis* oospores (B.04), showing extended wings, on average 25.04 μm wide, are reported in Figure 3.8.

Due to the presence of sterile thalli in populations A.04, B.03 and C.02, the traits related to the antheridia and archegonia (oos.v, oos.r, oog.v, oog.r, oc.v, oc.r) were not included in the fuzzy clustering and NMDS analysis on the morphometric traits, in order to preserve the largest number of observations. The attribution of each population to *Ch. globularis*, *Ch. gymnophylla*, or *Ch. vulgaris* based on fuzzy clustering (Figure 3.2) was similar to the one obtained using dichotomous keys. The analysis, moreover, highlighted the tendency of each

Table 3.1: Morphological traits analysed on the 12 Charophyte populations reported in Figure 2.8, with indication of the abbreviations used in the text.

	Number	Length	Diameter	Size	Ratio
Internodes	i.n.	i.l.	i.w.	i.v.	i.r.
Spines		s.l.	s.w.	s.v.	s.r.
Branchlets	b.n.				
Ecorticate cells	ec.n.	ec.l.	ec.w.	ec.v.	ec.r.
Corticate cells	cc.n.	cc.l.	cc.w.	cc.v.	cc.r.
Oospore		oos.l	oos.w	oos.v.	oos.r.
Oogonia		oog.l	oog.w	oog.v.	oog.r.
Coronula		oc.l	oc.w	oc.v.	oc.r.

thallus to exibit the traits typical of a single species or intermediate traits. With the exception of population A.01, close to the boundary between *Ch. gymnophylla* and *Ch. vulgaris*, all the populations were clearly classified in one group only.

The conditional recursive partitioning Figure 3.3 tree resolved the ambiguous positioning of A.01 in the fuzzy clustering, attributing the population to *Ch. gymnophylla* based on the presence of reproductive structures on ecorticate cells. In particular, the cortex type allows to differentiate *Ch. globularis* from the other species, whereas the type of cells bringing reproductive structures allows to differentiate *Ch. gymnophylla* and *Ch. vulgaris*. The size of internodes and of corticate cells provided also further differentiations among populations within single species.

NMDS analysis clearly differentiated the confidence ellipse relative to the 3 species, especially in relation to the proportion of ecorticate cells in radii and to the size of corticate and ecorticate cells. (Figure 3.4). The relative positioning of the confidence ellipses relative to the species was similar in the NMDS based on the concentrations of chlorophyll *a*, chlorophyll *b*, pheophytin *a*, pheophytin *b*, and total carotenoids, reported in Table 3.4, although the confidence ellipse for

Table 3.2: Morphological traits (mean: upper table; s.e.m.: lower table) of the thalli from the 12 Charophyte populations reported in Figure 2.8. Abbreviations are reported in Table 3.1. Units for the number of internodes, branchlets, corticate and ecorticate cells are in counts, units for lengths and widths are in μm, unless otherwise specified.

Population	Species	i.n.	i.l. (mm)	i.w.	s.l.	s.w.	b.n.	ec.n.	cc.n.	ec.l.	ec.w.	cc.l.	cc.w.
A.01	*Ch. gymnophylla*	8	25.73	502	54.9	23.12	5.1	1.33	2.512	982.1	148.49	1205.3	174.81
A.02	*Ch. vulgaris*	9	17.918	495.3	62.79	36.25	4.942	1.148	2.25	1139	153.84	1238.7	470
A.03	*Ch. vulgaris*	8	46.44	650.1	100.32	44.79	5.252	1.15	2.104	1028.8	157.32	1431.3	184.3
A.04	*Ch. globularis*	11	12.642	387.8	49.35	49.35	3.754	1	2.558	970	298	1152.5	157.76
A.05	*Ch. globularis*	7	23.83	388.66	73.18	66.8	5.246	1.1	3.128	1027	140.18	1058	144.52
B.03	*Ch. vulgaris*	6	23.77	432.4	87.8	33.46	3.956	1.018	1.95	1384	221.11	1168	234.6
B.04	*Ch. globularis*	7	11.75	296.46	63.3	53.4	5.13	1.046	1.898	1325	380	1427	189.59
B.21	*Ch. gymnophylla*	12	9.77	315.09	103	65.15	6.57	1.548	1.152	2098	306.9	2112	887
C.02	*Ch. gymnophylla*	8	13.73	373.23	79.5	65.3	5.754	1.382	1.122	2017	580	2234	236.3
C.12	*Ch. vulgaris*	7	48.09	749.8	104.77	88.4	5.676	1.118	2.006	1091	183.86	1307.5	210.73
P.01	*Ch. gymnophylla*	9	32.54	558.3	86.93	29.49	4.414	1.958	1.516	1162.3	162.58	1245.8	171.15
T.01	*Ch. vulgaris*	9	28.01	465.1	49.47	37.58	4.746	1.17	2.084	1060.3	157.4	1218.7	171.07

Population	Species	i.n.	i.l. (mm)	i.w.	s.l.	s.w.	b.n.	ec.n.	cc.n.	ec.l.	ec.w.	cc.l.	cc.w.
A.01	*Ch. gymnophylla*	1	1.27	7.12	3.42	2.04	0.259	0.078	0.117	25.7	2.76	31.0	4.78
A.02	*Ch. vulgaris*	1	0.568	29.6	5.58	4.38	0.339	0.090	0.108	108	6.53	83.1	301
A.03	*Ch. vulgaris*	1	4.97	43.5	5.25	1.98	0.209	0.070	0.052	42.6	3.55	47.3	9.40
A.04	*Ch. globularis*	1	0.690	11.2	3.77	3.77	0.752	0.000	0.342	124	157	19.2	2.27
A.05	*Ch. globularis*	1	2.00	9.61	4.58	20.3	0.145	0.045	0.156	131	8.63	34.0	3.33
B.03	*Ch. vulgaris*	1	3.73	14.4	12.9	1.24	0.732	0.018	0.136	136	5.15	107	12.1
B.04	*Ch. globularis*	1	3.34	5.61	11.0	10.4	0.175	0.030	0.240	165	205	129	7.25
B.21	*Ch. gymnophylla*	1	1.23	6.38	20.1	2.63	0.586	0.101	0.082	110	15.6	263	521
C.02	*Ch. gymnophylla*	1	2.36	6.09	16.1	11.2	0.580	0.080	0.061	128	385	179	11.3
C.12	*Ch. vulgaris*	1	4.55	39.0	6.57	12.4	0.212	0.044	0.052	66.3	4.81	52.7	9.20
P.01	*Ch. gymnophylla*	1	1.50	29.9	6.29	4.41	0.320	0.028	0.102	67.5	4.26	80.5	3.92
T.01	*Ch. vulgaris*	1	3.98	12.0	2.43	7.78	0.154	0.052	0.101	42.7	2.98	41.5	3.43

Table 3.3: Morphological traits (mean: upper table; s.e.m.: lower table) of the antheridia and archegonia from the 12 Charophyte populations reported in Figure 2.8. Abbreviations are reported in Table 3.1. A "-" means that only 1 observation was recorded, and there was not enough information to calculate s.e.m. Units are in μm.

Population	Species	oos.l.	oos.w.	oc.l.	oc.w.	oog.w.
A.01	*Ch. gymnophylla*	404.26	297.01	126.16	136.54	249.53
A.02	*Ch. vulgaris*	429.05	225.93	108.4	119.19	186.65
A.03	*Ch. vulgaris*	382.75	209.6	70.94	102.61	207.69
A.04	*Ch. globularis*	525.9	314	134.38	130.24	204.42
A.05	*Ch. globularis*	578.3	332.04	113.09	123.04	143.77
B.03	*Ch. vulgaris*	516.82	341.65	129.12	166.92	195.93
B.04	*Ch. globularis*	568.77	301.94	148.98	132.43	218.02
B.21	*Ch. gymnophylla*	277.98	242.88	91.47	97.64	233.74
C.02	*Ch. gymnophylla*	165.31	110.31	56.06	66.89	186.93
C.12	*Ch. vulgaris*	462.19	356.16	98.84	132.39	306.66
P.01	*Ch. gymnophylla*	427.98	227.42	115.88	117.87	195.69
T.01	*Ch. vulgaris*	416.9	248.41	112.63	125.52	230.53

Population	Species	oos.l.	oos.w.	oc.l.	oc.w.	oog.w.
A.01	*Ch. gymnophylla*	4.85	11.35	6.67	6.46	28.99
A.02	*Ch. vulgaris*	48.2	34.14	8.13	7.63	13.22
A.03	*Ch. vulgaris*	19.87	7.55	8.77	4.49	12.66
A.04	*Ch. globularis*	-	-	-	-	-
A.05	*Ch. globularis*	15.14	16.04	1.56	9.07	36.14
B.03	*Ch. vulgaris*	-	-	-	-	4.41
B.04	*Ch. globularis*	26.92	17.94	17.08	8.09	14.43
B.21	*Ch. gymnophylla*	41.92	50.22	15.57	14.91	29.4
C.02	*Ch. gymnophylla*	15.99	16.01	0.71	5.68	7.48
C.12	*Ch. vulgaris*	13.2	11.43	2.89	10.07	11.09
P.01	*Ch. gymnophylla*	11.19	19.39	7.37	4.48	1.58
T.01	*Ch. vulgaris*	21.21	27.03	7.8	3.87	4.07

Ch. vulgaris overlapped the confidence ellipses of *Ch. globularis* and *Ch. gymnophylla*, which were clearly separated (Figure 3.4). The coefficient of determination for the linear models relating the distances in the NMDS spaces with the original distances were equal to r^2 = 0.901 and r^2 = 0.988 for the morphometric trait and photosynthetic pigment datasets, respectively (Figure 3.5).

Carbonate encrustation (Figure 3.6) ranged from ~50% d.w. to more than 80% d.w. and showed significant differences among among sampling sites (P < 0.001) and among the species (P < 0.001), with

Table 3.4: Concentration (mean: upper table; s.e.m.: lower table) of chlorophyll *a* (Chl a), chlorophyll *b* (Chl b), pheophytin *a* (Pheo a), pheophytin *b* (Pheo b), and total carotenoids (Car). Units are in μg g^{-1} f.w.

Population	Species	Chl a	Chl b	Pheo a	Pheo b	Car
A.01	*Ch. gymnophylla*	150.27	93.75	69.86	< LOD	121.73
A.02	*Ch. vulgaris*	293.2	121.69	27.08	0.766	194.22
A.03	*Ch. vulgaris*	181.62	76.28	27.03	2.227	102.9
A.04	*Ch. globularis*	597.9	261.9	52.89	2.45	243.41
B.03	*Ch. vulgaris*	151.8	52.68	19.88	24.12	65.64
B.04	*Ch. globularis*	196.5	81.56	8.64	< LOD	96.81
B.21	*Ch. gymnophylla*	97.64	39.66	7.43	5.147	33.278
C.02	*Ch. gymnophylla*	167.5	99.1	76.2	83.8	162.4
C.12	*Ch. vulgaris*	217.13	86.39	13.9	0.2	127.8
P.01	*Ch. gymnophylla*	191.56	93.67	46.53	0.162	113.44
T.01	*Ch. vulgaris*	254.25	103.35	16.71	0.493	123.93

Population	Species	Chl a	Chl b	Pheo a	Pheo b	Car
A.01	*Ch. gymnophylla*	6.94	3.55	3.22	< LOD	2.29
A.02	*Ch. vulgaris*	17.0	7.35	1.54	0.498	7.04
A.03	*Ch. vulgaris*	7.43	2.86	1.58	0.602	5.57
A.04	*Ch. globularis*	36.0	18.9	5.95	1.16	8.01
B.03	*Ch. vulgaris*	11.1	4.45	2.13	2.11	4.65
B.04	*Ch. globularis*	16.4	7.07	0.870	< LOD	5.60
B.21	*Ch. gymnophylla*	4.00	1.43	1.11	0.773	0.286
C.02	*Ch. gymnophylla*	19.8	15.1	15.9	19.8	30.1
C.12	*Ch. vulgaris*	7.62	2.73	3.20	0.200	11.1
P.01	*Ch. gymnophylla*	5.43	5.00	3.48	0.162	4.09
T.01	*Ch. vulgaris*	8.42	3.11	1.57	0.493	3.79

Ch. gymnophylla and *Ch. vulgaris* exhibiting higher values than *Ch. globularis*. Conversely, epiphyte diatom biomass (Figure 3.7) did not differed among species (for $\alpha = 0.05$), but only among sampling sites ($P < 0.001$).

The binary HPLC method developed allowed the separation and the identification of 17 pigments (Table 3.5 and Figure 3.9). Main charophyte pigments were detected in all the samples, with variations in the abundance of chlorophyllides *a* and *b* and γ-carotene and α-carotene between *Ch. globularis* and the other two species (Figure 3.9).

Table 3.5: HPLC pigment profile of *Chara* spp., with indication of peak retention times and resolution.

Peak	Compound	Retention time (min)	Resolution
1	Chlorophyllide a	3.259	3.700
2	Chlorophyllide b	4.063	9.578
3	Neoxanthin	6.294	6.932
4	Violaxanthin	7.840	2.511
5	Antheraxanthin	8.480	9.008
6	Lutein	10.444	6.588
7	*cis*-Zeaxanthin	11.461	1.397
8	*trans*-Zeaxanthin	11.688	15.718
9	Chlorophyll *b*	14.247	2.392
10	Vinyl-chlorophyll *b*	14.617	2.59
11	Pheophitin *b*	15.070	4.880
12	Chlorophyll *a*	15.947	1.306
13	Vinyl-chlorophyll *a*	16.209	1.409
14	Pheophitin *a*	16.508	13.452
15	γ-Carotene	19.470	2.351
16	α-Carotene	20.024	2.659
17	β-Carotene	20.649	

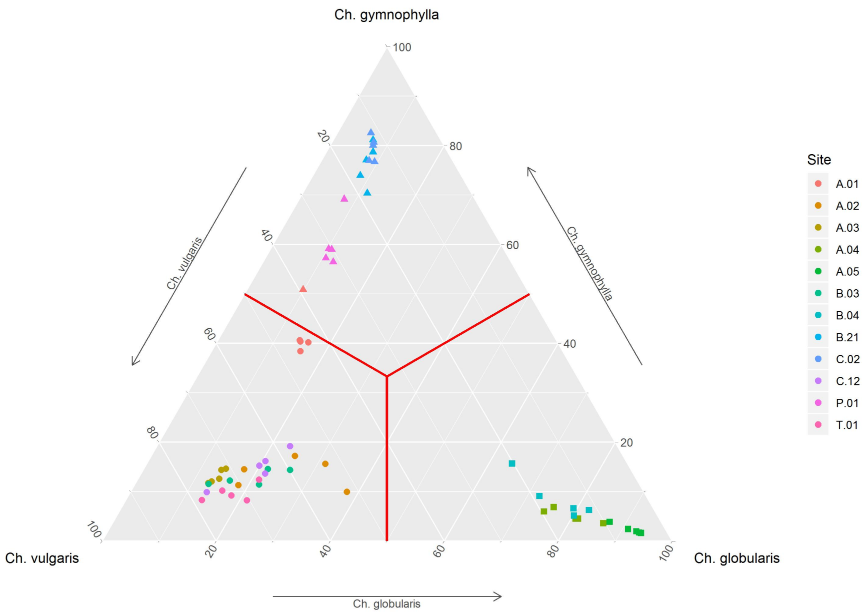

Figure 3.2: Ternary diagram of the probability memberships of each thallus to *Ch. globularis* (■), *Ch. gymnophylla* (●), and *Ch. vulgaris* (▲) according to the fuzzy clustering. Populations are coded in different colors according to the legend.

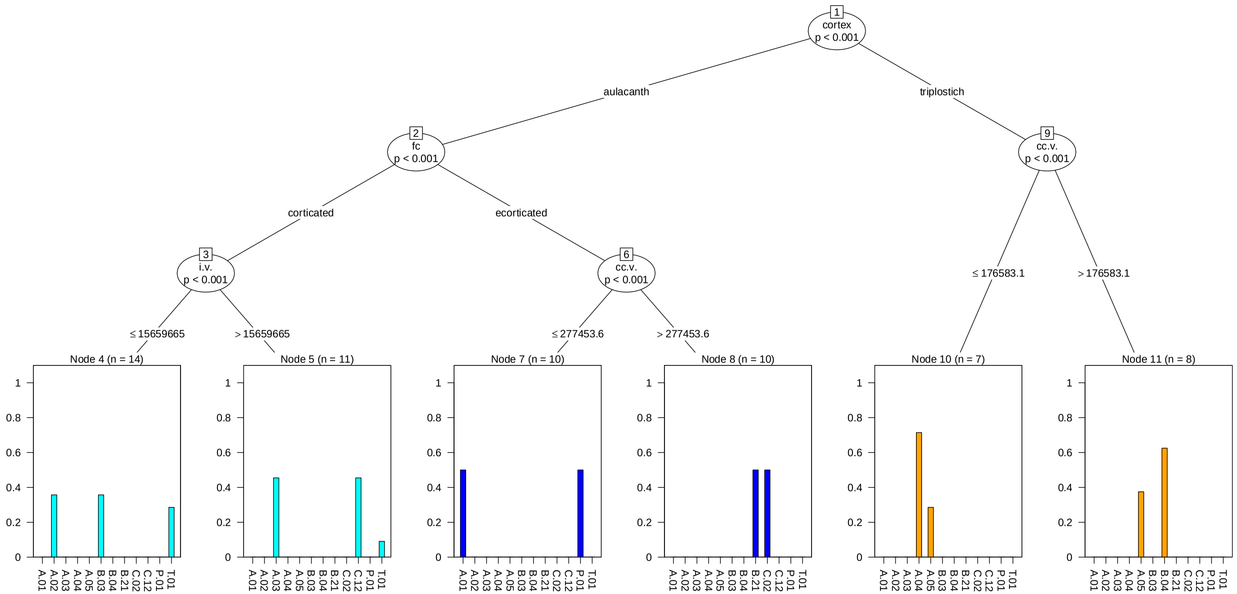

Figure 3.3: Conditional recursive partitioning tree based on charophyte morphometric traits. Colors indicate to which species populations belong to: *Ch. globularis* (—), *Ch. gymnophylla* (—), and *Ch. vulgaris* (—). Node probabilities and splitting rules are also reported.

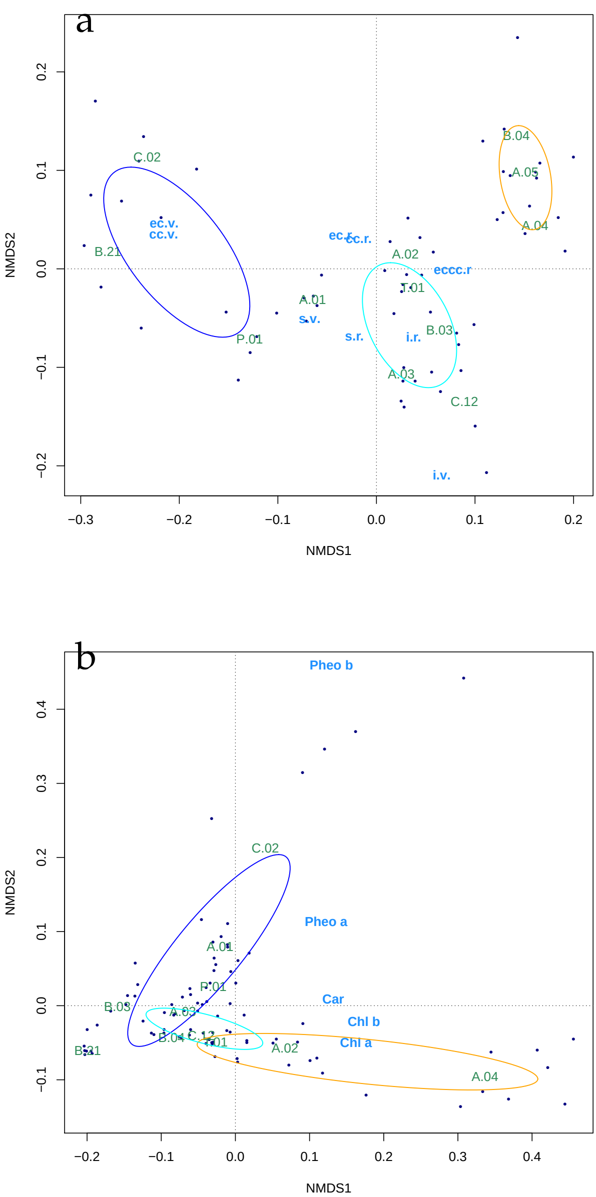

Figure 3.4: NMDS biplots based on the Charophyte morphometric traits (a) and photosynthetic pigment concentrations (b), with the superimposition of confidence ellipses (for $\alpha = 0.05$) relative to *Ch. globularis* (—), *Ch. gymnophylla* (—), and *Ch. vulgaris* (—). The centroid for each population are also shown. `eccc.r`: proportion of ecorticate cells on the total cell number in radii.

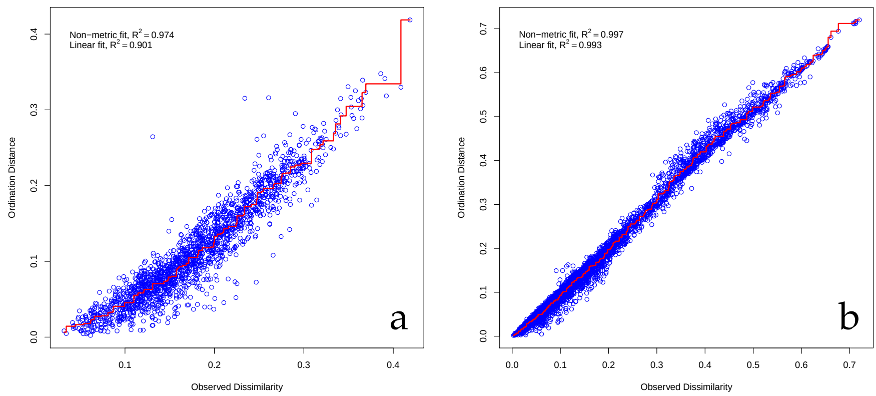

Figure 3.5: Stressplots relative to the NMDS on the Charophyte morphometric traits (a) and photosynthetic pigment concentrations (b). The coefficient of determination relative to the linear and non-linear regressions between the distances in the NMDS spaces and the original distances are also reported.

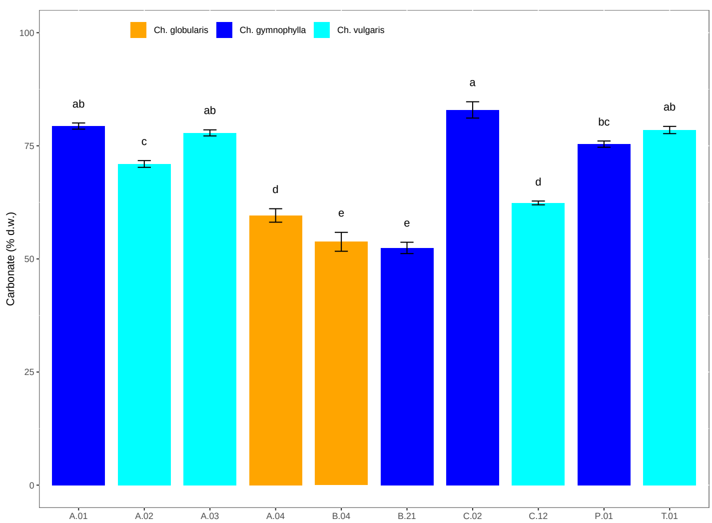

Figure 3.6: Average mass, in percent to thallus dry weight, of deposited carbonates on Charophyte thalli. Different letters indicate significant differences among sites according to the estimated marginal means test (for $\alpha = 0.05$). Colors indicate species according to the legend.

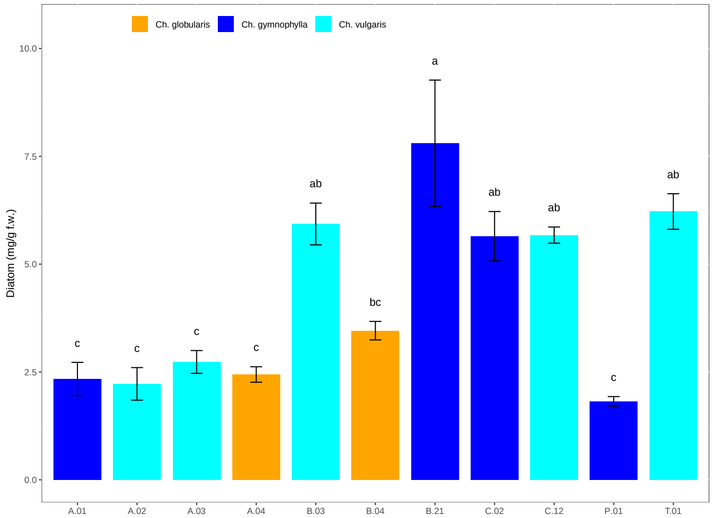

Figure 3.7: Average mass, in percent to thallus fresh weight, of epiphyte diatoms on Charophyte thalli. Different letters indicate significant differences among sites according to the estimated marginal means test (for $\alpha = 0.05$). Colors indicate species according to the legend.

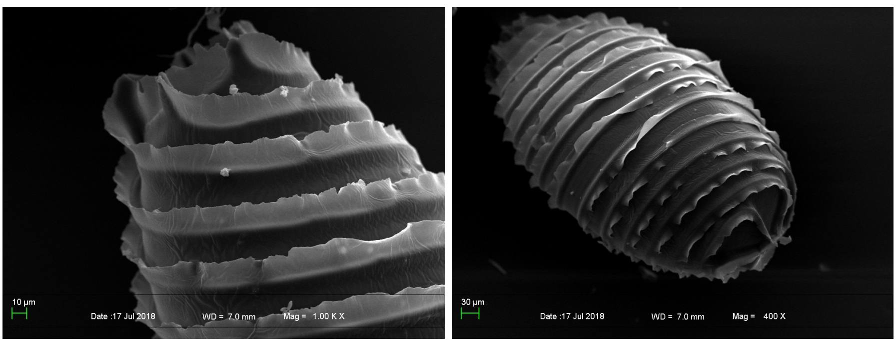

Figure 3.8: SEM images of *Ch. globularis* oospores showing extended wings.

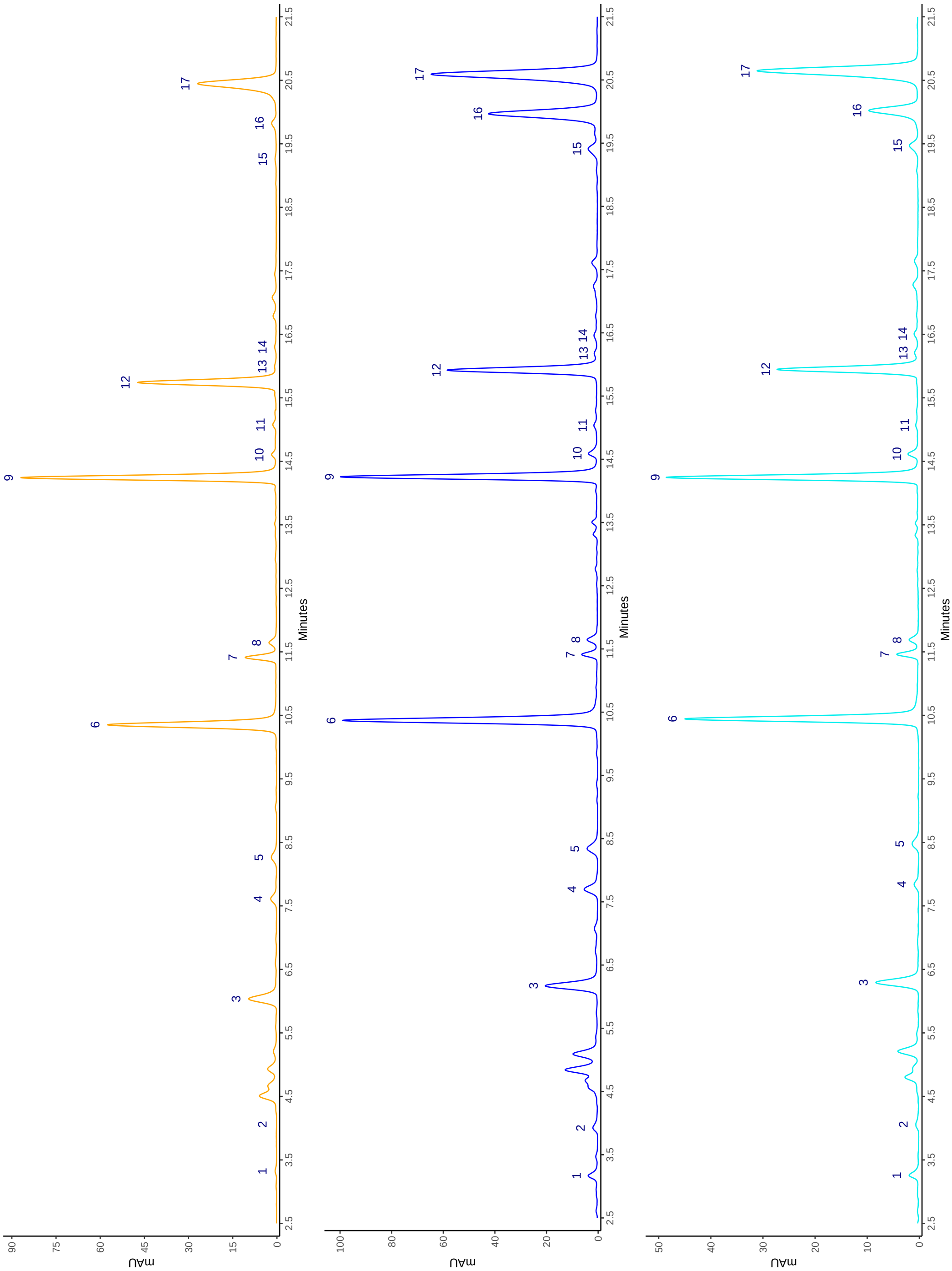

Figure 3.9: Chromatograms of the pigment extracts of *Ch. globularis* (—), *Ch. gymnophylla* (—), and *Ch. vulgaris* (—). Peak identification is reported in Table 3.5.

3.2 Biomonitor validation

The Mantel tests and the NMDS analyses were based on the Manhattan distance metric, which provided the best NMDS stress figures for all the datasets. Significant correlations between the distance matrices for *M. aquatica* and *H. nodiflorum* and for *Ch. gymnophylla* and *F. antipyretica* were highlighted by the Mantel correlation tests (Table 3.6). Dataset scaling in the [0, 1] interval increased the Mantel correlation coefficients in respect to the row dataset in the case of *M. aquatica* vs. *H. nodiflorum*, but not in the case of *Ch. gymnophylla* vs. *F. antipyretica* (Table 3.6).

Table 3.6: Results of the Mantel correlation tests based on the Manhattan distance metric.

	M. aquatica vs. *H. nodiflorum*	
	r	P-value
Raw data	0.1753	< 0.05
Scaled data	0.4873	< 0.001
	Ch. gymnophylla vs. *F. antipyretica*	
	r	P-value
Raw data	0.5155	< 0.01
Scaled data	0.4960	< 0.01

The linear regressions between the original distances and those from the NMDS spaces had determination coefficients $0.921 < r^2 < 0.989$ (Figure 3.10).

The NMDS for passive biomonitors based on the raw data highlighted a large overlap of the confidence ellipses for *H. nodiflorum* in 2016 and *M. aquatica* in 2016 and 2017, with a clear separation of the *H. nodiflorum* 2017 ellipse from the others (Figure 3.11). The differentiation was related to the higher concentrations, on average, of Cu and Mg, and the the lower concentrations of Pb and As in *H. nodiflorum* roots collected in 2017 (Figure 3.11). Confidence ellipses for *M. aquatica*

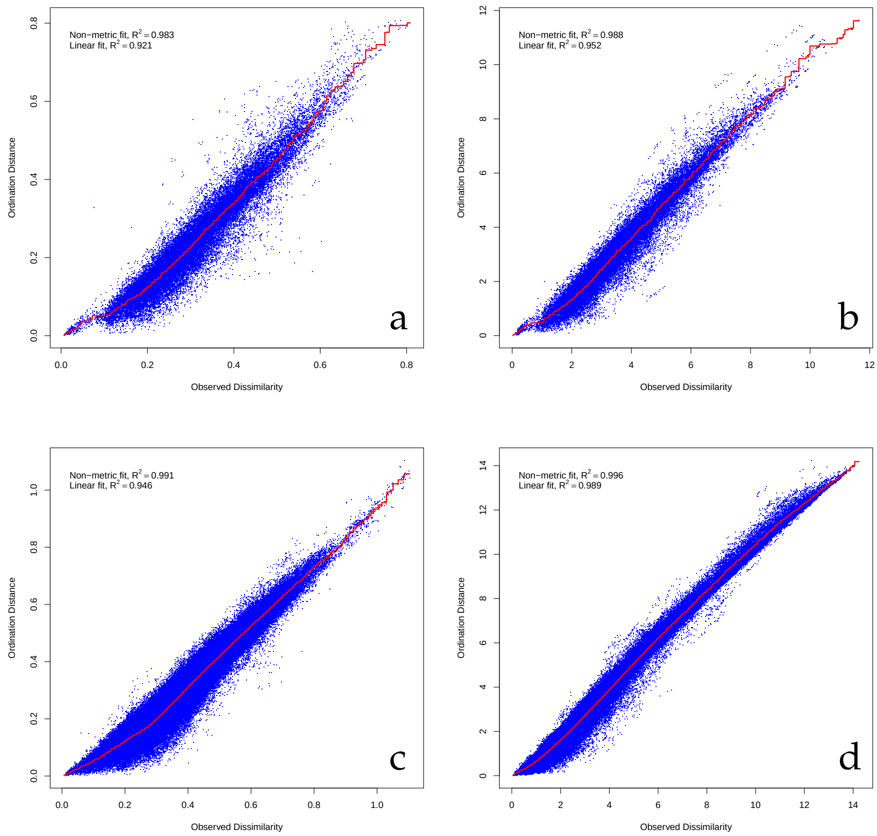

Figure 3.10: Stressplots relative to the NMDS on the *M. aquatica*/*H. nodiflorum* raw (a) and scaled (b) data, and to the NMDS on the *Ch. gymnophylla*/*F. antipyretica* raw (c) and scaled (d) data. The coefficient of determination relative to the linear and non-linear regressions between the distances in the NMDS spaces and the original distances are also reported.

and *H. nodiflorum* largely overlapped, instead, in the NMDS based on scaled data (Figure 3.11).

A clear-cut separation between the confidence ellipses for *Ch. gymnophylla* and *F. antiyretica* was highlighted by the NMDS based on the raw data, with the former exhibiting on average higher concentrations of As, Ca, K, Mg, Na, Pb, S, and Zn, and the latter higher concentrations of Cd, Co, Cr, Cu, Fe, Mn, Ni, and V (Figure 3.12). The differentiation

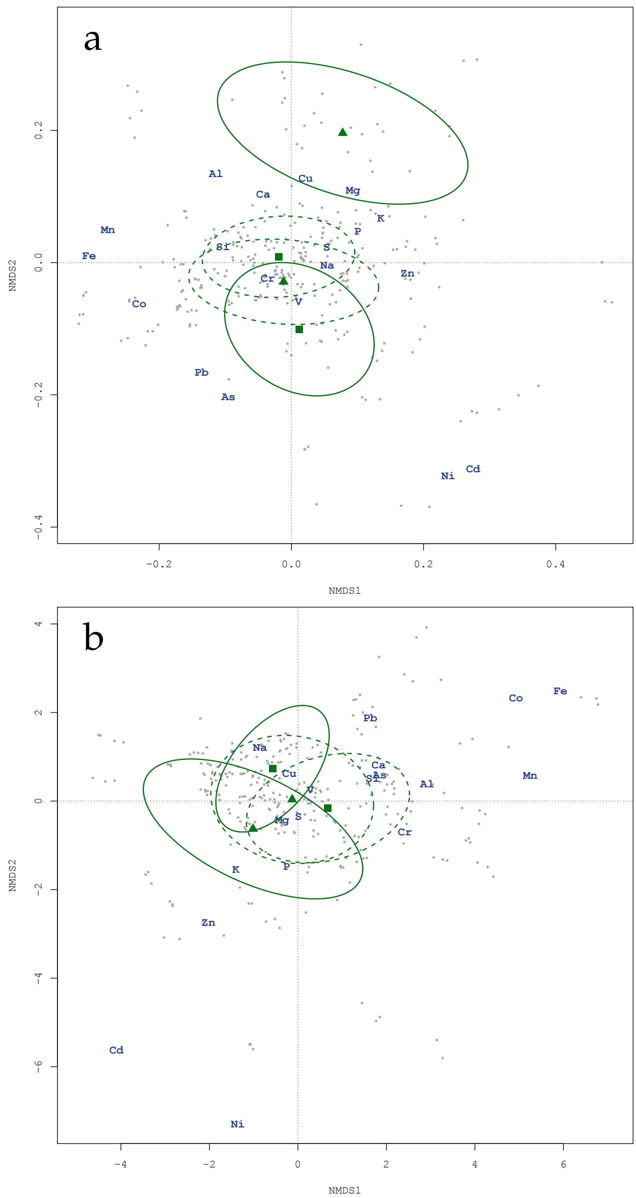

Figure 3.11: NMDS biplots based on raw (a) and scaled (b) PTE concentration data, with the superimposition of confidence ellipses (for $\alpha = 0.05$) relative to *M. aquatica* (- - -) and *H. nodiflorum* (—) in 2016 (■) and 2017 (▲).

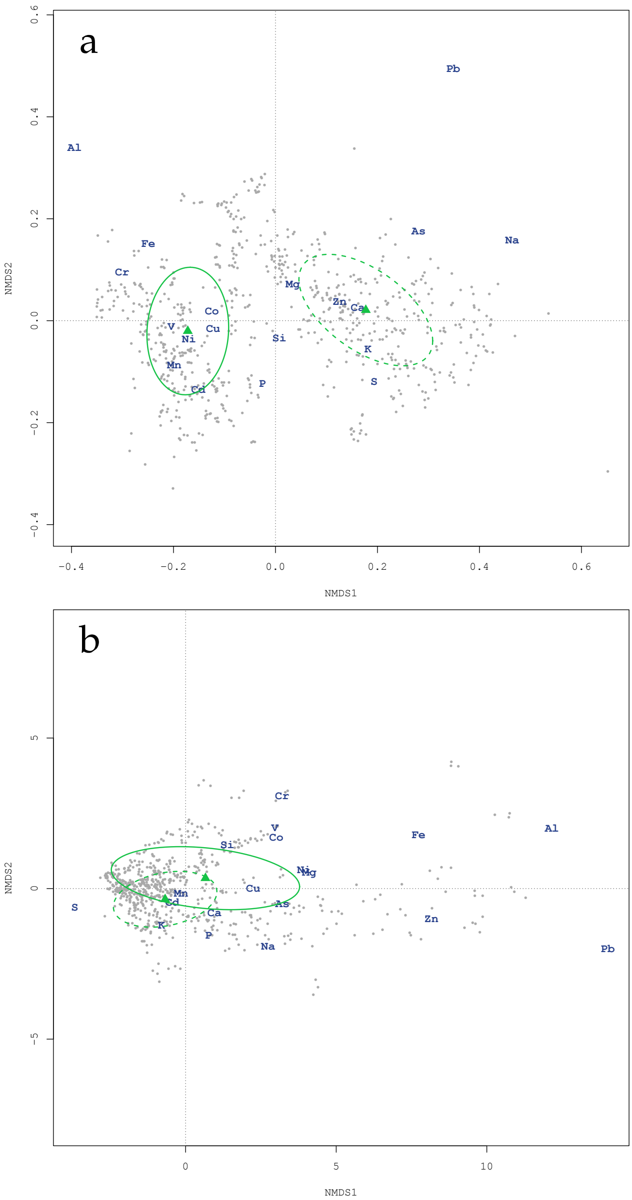

Figure 3.12: NMDS biplots based on raw (a) and scaled (b) PTE concentration data, with the superimposition of confidence ellipses (for $\alpha = 0.05$) relative to *Ch. gymnophylla* (- - -) and *F. antipyretica* (—) in 2017 (▲).

disappeared in the NMDS based on the scaled data, with the ellipses relative to *Ch. gymnophylla* and *F. antipyretica* encircling each other's centroids (Figure 3.12).

3.3 River quality

The connectivity diagrams developed for the Bussento, the Calore Salernitano and the joint river systems, relative to the sampling sites in which passive biomonitoring, active biomonitoring, water monitoring, and sediment analysis were performed, are reported in Figures 3.13 and 3.14.

Among the spatial weighting matrices developed for the Bussento river, the global tests using the passive biomonitoring data selected a binary weighted (*i.e.* with no weighting) Gabriel's graph, producing an adjusted-r^2 = 0.2813 and P < 0.01. The same connectivity topology was selected also for the spatial weighted matrices relative to the Calore Salernitano (adjusted-r^2 = 0.3531, P < 0.01) and the joint river systems (adjusted-r^2 = 0.3685; P < 0.01), although in either cases, a concave-up weighting scheme was choosen, with coefficients equal to 0.2 and 0.8, respectively. For the best spatial models, the forward selection algorithm selected 9 MEMs explaining the PTE variations in *M. aquatica* and *H. nodiflorum* in the Bussento river, 2 MEMs for the Calore Salernitano, and 11 MEMs for the joint river systems.

The connectivity topologies selected based on the active biomonitoring data varied among the Bussento, the Calore Salernitano, and the joint river systems. The global tests selected a relative neighbourhood graph either in the case of the Bussento (adjusted-r^2 = 0.5257, P < 0.01) or the joint river systems (adjusted-r^2 = 0.4324, P < 0.01), with the former unweighted and the latter linearly weighted. In the case of the Calore Salernitano, a Delaunay triangulation with concave-up (coefficient equal to 0.8) weighting was selected, producing an adjusted-r^2 = 0.6536 and P < 0.01. The MEMs explaining the PTE variations in *Ch. gymnophylla* and *F. antipyretica* were 8 in the case of the Bussento, 10 in the case of the Calore Salernitano, and 12 in the case of the joint river systems.

The covariance-based RDAs using the selected MEMs as predictors and PTE concentrations in passive and active biomonitors in the Bussento, the Calore Salernitano, and the joint river systems as re-

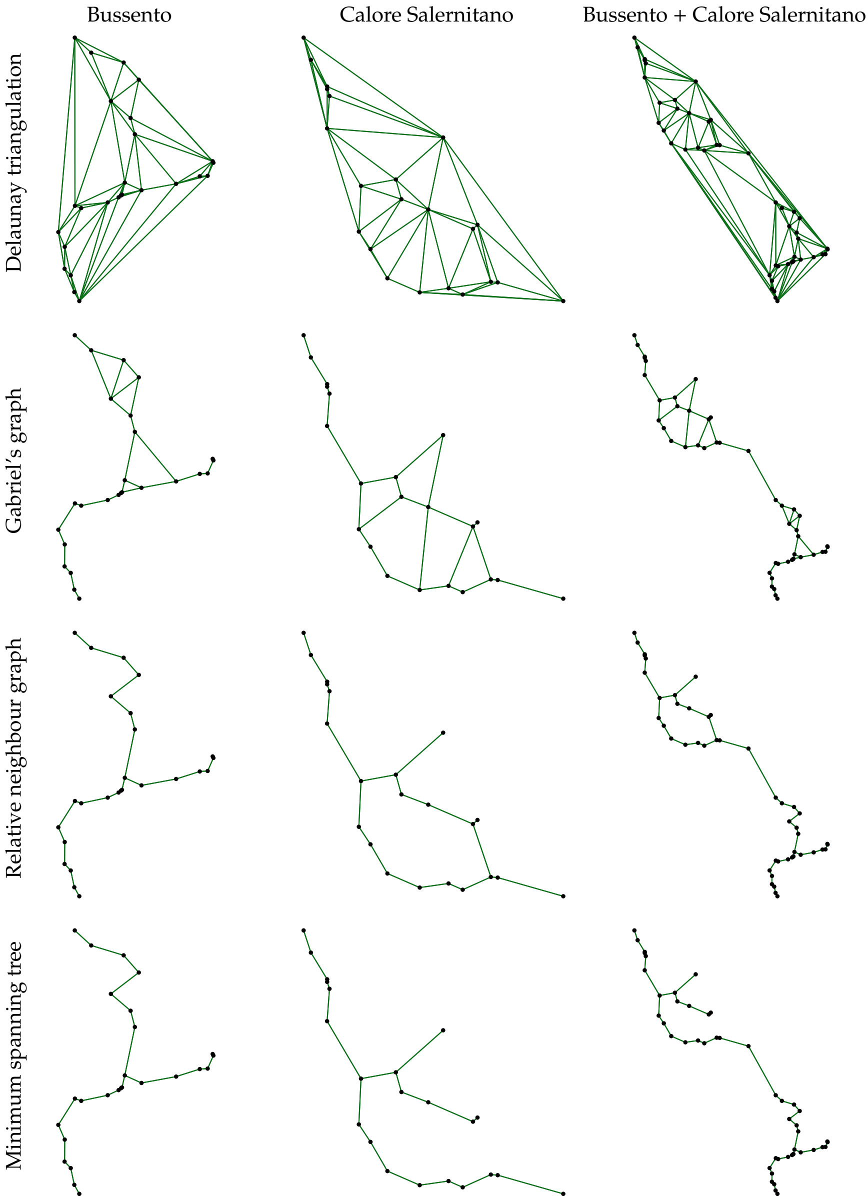

Figure 3.13: Connectivity diagrams developed for the Bussento, the Calore Salernitano and the joint river systems based on passive biomonitoring sites in 2016 or 2017. Spatial weighting matrices were computed through weighting of the diagrams.

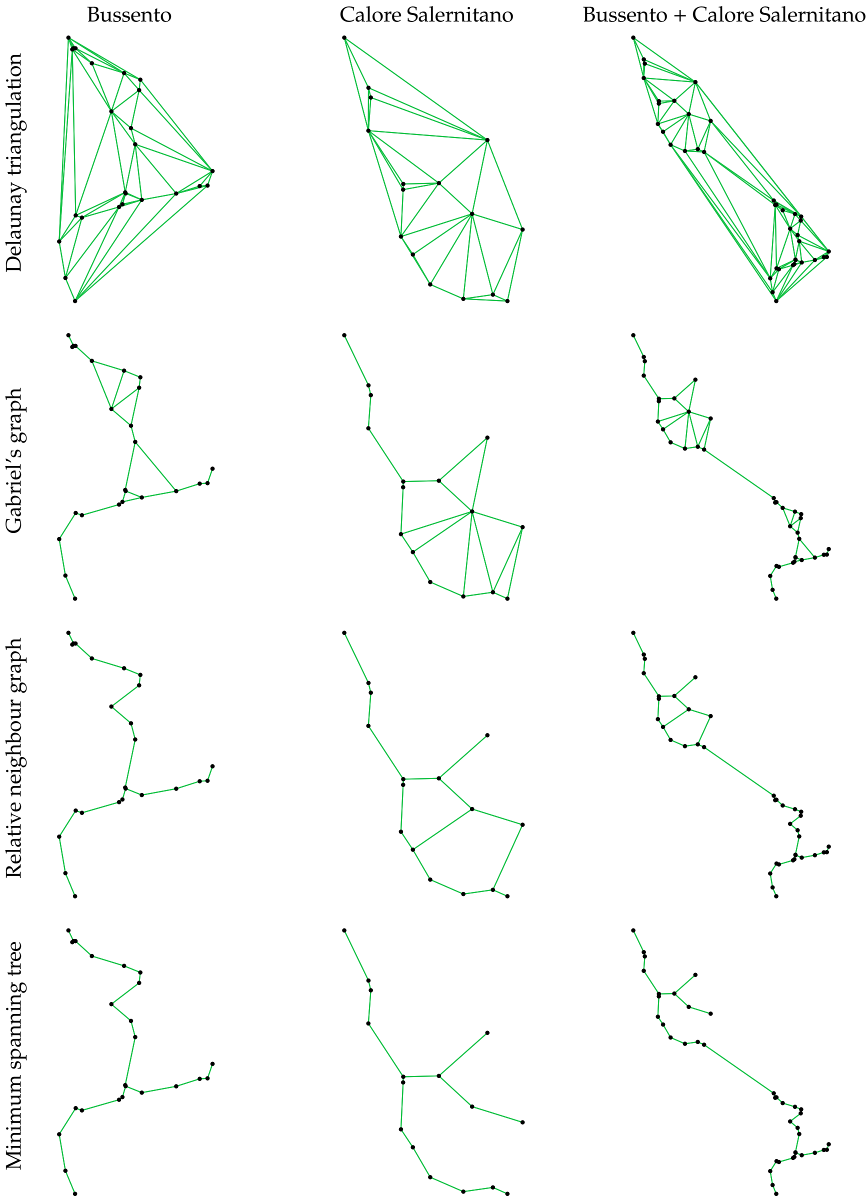

Figure 3.14: Connectivity diagrams developed for the Bussento, the Calore Salernitano and the joint river systems based on active biomonitoring sites. Spatial weighting matrices were computed through weighting of the diagrams.

sponse variables are reported in Figure 3.15. The distribution of the PTEs in *H. nodiflorum* and *M. aquatica* in the RDA space relative to the Bussento river, were primarily related to the directions described by MEMs 14, 13 and 15, and by MEMs 1, 2, and 6 ($P < 0.05$ for all MEMs). MEMs 1, 2, and 11 ($P < 0.001$ for all MEMs), instead, primarily determined the distribution of PTEs in *F. antipyretica* and *Ch. gymnophylla*. In the case of the RDAs relative to the Calore Salernitano river, MEM 1 ($P < 0.01$) appears to dominate the distribution of the PTEs from passive biomonitors, whereas 2 main groups of MEMs determined the distribution of PTEs from active biomonitors: Cd, K, P, and S were primarily related to MEMs 15, 11, and 3 ($P < 0.01$, $P < 0.05$, and $P < 0.05$), and the other PTEs to MEMs 10, 14, 2, and 9 ($P < 0.01$ for all MEMs). MEM 3 ($P < 0.01$) explained most of the variance in PTE distribution in the RDA triplot based on passive biomonitoring data relative to the joint river sistems, followed by MEMs 19 and 14, and by MEM 4 ($P < 0.05$ for all MEMs). Numerous MEMs, instead, contributed to explain the variance in the PTE concentrations in active biomonitors in the case of the joint river system: 2 ($P < 0.001$), 1, 26, 33, 7, 38, 3, and 21 ($P < 0.05$ for all MEMs).

Mantel correlograms (Figure 3.16), idicate significant spatial correlations, albeight with low values, in the case of the joint *Ch. gymnophylla*/*F. antipyretica* dataset, but not in the case of the joint *H. nodiflorum*/*M. aquatica* dataset. Specifically, positive correlations ($r = 0.050$ and $r = 0.071$; $P < 0.05$ in both cases) were observed in the 1.8 Km and 5.4 Km lag classes, and a negative correlation ($r = -0.124$; $P < 0.01$) was observed for the 12.6 Km lag class.

The PTE concentrations measured in the Bussento and Calore Salernitano in *H. nodiflorum* and *M. aquatica* in 2016 and 2017 are reported in Tables A.1, A.3, A.5, A.7, A.9 and A.11, and those in *F. antipyretica* and *Ch. gymnophylla* in 2017 are reported in Tables B.1, B.3, B.5 and B.7.

The multivariate spatial outlier maps, according to Filzmoser (2005), in relation to the macronutrient, micronutrient, and non-essential element concentrations in *H. nodiflorum* and *M. aquatica*, and in *Ch. gymnophylla* and *F. antipyretica* are shown in Figures 3.17 and 3.18,

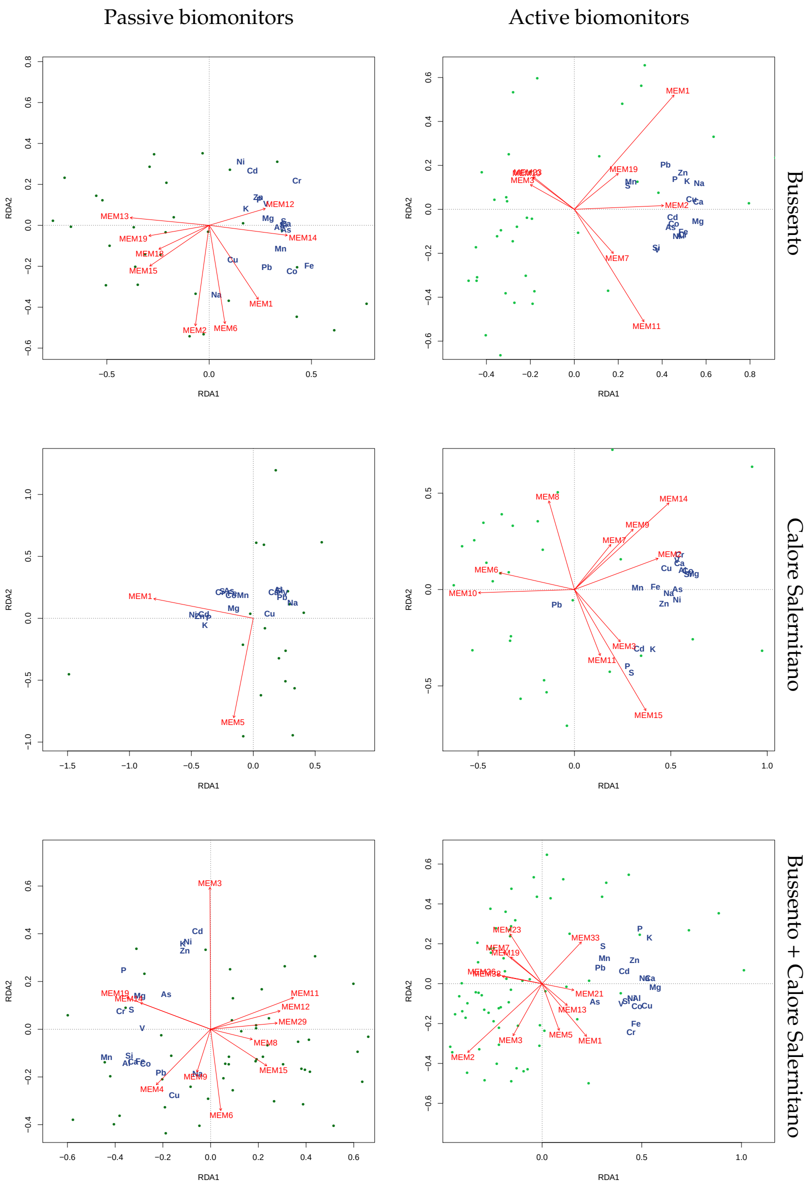

Figure 3.15: RDA triplots computed using the selected MEMs as predictors and the PTE concentrations in passive and active biomonitors in the Bussento, the Calore Salernitano, and the joint river systems as dependent variables. For the interpretation of MEMs, refer to Figures E.1 to E.6.

respectively. The analysis produced similar maps for micronutrients and non-essential elements, both in the case of passive biomonitoring data and in the case of active biomonitoring data, with the identification of common spatial outliers. In particular, 6 (B.11, B.21, B.23, B.24, C.03, C.09) common spatial outliers among micronutrients and non-essential elements were identified based on passive biomonitoring data and 12 (B.18, B.20, B.21, B.25, B.26, B.27, B.29, C.03, C.07, C.15, C.19, C.20) using active biomonitoring data. PTE concentrations in *H. nodiflorum* and *M. aquatica* identified 9 additional sites as spatial outliers for micronutrients: B.01, B.02, B.09, B.10, B.14, B.17, B.18, C.05, and C.12, and 2 additional sites for non-essential elements: C.06 and C.15. Based on PTE concentrations in *Ch. gymnophylla* and *F. antipyretica*, 3 (B.11, B.12, B.17), and 4 (B.14, B.19, C.06, C.13) outliers were unique to micronutrients and non-essential elements, respectively. Macronutrients in passive biomonitors identified sites B.05, B.06, B.09, B.14, B.16, B.17, B.24, B.25, C.03, and C.09, as spatial outliers, some of them identified also by the macronutrient concentrations in active biomonitors (B.11, B.14, B.17, B.18, B.19, B.20, B.21, B.25, B.26, B.27, B.28, B.29, C.03, C.07, and C.19). Overall, sites B.21, C.09 and, to a lesser extent, C.03, were the ones showing the largest deviations from the others in relation to micronutrients and non-essential elements, and also in relation to macronutrients in the case of active biomonitors. Ni, Cd, Fe, Co, As, P, S, and Ca were the elements with the largest contribution to the outlyingness definition based on PTE concentrations in *H. nodiflorum* and *M. aquatica*, whereas also Al, V, Pb, Zn, Si, Mg, and K contributed to identify outliers in the case of *Ch. gymnophylla* and *F. antipyretica*.

The total PTE concentrations in sediments and their concentrations in the exchangeable, bound to Fe-Mn oxides, bound to organic matter, and residual fractions are reported in Tables C.1, C.3, C.5, C.7 and C.9.

The singular value decomposition of the 3-mode compositional tensor, describing the pattern of PTE distribution within the exchangeable, bound to Fe-Mn oxides, bound to organic matter, and residual fractions, extracted 9 tensors individually explaining a percentage of the total variance > 1% and cumulatively the 88.07% of the total vari-

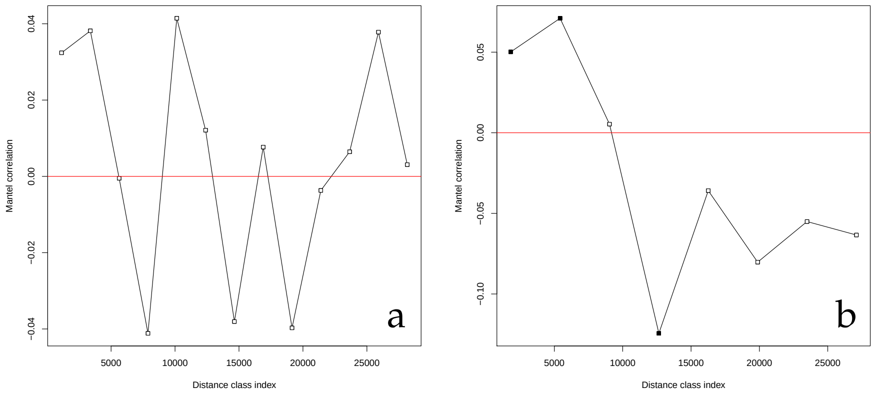

Figure 3.16: Mantel correlograms based on data from *H. nodiflorum* and *M. aquatica* (a), and from *F. antipyretica* and *Ch. gymnophylla*. Black squares indicate significant (for $\alpha = 0.05$) spatial correlations.

ance. The 1st tensor alone justified the 69.82% of the total variance, and the 2nd the 5.00%. The biplot obtained projecting the modes n. 2 (ilr-transformed relative abundances within the BCR fractions) and n. 3 (PTE abundances) onto the 1st and 2nd tensors produced the outline of Figure 3.19. The 1st axis points toward an increase in the residual fraction, whereas the 2nd toward an increase in the fraction bound to Fe-Mn oxides. Element distributions highlight 2 main gradients in relation to the tensors: the first beginning with Ca, showing the lowest abundance in the residual fraction together with Cd, and ending with Fe, showing the highest concentrations in the residual fraction, and the second beginning with K and S, with the lowest abundance in the fraction bound to Fe-Mn oxides, and ending with Mn, for which the fraction bound to Fe-Mn oxides dominated upon the others. The distribution of each element within the 4 BCR fractions in each site is reported as stacked bar plots in Figure 3.22.

The dendrogram computed from the loadings of mode n. 1 onto the 9 tensors selected by the PTA-3 algorithm (Figure 3.23), associating the sites in relation to the similarities in PTE distribution among the BCR fractions, differentiated the sites C.15, C.16, and C.17, located

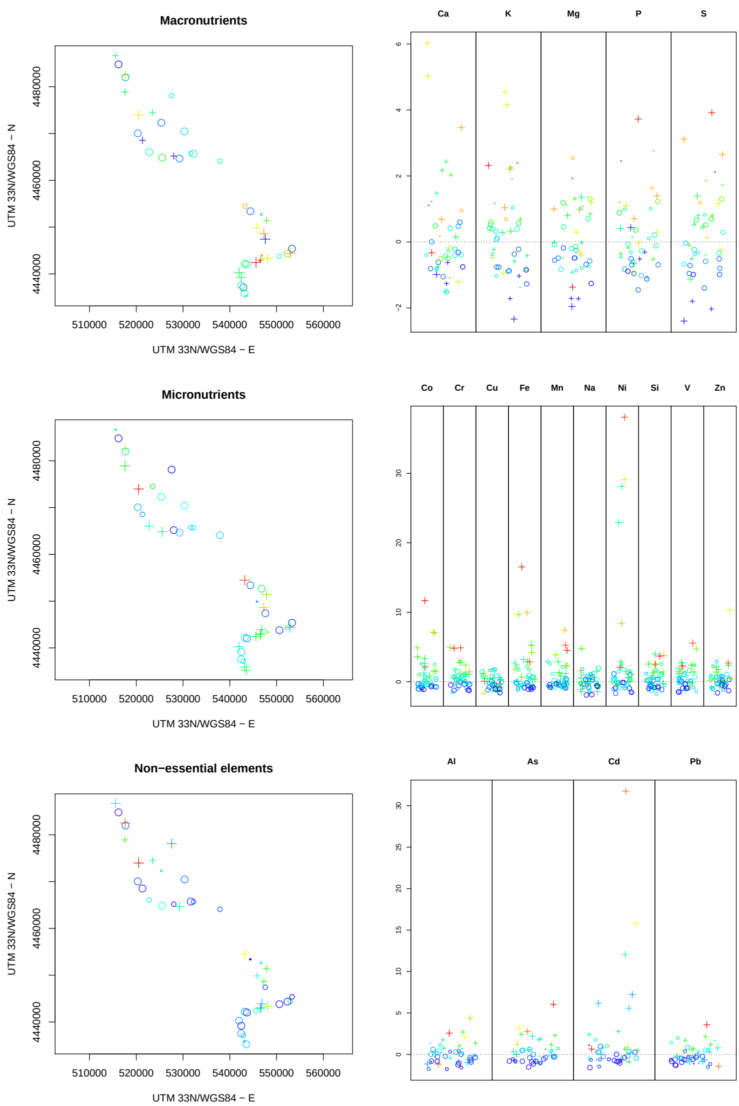

Figure 3.17: Multivariate spatial outlier plots (left) and break-down of each PTE contribution (right), based on PTE concentrations in roots of *H. nodiflorum* and *M. aquatica* in 2016 and 2017. PTE values on the right are centered and scaled according to the MCD estimates. Crosses represent spatial outliers, colored according to their position with respect to the multivariate data distribution (blue: low values, red: high values).

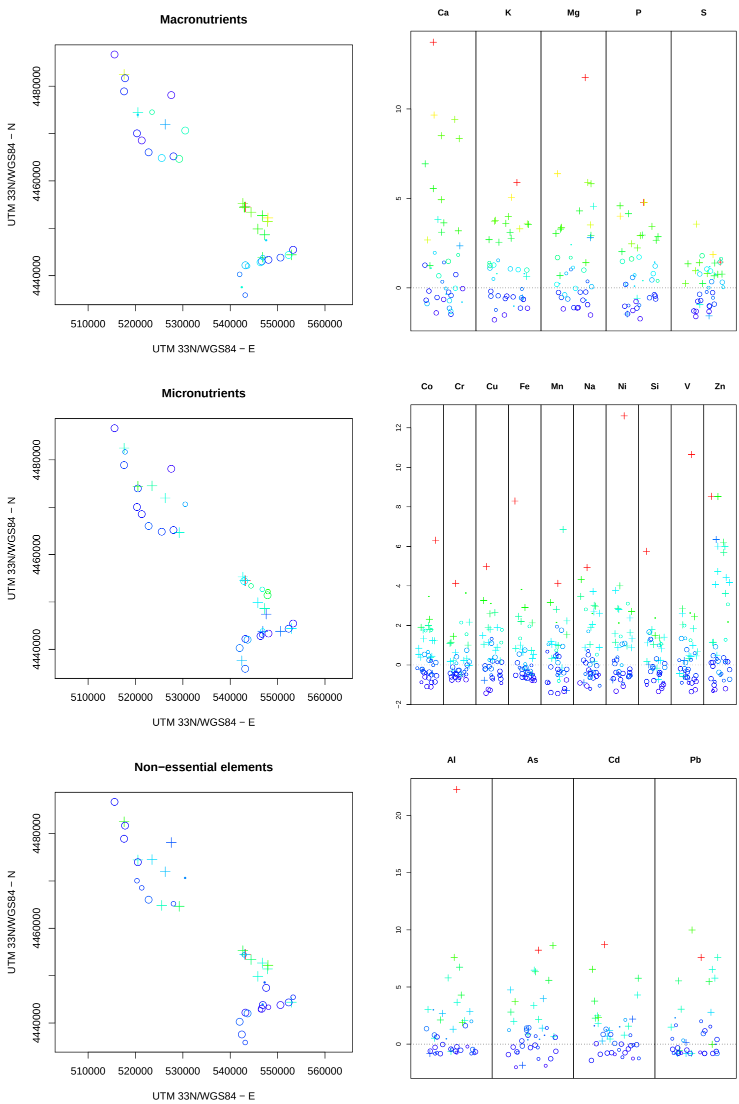

Figure 3.18: Multivariate spatial outlier plots (left) and break-down of each PTE contribution (right), based on PTE concentrations in roots of *F. antipyretica* and *Ch. gymnophylla* in 2016 and 2017. PTE values on the right are centered and scaled according to the MCD estimates. Crosses represent spatial outliers, colored according to their position with respect to the multivariate data distribution (blue: low values, red: high values).

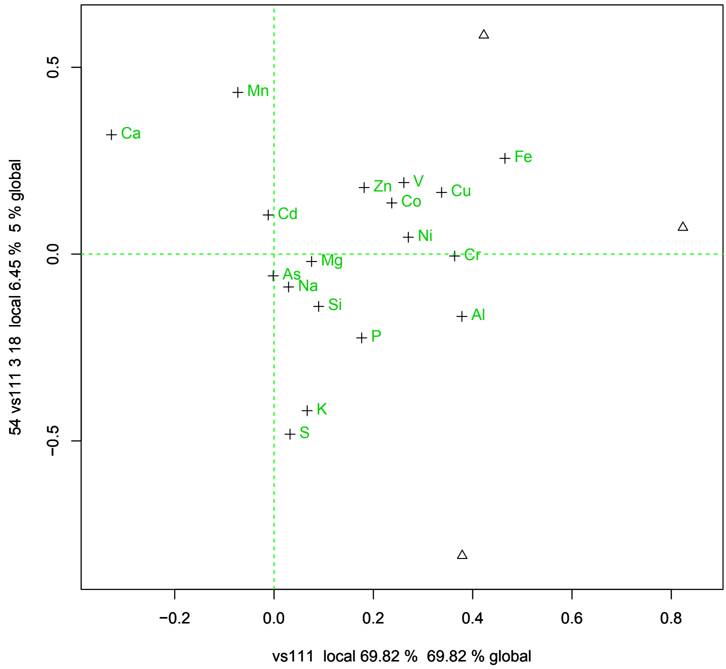

Figure 3.19: Biplot of the projections of modes n. 2 and n. 3 onto the 1st and 2nd tensors obtained through the PTA-3 algorithm on the 3-mode compositional tensor.

in the upper stretch of the Calore Salernitano, from the others. In addition, two other main clusters were highlighted, one comprising most of the sites on the Bussento-Bussentino river system, and another futher splitted into a cluster comprising sites B.02, B.16, and B.18, and a cluster comprising the rest of the sites on the Calore-Rio Pietra-Fasanella river system, respectively. Terminal leaves were in some cases associated based on their geographical distance, as in the case of the clusters B.16-B.17 and B.21-B.27.

The ternary diagram showing the composition in terms of quartz, calcite and dolomite of the sediments from the 18 sites on the Bussento and Calore Salernitano rivers is represented in Figure 3.24. Sites lies along a gradient of relative abundances of quartz and calcite, with percentages of dolomite lower than 20%. The only exception was site B.21, with ~60% of dolomite and similar contents of calcite and quartz.

The site lie on the boudary of the 3σ confidence interval, whereas all the others are enclosed within the 2σ limit.

The ilr-transformed percentages of quartz, dolomite, and calcite are significant ($P < 0.001$) in determining the site and element distributions in the RDA triplot using the total PTE concentrations in sediments as response variables, but fail to differentiate the two river systems (Figure 3.25). The sites belonging to the Bussento and the Calore Salernitano were, instead, clearly separated on the RDA triplot computed using the ilr-transformed variables as predictors and the loadings of the mode n. 1 compositional tensor upon the 9 selected tensors as response variables. Even in this case, the axes were significant ($P < 0.001$) in determining the distribution of sites and response variables within the RDA space (Figure 3.25).

The NMDS based on total PTE concentrations in sediments (Figure 3.26) differentiated the sites on the Calore Salernitano from those on the Bussento river, the former characterised by higher concentrations of P and As, and the latter characterised by higher concentrations of K. Moreover, each group was further differentiated into 2 main clusters. For the sites on the Calore Salernitano river, C.15, C.16, and C.17, were characterised by higher Cd, S, and Na concentrations, whereas C.01, C.03, C.06, C.09, and C.10, by higher Si, Cu, Al, Cr, Fe, Zn, Co, and Ni concentrations. For the sites on the Bussento river, B.21, B.22, and B.22, differentiated from the others in relation to their higher Mg, K and Ca concentrations, whereas the other sites were characterised by higher concentrations of the same elements characterising the cluster of sites C.01, C.03, C.06, C.09, and C.10. No clear association of sites B.21 and C.03 with high concentrations of Cd and Ni, highlighted by both passive and active biomonitors, was observed in relation to sediment total concentrations. The same holds true also for the NMDS based on each BCR fraction, shown in Figures 3.27 to 3.30. The NMDS biplots based on the PTEs bound to Fe-Mn oxides and organic matter fractions data (Figures 3.28 and 3.29) highlight a grouping structure similar to the one described for the NMDS based on total PTE concentrations, with sites C.01, C.03, C.06, C.09, and C.10 grouped together and a position of site B.21 on the higher end of the Mg vector. Conversely, the NMDS based on PTEs bound to the exchangeable and the residual fractions data (Figures 3.27 and 3.30) did not show any clear differentiation of the sites, with the exception of site C.06 in relation to Fe exchangeable concentration. The stresspots relative to the NMDS based on the total PTE concentrations and on the PTE concentrations in each BCR fraction are reported in Figure 3.31, highlighting coefficients of determination relative to the linear regression between the distances on the NMDS spaces and the original distances always higher than 0.9, with the exception of the NMDS based on PTE concentrations in the exchangeable fraction (r^2 = 0.773).

PTE concentrations in water in the Bussento and Calore Salernitano rivers in 2016 and 2017 are reported in Tables D.1 and D.3, respectively, whereas ORP, dissolved O_2, electrical conductivity, pH, and concentration of anions, photosynthetic pigments, TC, IC, TOC, and TN are reported in Tables D.2 and D.4. The multivariate outlier maps relative to the macronutrient, micronutrient and anion concentrations in water in 2016 and 2017 are reported in Figures 3.32 and 3.33, respectively. The outlier maps relative to the non-essential elements in 2016 and 2017 were not produced due to their concentrations below the limits of detection (Al: 1 μg L^{-1}, As: 2 μg L^{-1}, Cd: 0.1 μg L^{-1}, Pb: 1 μg L^{-1}). With the exception of sites B.08 and B.11 in 2016 and sites C.03 and C.07 in 2017, all the spatial outliers (B.01, B.14, B.16, C.01, C.02. C.03, C.04, C.05, C.07, C.16, C.17, C.18 in 2016, and B.16, B.21, B.25, B.27, C.01, C.02. C.03, C.04, C.05, C.07, C.20, C.21 in 2017) identified based on anion concentrations were selected also based on macronutrient concentrations. In addition, the analysis on macronutrient concentrations selected also sites B.13, B.19, and C.10 in 2016, and sites B.13, B.15, B.24, B.28, and C.09. The number of outliers detected based on micronutrient concentrations was greater in 2016 than in 2017, with 8 sites selected on the Bussento river (B.01, B.04, B.13, B.14, B.16, B.17, B.19, B.20) and 7 on the Calore Salernitano river (C.01, C.02, C.03, C.06, C.16, C.17, C.18), whereas 6 sites were altogether identified in 2017 (B.16, B.21, B.25, B.27, B.28, B.29, C.15). The elements mostly contributing to the outlyingness definition in 2016 were P, K, Fe, Mn, Zn and Na, together with chlorides and nitrates. In 2017, all the macronutrients and anions contributed to the definition of the spatial outliers, together with Cu, Cr, Co and Si. The multivariate outlier maps (Figure 3.34) based on photosynthetic pigments, TOC and TN indicated sites B.01, B.02, B.03, B.04, B.05, B.16, B.17, C.01, C.04, C.05, C.09, C.13, and C.16 as outliers in 2016, and sites B.04, B.06, B.10, B.12, B.14, B.15, B.16, B.21, B.25, C.01, C.03, C.05, C.11, C.12, C.14, C.19, and C.20 in 2017. Chlorophylls and total carotenoids contributed mostly to the outlyingness definition both in 2016 and 2017, with a contribution of TN in 2017.

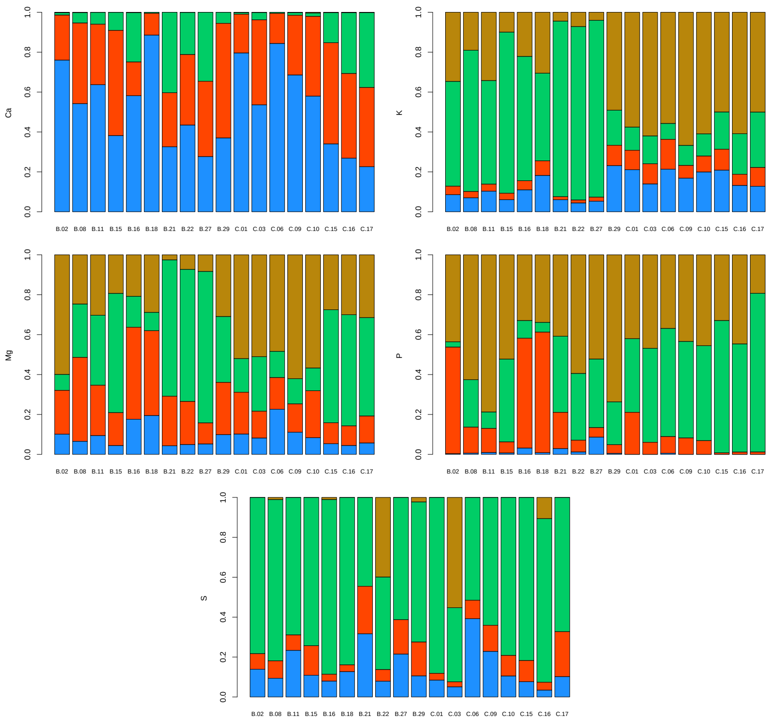

Figure 3.20: Stacked barplots of the macronutrient (Ca, K, Mg, P, S) concentration distribution in the 4 BCR fractions: exchangeable (■), bound to Fe-Mn oxides (■), bound to organic matter (■), residual (■).

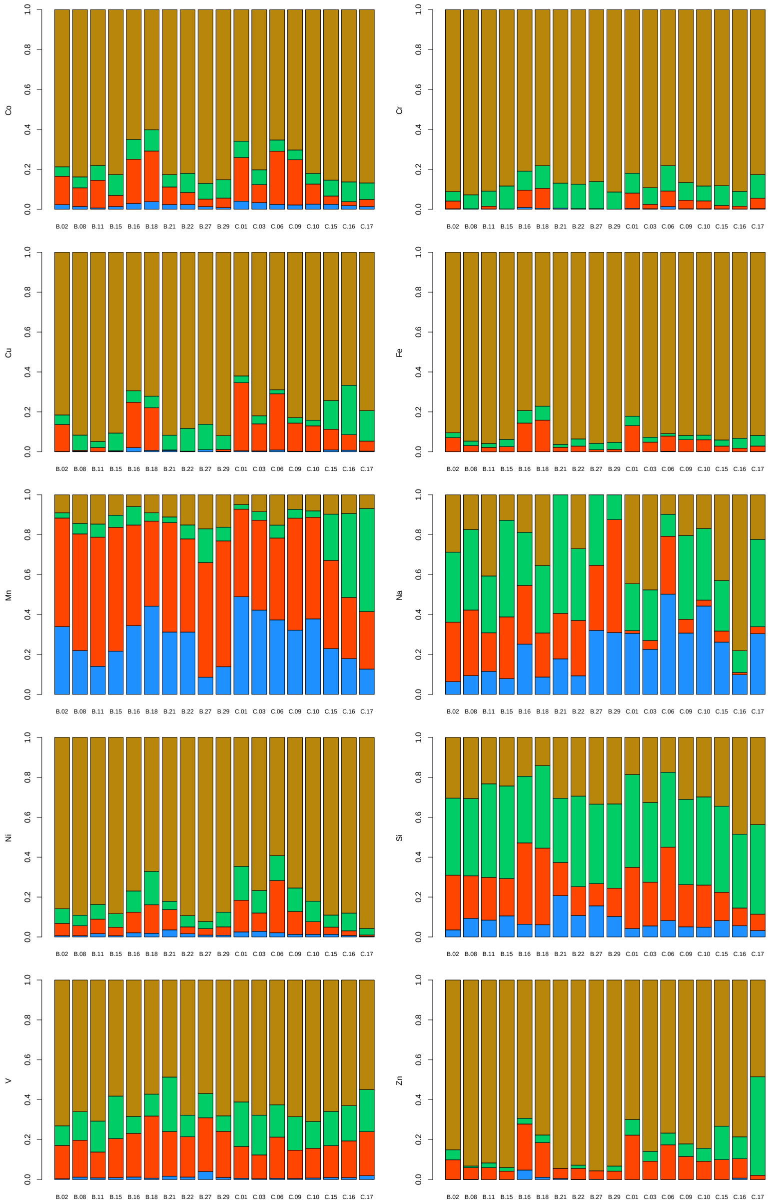

Figure 3.21: Stacked barplots of the micronutrient (Co, Cr, Cu, Fe, Mn, Na, Ni, Si, V, Zn) concentration distribution in the 4 BCR fractions: exchangeable (■), bound to Fe-Mn oxides (■), bound to organic matter (■), residual (■).

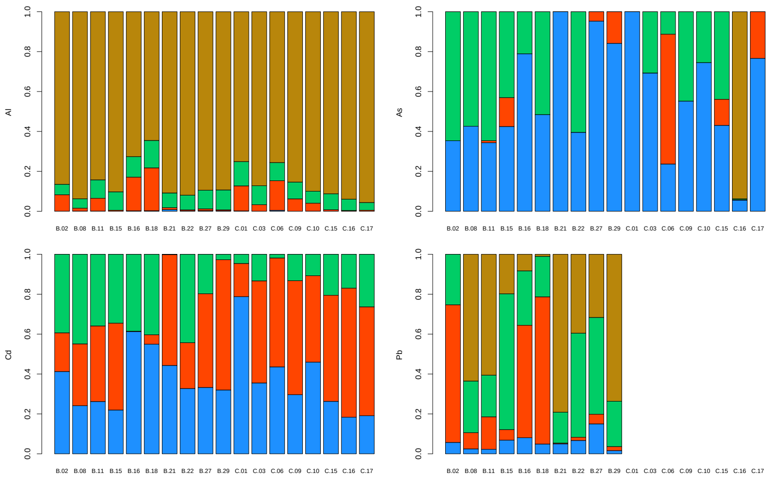

Figure 3.22: Stacked barplots of the non-essential element (Al, As, Cd, Pb) concentration distribution in the 4 BCR fractions: exchangeable (■), bound to Fe-Mn oxides (■), bound to organic matter (■), residual (■).

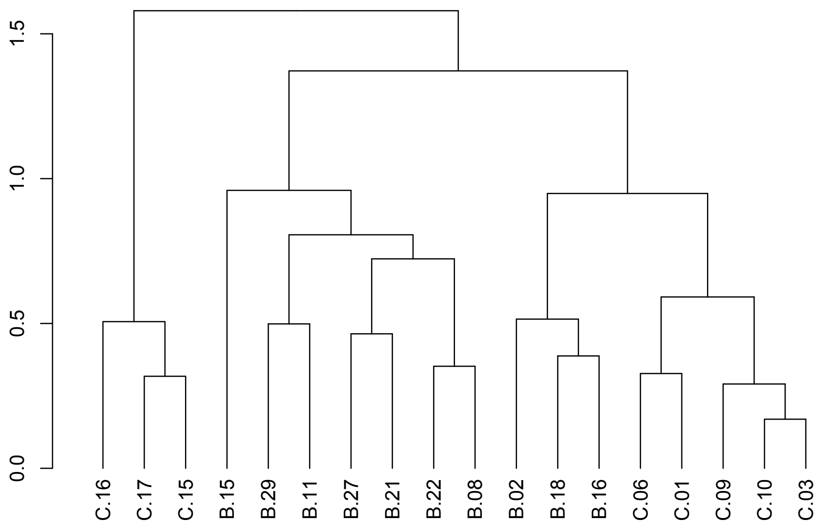

Figure 3.23: Dendrogram based on the Euclidean distance matrix of the projections of mode n. 1 onto the 9 tensors explaining more than 1% of the total variance in the 3-mode compositional tensor.

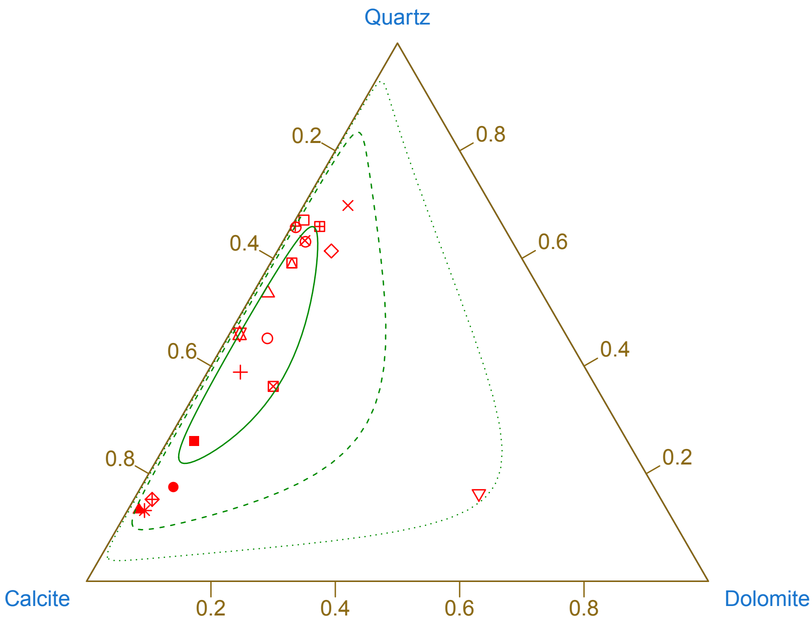

Figure 3.24: Ternary diagram showing the estimated relative abundance of quartz, calcite and dolomite in the sediments of the 18 sites on the Bussento and Calore Salernitano rivers: B.02 (□), B.08 (○), B.11 (△), B.15 (+), B.16 (×), B.18 (◇), B.21 (▽), B.22 (⊠), B.27 (✳), B.29 (⌖), C.01 (⊕), C.03 (⧖), C.06 (⊞), C.09 (⊗), C.10 (⍓), C.15 (■), C.16 (●), C.17 (▲). Confidence ellipses for 1σ (—), 2σ (- - -), and 3σ (· · ·) are also shown.

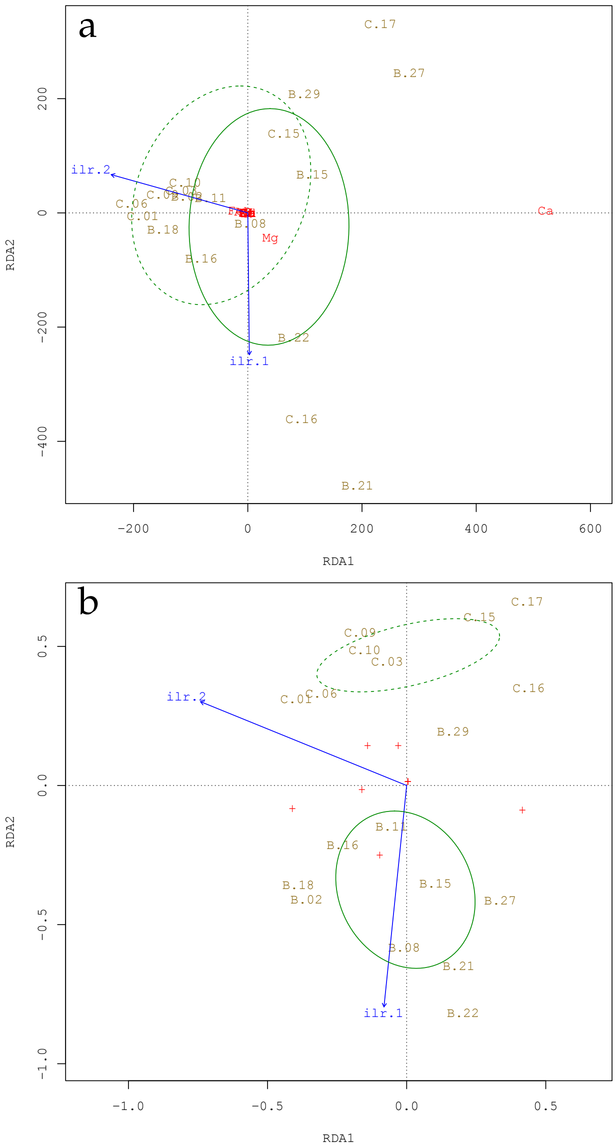

Figure 3.25: RDA triplots computed using the ilr-transformed percentages of quartz, calcite, and dolomite as predictors and the total PTEconcentrations (a) and the loadings of the mode n. 1 compositional tensor upon the 9 selected tensors as response variables (b). Confidence ellipses (for $\alpha = 0.05$) relative to the Bussento (—) and the Calore Salernitano (- - -) rivers are also shown.

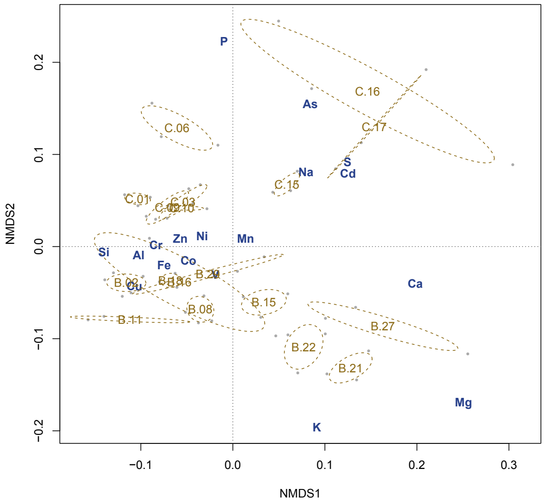

Figure 3.26: NMDS biplot relative to the total PTE concentrations in sediments of the 18 sites on the Bussento and the Calore Salernitano rivers. Confidence ellipses (for $\alpha = 0.05$) relative to each sites are also shown.

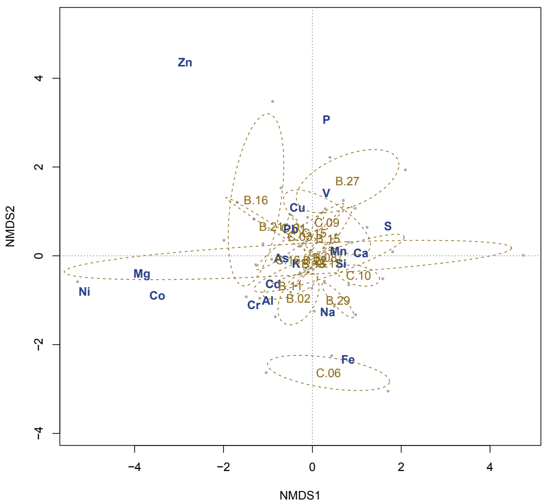

Figure 3.27: NMDS biplot relative to the PTE concentrations in the exchangeable fraction in sediments of the 18 sites on the Bussento and the Calore Salernitano rivers. Confidence ellipses (for $\alpha = 0.05$) relative to each sites are also shown.

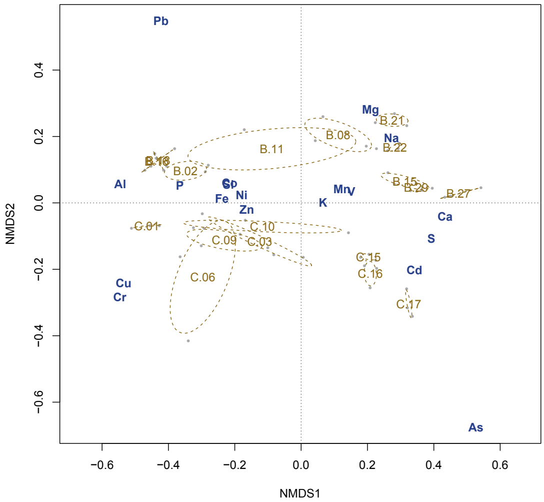

Figure 3.28: NMDS biplot relative to the PTE concentrations bound to Fe-Mn oxides in sediments of the 18 sites on the Bussento and the Calore Salernitano rivers. Confidence ellipses (for $\alpha = 0.05$) relative to each sites are also shown.

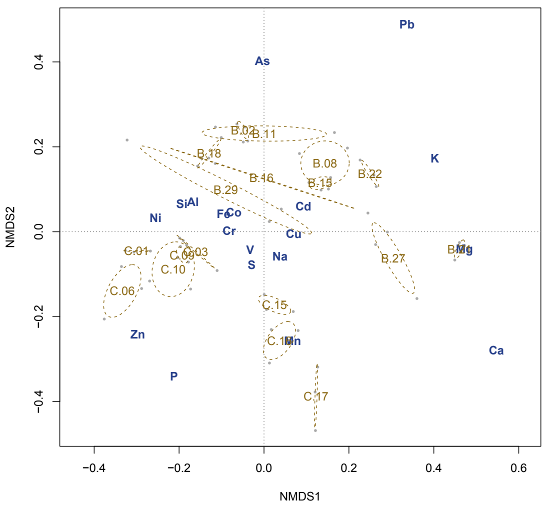

Figure 3.29: NMDS biplot relative to the PTE concentrations bound to the organic matter in sediments of the 18 sites on the Bussento and the Calore Salernitano rivers. Confidence ellipses (for $\alpha = 0.05$) relative to each sites are also shown.

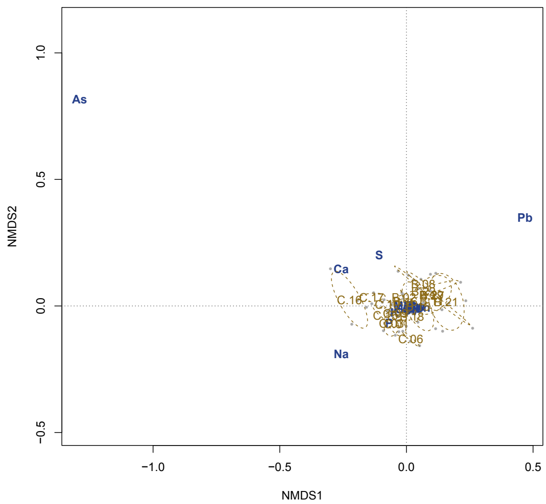

Figure 3.30: NMDS biplot relative to the PTE concentrations in the residual fraction in sediments of the 18 sites on the Bussento and the Calore Salernitano rivers. Confidence ellipses (for $\alpha = 0.05$) relative to each sites are also shown.

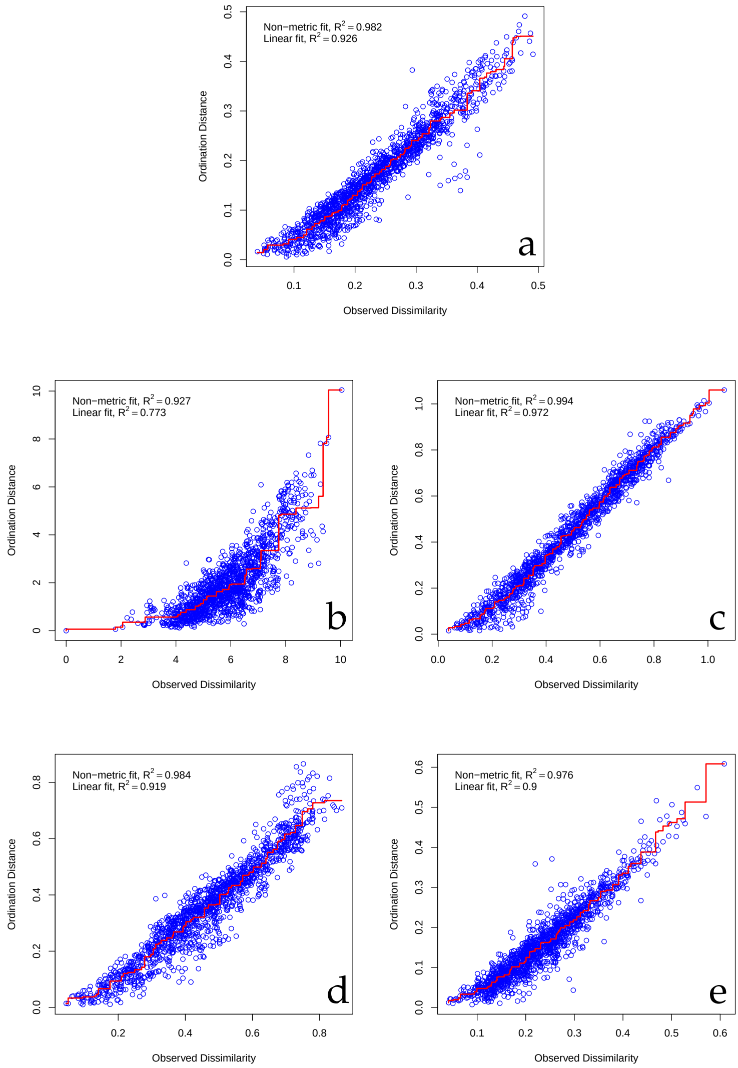

Figure 3.31: Stressplots relative to the NMDSs based on the total PTE concentrations (a) and on the PTE concentrations in the exchangeable (b), bound to Fe-Mn oxides (c), bound to organic matter (d), and residual (e) fractions. The coefficient of determination relative to the linear and non-linear regressions between the distances in the NMDS spaces and the original distances are also reported.

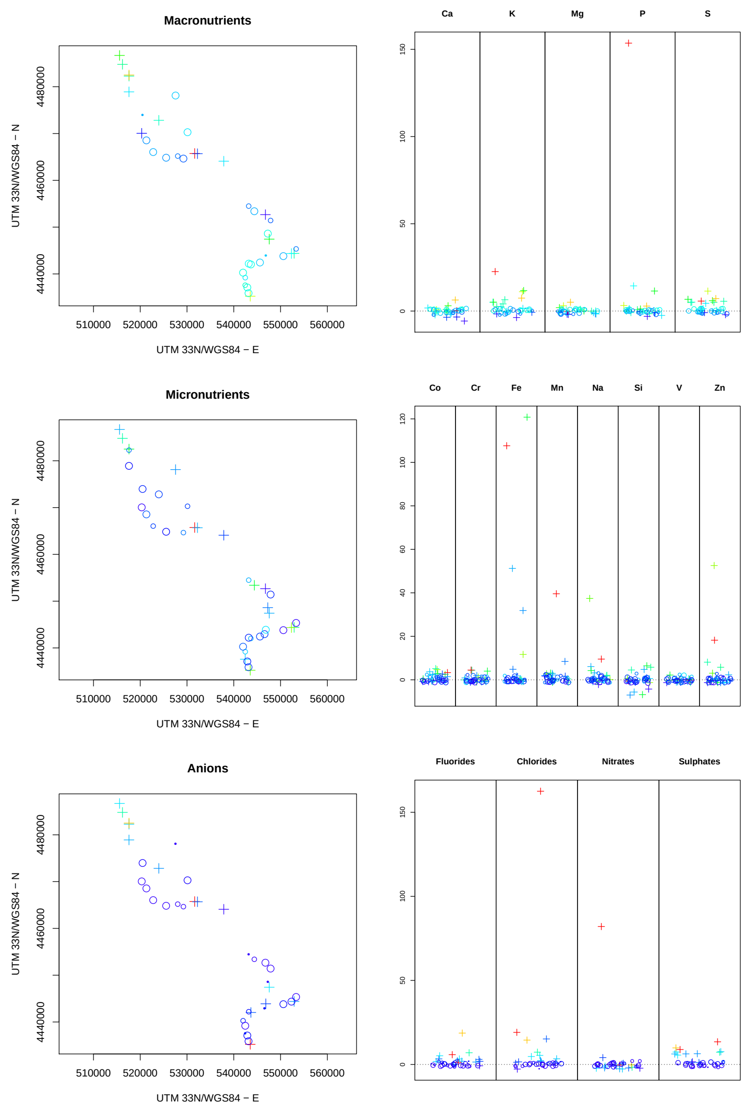

Figure 3.32: Multivariate spatial outlier plots (left) and break-down of the contribution of each variable (right), based on macronutrient, micronutrient, and anion concentrations in water in 2016. Values on the right are centered and scaled according to the MCD estimates. Crosses represent spatial outliers, colored according to their position with respect to the multivariate data distribution (blue: low values, red: high values).

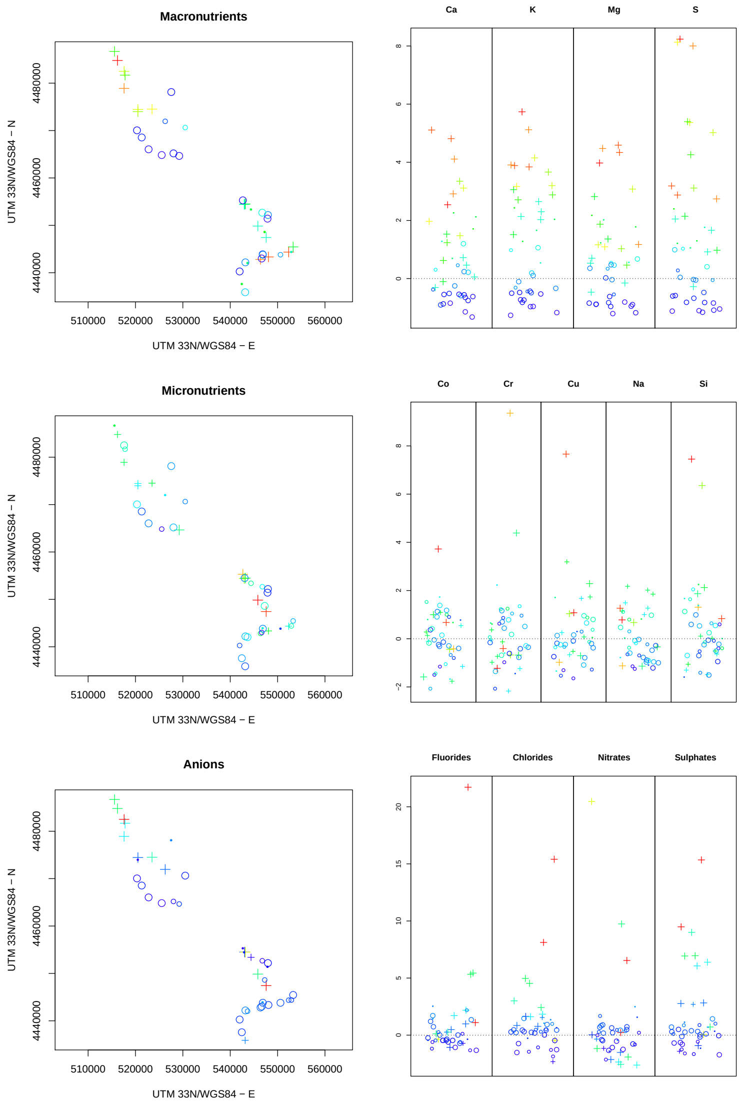

Figure 3.33: Multivariate spatial outlier plots (left) and break-down of the contribution of each variable (right), based on macronutrient, micronutrient, and anion concentrations in water in 2017. Values on the right are centered and scaled according to the MCD estimates. Crosses represent spatial outliers, colored according to their position with respect to the multivariate data distribution (blue: low values, red: high values).

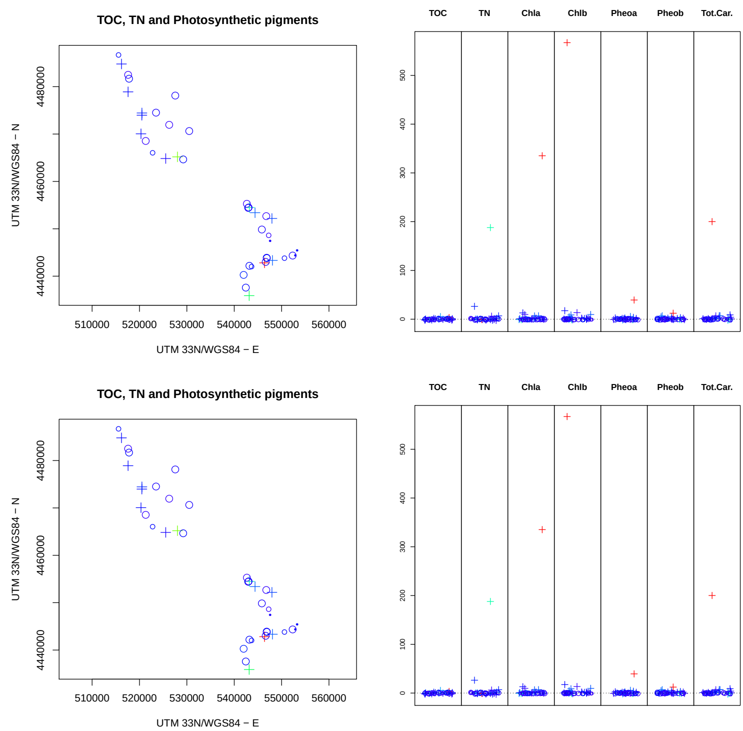

Figure 3.34: Multivariate spatial outlier plots (left) and break-down of the contribution of each variable (right), based on TOC, TN and photosynthetic pigments in water in 2016 (upper panels) and 2017 (lower panels). Values on the right are centered and scaled according to the MCD estimates. Crosses represent spatial outliers, colored according to their position with respect to the multivariate data distribution (blue: low values, red: high values).

Chapter 4

Discussion

The project engaged in the concept of integrated monitoring in its broadest definition, involving multiple and deeply interwined activities, which allowed to fulfill its three main goals and point out where future efforts should be directed.

Accurate spatial gradients of PTE concentrations were highlighted through the joint use of ensembles of both passive and active biomonitors, in turn allowed by the validation of the novel biomonitors and the evaluation of local biodiversity. In this context, the Charophyte flora of the "Cilento, Vallo di Diano e Alburni" National Park is characterised by an exceptional biodiversity, completely overlooked to date. Indeed, of all the species observed in the area, 3 were never recorded at the regional level according to the most recent and authoritative revision of the Italian flora (Bazzichelli and Abdelahad, 2009), and *Ch. vulgaris* var. *papillata* was never observed even at the national level (Bazzichelli and Abdelahad, 2009; Guiry and Guiry, 2018). All the species represent thus novel additions to the Charophyte flora of either Campania or Italy. Albeit the current taxonomic position of *Ch. vulgaris* var. *papillata* poses it as a variety of a subcosmopolitan and widespread species, *Ch. vulgaris*, its recording is of paramount importance considering the limited known distribution of the taxon (Guiry and Guiry, 2018) and the uncertainties in Charophyte taxonomy. Indeed, the entire group is currently under intensive taxonomical revisions, thanks to novel molecular data, which are changing the taxonomical ranking of numerous entities and shedding light on their morphological plasticity (Schneider et al., 2015; Nowak et al., 2016; Schneider et al., 2016; Urbaniak and Sakayama, 2017). Recent advances point toward an alleged lower number of species, as compared to morphometric taxonomies, but with extreme plasticity in their morphological traits. The variations result from the interaction of genetic and environmental determinants, possibly through the involvement of epigenetic alterations (Nowak et al., 2018; Puche et al., 2018), and the efforts of several groups are rapidly converging to clarify these topics (Beilby et al., 2018).

Our data also highlighted extreme plasticity in population traits, although the relative contribution of specific and environmental determinants varied in relation to the kind of traits. Of the 17 populations observed during the three years of the research, we were able to collect information on the morphology, photosynthetic pigments, and carbonate encrustation of 12, due to the disappearence of some populations during the sampling. On the positive side, 4 of the missing populations belonged to *Ch. gymnophylla* or *Ch. vulgaris*, already accounting for 70% of the studied populations. On the negative side, the unique population of *Ch. vulgaris* var. *papillata* was lost. Focused explorations are thus needed to ascertain wether the taxon got extincted in the area or still survives with other populations. Morphological, biochemical (photosynthetic pigment concentrations), and ecological (carbonate encrustation, epiphyte diatom biomass) traits lie on a gradient of increasing environmental contribution and decreasing species-specificity. Indeed, the differentiation between *Ch. gymnophylla* and *Ch. vulgaris*, based on their morphology, disappears in relation to their photosynthetic pigment concentrations and carbonate encrustation, and all the species became indistinguishable when considering the epiphyte diatom load on the surface of thalli. Ecological traits, in particular, can be deeply modified by the environment and may exhibit wide temporal fluctuations, although species-specific traits can play an inportant role in the carbonate deposition process

(Herbst et al., 2018a,b) and may favour or hinder the colonization of thalli by epibionts (Sviben et al., 2018).

The differentiation between *Ch. gymnophylla* and *Ch. vulgaris* assumes particular importance in the context of the systematic position of the species which, due to the presence of populations with intermediate traits, were long considered to belong to the same taxon. Our analysis shows, instead, that the species can be clearly distinguished based on the presence of reproductive structures on the radii corticate cells, on the corticate cell number and on the size of internodes.

The possibility to unambiguously identify *Ch. gymnophylla* and *Ch. vulgaris* has pivotal consequences for their use in freshwater biomonitoring, allowing the accurate definition of the source material, especially in the case of sympatric populations. Indeed, our analysis allowed to definitely attribute the source population for bag preparation to *Ch. gymnophylla* and to ascertain its distribution in the Bussento and Calore Salernitano rivers, preliminary steps to its validation as a novel active biomonitor.

Usually, the validation of novel bioaccumulators is carried out by studying the kinetics of pollutant accumulation in controlled conditions (see for example Díaz et al., 2012). This approach is invaluable in providing key parameters like pollutant accumulation rate, saturation time and range of linearity in biomonitor responses. However, field conditions rarely match the experimental settings employed in mesocosm studies, making the direct translation of these parameters to field applications questionable. Indeed, the complex network of interactions with the abiotic and biotic environment experienced by biomonitors in the field shapes their responses, which cannot be predicted by simple kinetics. The actual validation of novel biomonitors mandate thus the study of their field behaviour in relation to pollution gradients, that, although conceptually simple, requires independent information on stationary spatial gradients of pollutants in bioavailable form. As specified in the Introduction section, chemical analyses of water and sediments can rarely provide such information, and the validation of novel biomonitors often relies on comparing the obtained gradients with the distribution of known pollution sources. Examples of this approach are in Lafabrie et al. (2007), Baldantoni and Alfani (2016), and De Nicola et al. (2017). Recently, the introduction of chemical matrices mimicking the behaviour of bioaccumulators, like Diffusive Gradients in Thin films (DGTs), but with a lower sensitivity to environmental variations, provided researchers with a seemingly reliable reference for the validation of biomonitors *in situ* (Jordan et al., 2008; Waltham et al., 2011; Philipps et al., 2018a). DGTs, however, are not a perfect reference, representing a model system with substantially different sensitivity to environmental factors and to the analytes accumulated in respect to biomonitors (Peters et al., 2003; Philipps et al., 2018a,b), and sometimes DGT and biomonitor were employed in conjunction to improve accuracy of environmental monitoring rather than to validate biomonitors (Stark et al., 2006; Diviš et al., 2012). Moreover, in some cases the situation was even reversed, with the responses of DGTs validated against known bioaccumulators, like *F. antipyretica* (Ferreira et al., 2013).

The use of established biomonitors, validated by means of multiple techniques in multiple occasions, as improved references over DGTs and similar chemical matrices is a straightforward consequence of these considerations, provided they have similar behaviour toward pollutant accumulation in respect to the novel biomonitors. Obviously, the main limitation of the this approach lies on the requirement of concomitant occurrence of both biomonitors in several locations along spatial gradients of environmental pollution, a constraint of limited relevance in active biomonitoring, though. This approach was adopted in the present research to validate *Ch. gymnophylla* and *M. aquatica* as novel active and passive biomonitors, respectively. The effectiveness in biomonitoring studies of the references chosen, *F. antipyretica* and *H. nodiflorum*, was repeatedly assessed in both controlled and field conditions. *H. nodiflorum* was shown by Vlyssides et al. (2005) to exhibit Michaelis–Menten kinetics in the accumulation of several metals, notably Cd, Cr, Cu, Pb, Mn, Ni, Hg, As, Zn, and Sn. Its definite field validation as an exemplary biomonitor for Mediterranean river, however, was carried out by Baldantoni and Alfani (2016), who demonstrated how the roots of this species were able to provide spatial gradients fitting the distribution of known pollution sources, and averaged over the responses of 6 others candidate biomonitors. *F. antipyretica* currently represents the *de facto* standard in river "bryomonitoring" of PTEs, radionuclides, and organic pollutants (Augusto et al., 2011; Favas and Pratas, 2013; Gecheva and Yurukova, 2014; Debén et al., 2018). Its effectiveness has been recognised since 1981 (Ledl et al., 1981), but it is only in recent years that river biomonitoring using mosses bacame an established technique and the number of studies employing *F. antipyretica* has increased (Debén García et al., 2017). As in the case of *H. nodiflorum*, also for this species Michaelis–Menten kinetics in PTE accumulation were described, although the actual kinetics may vary in relation to exposure time and pollutant concentrations (Díaz et al., 2012).

The uniform responses between the couples of passive biomonitors and active biomonitors are remarkable, extending beyond similarities in gradients to involve also absolute concentrations in the case of *M. aquatica* and *H. nodiflorum*. Revealing in this context is the wide overlap of the confidence ellipses for the two species in 2016 and 2017 in the NMDS space, even in the case of raw data, where the unique group differentiating from the others was the one relative to *H. nodiflorum* in 2017. As expected in relation to the stationary nature of the gradients obtained through biomonitoring (Baldantoni and Alfani, 2016), *M. aquatica* provided the same PTE concentration patterns in both the years, substantially overlapping with those of *H. nodiflorum* in 2016. The differentiation between *H. nodiflorum* in 2017 and the others, however, disappeared when scaling the data, suggesting the presence of some sites where only *H. nodiflorum* was collected and showed unusually high PTE concentrations. A possible site showing these characteristics was B.21, one of the springs of the Bussento in the Sanza district, exhibiting exceedingly high PTE concentrations in biomonitors in both the years, but where *M. aquatica* did not occur in 2017. The hypothesis is further supported by the increase in the Mantel correlation through data scaling, indicating that the presence of unusual PTE concentration values in a single set of data was responsible for the differences between the biomonitors, rather than PTE bioaccumulation patterns. Accordingly, data scaling did not substantially affect the Mantel correlation between *Ch. gymnophylla* and *F. antipyretica*, although wide differences in absolute PTE concentrations were highlighted by the NMDS based on the row data. In particular, the two species showed different selectivities toward PTEs, with *F. antipyretica* accumulating higher concentrations of Al, Cd, Co, Cr, Cu, Fe, Mn, Ni, and V, and *Ch. gymnophylla* accumulating higher concentrations of As, Ca, K, Mg, Na, Pb, S, and Zn. Irrespective of these variations, attributable to morpho-physiological differences between the two species (Naser et al., 2011; De Nicola et al., 2013), however, the patterns of PTEs were largely in agreement, as denomstrated by the high Mantel correlations and the wide overlap between their relative confidence ellipses following data scaling. In this context, it is worth considering the conservative-oriented choices in the techniques employed in data analysis. On the exploratory side, the NMDS with the superimposition of confidence ellipses does not donsider *a priori* subdivisions of observations into several groups, as in CVA, but rather tries to preserve the original distances while shrinking the multivariate space onto a predefined set of axes (Podani, 2005; Podani and Morrison, 2017). As a result, positions in NMDS space represent only the relative distances among observations: if groups differ in absolute concentrations or PTE accumulation patterns, their differences are projected onto the NMDS space, allowing an *a posteriori* group differentiation, the opposite happening for the similarities. On the inferential side, the Mantel correlation test is known to have significantly lower power in detecting significant correlations as compared to univariate techniques like the Pearson's or the Spearman's correlation tests (Legendre and Legendre, 2012). The values obtained for the correlations between the pairs of active and passive biomonitors represent thus exceptional agreements between the *patterns of distances* in the original matrices.

Providing spatial concentration patterns of PTE concentrations comparable to some of the best biomonitors in their classes, both *M. aquatica* and *Ch. gymnophylla* can be considered valuable passive and active bioaccumulators, respectively, for Mediterranean river biomonitoring. Moreover, on the practical side, both the species have some advantages over their references. On the one hand, *M. aquatica* showed to be more widespread than *H. nodiflorum*, at least in the Bussento-Bussentino and the Calore Salernitano-Rio Pietra-Fasanella river systems, allowing a wider spatial covering of passive biomonitoring. On the other hand, *Ch. gymnophylla*, as most Charophytes, exhibit high grow rates and biomass production (Laffont-Schwob et al., 2015), can be easily cultivated (Nowak et al., 2018), allowing virtually uncontaminated source material, and can be dried and pulverised with more ease than *F. antipyretica* (no need of liquid nitrogen freezing), simplifying laboratory operations.

In the context of river monitoring, the coherent behaviour of both the passive and active biomonitors ensured the accurate derivation of spatial PTE concentration gradients. Overall, most of the variations in PTE concentrations appear at local or medium scale, with seemingly no large-scale gradients. All of the MEMs extracted, in fact, represent local and medium spatial scales, even the lower order ones, usually describing large spatial scales (Dray et al., 2006; Bauman et al., 2018). The most important MEMs extracted in relation to the patterns of PTE concentrations in active biomonitors, however, tend to represent variations at scales larger than in those extracted using passive biomonitoring data, especially in the case of the Bussento river. The Mantel correlograms further support this scenario, indicating that local alterations do not propagate in space, except for small distances when considering PTE concentrations in *F. antipyretica* and *Ch. gymnophylla*. Indeed, a slight positive autocorrelation at the lower distance classes was observed in PTE concentrations in active biomonitors only, rapidly falling to negative values and then to null autocorrelations. This occurrence is usually related to the presence of strong local determinants of the observed patterns (Borcard et al., 2011), indicating that PTE concentration patterns tend to be similar within small spatial ranges, and quickly vary with increasing distances.

As expected based on the similar spatial scales represented by MEMs, all the PTEs exhibit similar behaviour in respect to the MEMs in the RDAs, indicating common local sources of variations for all of them. Notable exceptions, however, are the associations among Cd, K, Ni and Zn, and among Al, As, Ca, Co, Fe, Mn, Pb, and Si, especially evident in the RDAs based on PTE concentrations in *H. nodiflorum* and *M. aquatica*. In this context, the comparison of the spatial outlier maps and the raw data indicate the presence of localized hot-spots of PTE concentrations in biomonitor roots in several sites along the course of the Bussento and the Calore Salernitano rivers, notably B.11, B.17, B.18, B.21, B.25, B.26, C.03, and C.09. Among them, the sites B.17, B.18 and B.26, located on the upper course of the Bussento river, B.25, on the Ciciriello river, a tributary of the Bussento, and C.09, on the middle course of the Calore Salernitano river, are especially associated to high concentrations of Al, As, Ca, Co, Fe, Mn, Pb, and Si. Conversely, the sites where the highest concentrations of Cd, K, Ni, Zn, and sometimes Cr, are invariably springs: B.21, in the upper course of the Bussento river, B.11, in the Morigerati district, where the Bussento emerges after its hypogeous course (Bovolin et al., 2017), and C.03, on the Calore Salernitano in the Castelcivita district, where water from most of the Alburni karst system emerges (Ducci et al., 2008). Conversely, the patchiness in hot-spot spatial distribution appears lower when considering the PTE concentration gradients derived from active biomonitoring. In this case, in fact, most of the sites on the upper course of the Bussento river were identified as spatial outliers, either in relation to macronutrient, micronutrient or non-essential element concentrations, along with localized hot-spots like C.03, C.09, C.15, C19, and C.20.

The absolute concentrations reached by several micronutrients and non-essential elements in biomonitors, especially the roots of *H. nodiflorum*, raise concerns when compared to reference concentrations, or concentrations derived from other studies employing the same species. Indeed, values up to two order of magnitude higher in respect to the

Standard Reference Plant (Markert et al., 2015) were recorded for some PTEs, notably Al, Fe, Ni and V, and up to one order of magnitude higher for several others, like As, Cd, Co, Cr, and Mn. Mn and Ni, in addition, reached in *H. nodiflorum* roots in sites B.17 and B.21 values more than $1 \cdot 10^3$ times higher in respect to the concentrations measured in the roots of the same species by Bonanno et al. (2017) and Bonanno and Vymazal (2017) in four areas affected by different levels of anthropogenic impacts. It is, however, the comparison of Ni concentrations in *H. nodiflorum* with those measured in the spring area of the Sarno river that raises the major concerns about river quality in several sites of the Bussento and Calore Salernitano rivers. Indeed, values up to $\sim$ 40 $\mu g \cdot g^{-1}$ were recorded in the spring area of the Sarno river (Baldantoni et al., 2018), whereas in C.03, and especially B.21 springs, values up to $\sim$ 250 $\mu g \cdot g^{-1}$ and $\sim$ 450 $\mu g \cdot g^{-1}$, respectively, were observed. The same considerations apply in the case of Cd, where concentrations up to $\sim$ 20 $\mu g \cdot g^{-1}$ and $\sim$ 14 $\mu g \cdot g^{-1}$ in C.03 and B.21, respectively, were observed, against an average concentration of 2.4 $\mu g \cdot g^{-1}$ in the spring area of the Sarno river (Baldantoni et al., 2018). *F. antipyretica*, although similarly highlighting B.21 as the most critical site, exhibits concentrations lower or in the same order of magnitude than those reported for the same species (Samecka-Cymerman et al., 2005; Samecka-Cymerman and Kempers, 1999) transplanted in sites downstream sewage sludge sources or growing on basaltic substrates.

The constant association of the highest PTE concentrations with springs is remarkable, and may be attributed either to groundwater contamination from anthropogenic activities or the crossing of PTE-enriched lithological layers, or to changes in PTE bioavailabilities. Sediment analysis, however, did not reveal neither the presence of peculiar mineralogical structures, apart from a relatively high abundance of dolomite in B.21, or higher total PTE concentrations, nor variations in the bioavailability of Ni, Cd, Cr, or V associated to the sites where bioaccumulators highlighted the highest concentrations. Indeed, PTE concentrations in the exchangeable fraction were relatively uniform across all the studied sites, with the exception of site C.06, in the upper course of the Fasanella river, characterised by higher Fe exchangeable concentrations, that did not reflect into higher concentrations in biomonitors, though. Although wider differences among sites were related to the PTE concentrations bound to Fe-Mn oxides and organic matter, neither the associations among PTEs observed in biomonitors nor the associations of sites based on the highlighted criticalities were observed in the NMDS spaces obtained from these data. Explanatory in this context is the clustering of sites based on their overall pattern of PTE bioavailabilities, grouping sites mostly in relation to their geographical proximity rather than to the criticalities detected through the biomonitoring.

The hypothesis of groundwater contamination assumes thus particular relevance, especially in relation to the known vulnerabilities of some of the studied areas. This is especially true for the site C.03, for which detailed studies are available (Ducci et al., 2008), coding this area as one at "high risk of groundwater contamination", and site B.21, characterised by a superficial basal plate with water circulation through debris (D. Guida, personal comuication).

A simple model of continuous emissions from the springs to the rivers, however, does not account for the PTE concentrations in water below the limits of detection for several micronutrients and non-essential elements. Moreover, it cannot explain the differences in the spatial scales of variation in the gradients obtained through passive and active biomonitoring. Indeed, the MEM spatial analysis, the Mantel correlograms, and the spatial outlier maps, provide a coherent scenario of the spatial scales relevant to *H. nodiflorum* and *M. aquatica*, and to *F. antipyretica* and *Ch. gymnophylla*, with the former reacting to conditions widely and rapidly changing in space, and the latter highlighting more gradual spatial changes. These differences may be attributable to the double interaction with sediments and water in the case of the rooted passive biomonitors, as compared to the unique interaction with water of the active biomonitors. Indeed, the interaction with sediments, intrinsically more variable in space, may be advocated to explain the finer spatial scales of vatiation in PTE concentrations highlighted by *H. nodiflorum* and *M. aquatica*. However, sediment analysis demonstrated a degree of spatial uniformity in bioavailable concentrations incompatible with the gradients obtained through passive biomonitoring. Albeit a role of sediments as modifiers of the uptake behaviour of *H. nodiflorum* and *M. aquatica* cannot be definitely excluded, major determinants for the observed gradients should be searched in water.

A refinement of the groundwater contamination model, accounting for erratic emission pulses, may solve this multi-faceted problem in its entirety. Indeed, pollution peak events got easily missed by water chemical monitoring, explaining the low PTE concentrations observed in water samples, but are integrated by biomonitors. The exposure time, however, shapes the obtained gradients, since the longer the exposure, the higher the likelihood of peak picking, and the deeper the differences between the source areas and their neighbourhood. A process similar to image staking in enhancing the signal from weak areas (Morozov and Dueker, 2003). Therefore, the longer exposure of *H. nodiflorum* and *M. aquatica* (6-7 months), in respect to *F. antipyretica* and *Ch. gymnophylla* (21 days) is possibly the key in explaining the differences in the spatial gradients they produced. This hypothesis is further supported by the season covered by passive biomonitoring, characterised by heavy rain events. Indeed, it is known that the hydrology of several groundwater systems in the area, notably C.03, behave according to a "piston-flow" model (Celico, 1994; Bovolin et al., 2015, 2017). The groundwater laminar flows and the presence of deposition ponds allow these systems to accumulate dissolved and suspended matter in the underground system, released in occasion of rain events increasing the pressure in the hydrological system (Ravbar et al., 2011; Ford and William, 2013). The outcomes are sudden and short-living emission pulses of ions and particulate matter (Ravbar et al., 2011; Bovolin et al., 2017), almost impossible to detect with water chemical monitoring, but easily recorded by biomonitors.

Water analyses, however, allowed to highlight kinds of criticalities undetectable using *H. nodiflorum* and *M. aquatica* or *F. antipyretica* and

Ch. gymnophylla. In particular, spatial outliers related to the presence of high anion concentrations (especially Cl^-, NO_3^-, and SO_4^{2-}), associated to high concentrations of macronutrients, were identified in the sites B.16, the at the mouth of the "La Rupe" ponor on the upper course of the Bussento river, C.16, in the Valle dell'Angelo district, on the upper course of the Calore Salernitano river, and in all the sites on the lower course of the Calore Salernitano river. The proximity of wastewater treatment plants and the absence of other known sources of organic matter and nutrients in soluble forms, allow the attribution of the outliers in the upper course of both the Bussento and the Calore Salernitano rivers to the presence of wastewater discharges within the rivers. This hypothesis, is further supported by the observation, during the 2016 sampling campaign, of floating sewage sludges in site C.16. Conversely, the diffuse high anion concentrations in the lower course of the Calore Salernitano, associated to the presence of high concentrations of photosynthetic pigments, indicating eutrophic conditions, match the distribution of intensive agricultural sistems settled along the river course. Soil leaching of soluble nutrients like, SO_4^{2-}, may thus explain the distribution of these analytes in river water.

Overall, three main criticalities were thus highlighted in the Bussento-Bussentino and Calore Salernitano-Rio Pietra-Fasanella river systems: i) the presence of springs occasionally emitting water with high PTE concentrations, ii) the presence of wastewater discharges and iii) the presence of nutrient leaching from agricultural soils. With the exception of the latter, the criticalities appear to be localized to few sites on both the river systems, an occurrence involving also the presence of high Al, As, Co, Fe, and Mn concentrations in a few sites, which are likely related to the presence of metallic structures or wastes in the riverbed.

The approach embraced for the research, joining chemical, physical, botanical, zoological, geological, cartographical and statistical skills, represents a true ecological strategy to the study of complex ecosystems, and an example of how multiple activities can be coupled to obtain a comprehensive view of freshwater ecosystem integrity. Despite the enormous efforts required, it is the unique approach capable of dealing with the complexity of ecological systems, and what it is advocated for to cope with the current global and local scale crises of the Anthropocene.

Contributions

The implementation of this research was allowed by the financial support of the "Cilento, Vallo di Diano e Alburni" National Park and the Ecology group of University of Salerno, which funded the three-years Ph.D. fellowship. The whole project was coordinated, on the Park side, by Dr. Laura De Riso, and on the University side by Prof. Daniela Baldantoni and Anna Alfani, Supervisor and Co-Supervisor of this Ph.D. thesis, respectively. A fruitful exchange of opinions with Prof. Domenico Guida and Dr. Maurizio Carotenuto (Co-Supervisors at University of Salerno), Prof. Gianluca Sarà (Co-Supervisors at University of Palermo) and Prof. Antonio Proto (Co-Examiner at University of Salerno) elevated the results of this research.

Appendix A

PTE concentrations in passive biomonitors

Table A.1: PTE concentrations (mean) in *H. nodiflorum* from the Bussento and Calore Salernitano rivers in 2016. Units are in μg g^{-1} d.w., unless otherwise specified.

Site	Al	As	Ca	Cd	Co	Cr	Cu	Fe	K	Mg	Mn	Na	Ni	P	Pb	S	Si	V	Zn
B.02	6502	0.323	6735	0.903	2.193	6.369	29.695	2880	16686	7024	191.05	14675.9	8.384	1404.15	0.513	2582.3	24850	53.33	57.16
B.03	4905	0.269	6332	0.972	3.239	4.702	26.748	2318.9	13260	5725.27	865.7	13645	9.974	1252.1	0.814	3218	26962.06	43.457	51.63
B.04	5150	0.213	5658	1.024	3.006	5.4	27.705	2670	15450	6438.3	518.98	13476.7	11.396	1405.31	0.745	3137.5	20439	47.545	56.1
B.05	1431.53	0.115	3996.5	1.01	1.661	2.233	39.396	862.1	22022	>8000	171.236	12423	8.775	1813.37	0.416	2714.5	5495.9	48.375	82.9
B.06	1853	0.165	5123	1.255	3.242	2.464	20.931	2738.3	18720.9	7617.2	471.16	13334.5	11.108	1034.81	0.457	2511.7	9211	43.19	57.251
B.07	3999	0.224	5439.5	1.311	2.086	4.619	27.673	1870.3	15623	>8000	398.41	11882	10.688	1550.7	0.879	2943.3	18259	51.272	69.15
B.08	3866	0.217	5274	1.208	2.032	5.451	16.959	1636	17348.5	6149.2	553.3	13374	24.197	1861.7	0.878	3001.1	20687	44.114	55.541
B.09	3319.9	0.458	7727	1.109	2.343	7.983	21.952	1508.1	28419	4936	940.02	12760	32.145	3354.94	1.87	6545.5	45817	38.201	148.19
B.10	2200	0.232	6722	1.82	3.475	6.757	8.515	1731.2	32709	>8000	1266.25	9832.2	74.617	2350.2	0.911	2881	11817	61.1	63.87
B.11	2373.8	0.206	6722	1.554	1.228	5.13	6.629	1027	15465	5709.9	162.91	6258.6	91.267	2589.6	0.902	3412.3	17513	40.023	61.42
B.15	307.6	0.068	4025	0.534	0.414	1.107	11.325	263.74	5385	>8000	34.369	11522	8.78	1056.3	1.319	2106.8	5611.1	44.777	85.5
B.16	5585	0.287	7517	0.946	4.79	5.51	24.63	3788	18016	5570	1038	16926	7.05	1768	1.344	2965	17092	45.66	130.14
B.17	6873.3	0.444	9858	0.838	7.865	6.879	16.91	9521.9	18619.1	6873.9	1626.3	15318.2	7.272	1711	2.213	4000.5	35938	51.642	43.287
B.18	6486	0.849	16340	1.454	17.93	8.143	17.23	23780	14377.2	>8000	1839.3	12575	10.079	1322.1	2.136	3172	22430	65.05	62.74
B.21	4693	0.514	6499	10.687	2.419	21.553	13.502	2158.9	20007	>8000	1841.5	9604	448.75	2266.9	1.073	3468.6	17597.5	78.418	126.176
C.03	1631	1.426	4742	20.265	2.302	8.055	7.472	2400	45827	4893	334	7296.4	246.91	2174.35	0.803	2848	14780	38.27	296.6
C.06	1254	0.135	8780	3.784	0.77	3.657	4.849	539.9	23789	6966	200.8	11463	4.127	1620.8	1.101	2336	12500	38.54	20.45
C.15	1422.2	0.408	4549	11.817	0.79	3.027	10.367	659.72	13610	5380.1	49.136	20211.3	10.693	1517.75	0.569	2484.65	9135	35.442	54.095

Table A.2: PTE concentrations (s.e.m.) in *H. nodiflorum* from the Bussento and Calore Salernitano rivers in 2016. Units are in μg g^{-1} d.w., unless otherwise specified.

Site	Al	As	Ca	Cd	Co	Cr	Cu	Fe	K	Mg	Mn	Na	Ni	P	Pb	S	Si	V	Zn
B.02	270	0.033	365	0.013	0.068	0.122	0.069	107	57.9	107	1.59	31.1	0.109	6.69	0.032	20.3	1380	1.02	1.38
B.03	147	0.012	655	0.041	0.003	0.158	0.451	48.0	219	9.92	33.1	175	0.112	27.3	0.063	47.5	4.80	0.828	1.74
B.04	227	0.002	484	0.023	0.078	0.027	0.248	227	195	71.9	8.39	73.2	0.153	5.90	0.022	29.0	549	0.668	1.20
B.05	7.12	0.016	67.1	0.015	0.022	0.034	0.128	11.6	141	-	0.525	159	0.062	5.86	0.141	28.5	80.8	0.139	0.335
B.06	121	0.010	472	0.018	0.050	0.109	0.193	56.6	24.3	55.7	6.99	63.1	0.163	5.35	0.090	14.5	567	0.502	0.630
B.07	143	0.008	18.0	0.026	0.098	0.109	0.499	57.1	175	-	8.74	112	0.135	24.3	0.036	55.1	728	0.872	2.10
B.08	406	0.013	268	0.024	0.051	0.352	0.289	158	91.9	21.4	13.3	70.9	0.201	15.4	0.085	69.7	978	0.872	0.895
B.09	92.5	0.019	868	0.018	0.027	0.170	0.175	28.7	341	50.9	2.93	247	0.278	5.58	0.102	71.0	439	0.490	3.60
B.10	181	0.012	441	0.033	0.073	0.206	0.062	80.6	120	-	5.07	63.3	0.239	14.8	0.106	72.2	135	2.94	1.30
B.11	18.8	0.013	167	0.016	0.029	0.085	0.026	10.4	219	37.6	1.45	75.8	0.479	11.4	0.134	52.6	446	0.315	2.08
B.15	21.1	0.011	388	0.022	0.003	0.096	0.276	2.41	240	-	0.787	258	1.37	18.1	0.601	63.0	25.7	0.755	3.26
B.16	1	0.002	2	0.001	0.03	0.07	0.04	9	2	3	3	6	0.01	8	0.005	3	5	0.01	0.02
B.17	90.8	0.009	124	0.018	0.062	0.035	0.192	91.1	43.4	43.8	2.89	70.8	0.265	11.4	0.088	14.8	222	0.483	0.615
B.18	519	0.063	1730	0.031	1.07	0.356	0.493	1430	63.6	-	97.0	136	0.281	15.0	0.092	22.7	1040	1.62	1.04
B.21	101	0.030	262	0.073	0.042	0.462	0.095	59.0	300	-	14.4	123	2.23	12.6	0.046	39.7	28.2	0.952	0.303
C.03	300	0.022	232	0.153	0.711	0.172	0.372	1230	259	144	237	50.1	3.21	5.32	0.256	41.1	1660	1.64	3.81
C.06	308	0.031	5190	0.049	0.057	0.741	0.399	81.5	225	617	11.4	312	0.014	65.7	0.540	146	1910	1.42	1.81
C.15	7.90	0.030	120	0.058	0.016	0.033	0.053	6.56	104	47.7	0.287	40.2	0.085	5.88	0.113	8.52	154	0.632	0.181

Table A.3: PTE concentrations (mean) in *H. nodiflorum* from the Bussento and Calore Salernitano rivers in 2017. Units are in $\mu g\ g^{-1}$ d.w., unless otherwise specified.

Site	Al	As	Ca	Cd	Co	Cr	Cu	Fe	K	Mg	Mn	Na	Ni	P	Pb	S	Si	V	Zn
B.02	3350	0.064	6760	0.324	0.499	2.42	15.8	1820	35220	4790	207	2910	3.53	1520	< LOD	1353	14860	6.13	48.2
B.04	5160	0.025	11710	0.548	0.44	3.94	22.24	1499	23600	11028	211.02	3687	3.011	1871	< LOD	2859	10220	10.44	58.05
B.06	3179.8	0.02	8160	0.41	1.303	1.941	18.002	1710.2	16564	11620	2786.5	3127	5.251	1024.8	0.01	2873.1	7855	10.331	63.06
B.07	7436	0.119	13546	1.132	1.161	5.908	27.1	4302	32960	12223	632.5	5269	8.346	3186	0.039	3291	31070	20.83	106.72
B.08	763	0.015	3040	0.203	0.264	0.682	6.86	263	15860	6140	177.5	4140	2.73	1174	< LOD	2222	4840	6.25	26.9
B.10	5949	0.136	18366	1.992	2.94	13.318	19.42	4957	31932	15426	1680	2787	69.18	4996	< LOD	4296	32142	27.80	162.45
B.11	3713	0.046	9780	0.852	0.422	4.919	9.207	1252	21812	11240	289.76	2985	20.126	2945.3	0.057	3211.9	11630	14.915	46.31
B.17	14820	0.074	33950	< LOD	4.77	10.656	25.81	21860	36340	11002	8986	5311	7.741	3133	0.16	4301	35740	22.32	106.03
B.18	4060	0.049	7710	1.105	0.766	2.97	43.2	1250	60000	6770	153	4250	8.8	1860	0.191	2220	10310	13.9	94.2
B.21	13950	0.197	17690	14.16	1.395	46.5	40.21	4168	41010	13420	5210	3233	293.59	5547	0.155	4070	29450	62.813	254.76
B.23	1158	0.036	3725	0.195	0.173	1.446	2.213	649.8	2907	1012	103.3	368.44	3.50	790	< LOD	467.64	6418	2.60	9.64
B.25	2112	0.057	7880	0.852	0.55	1.222	7.93	911	55530	7120	591	5540	1.945	1644	0.101	1617	8630	3.94	27.5
C.03	873.4	0.076	4610	8.263	0.18	4.216	6.678	357.6	43840	10366	51.87	3591.6	56.39	1965	< LOD	2719.5	3160	11.668	326.85

Table A.4: PTE concentrations (s.e.m.) in *H. nodiflorum* from the Bussento and Calore Salernitano rivers in 2017. Units are in μg g^{-1} d.w., unless otherwise specified.

Site	Al	As	Ca	Cd	Co	Cr	Cu	Fe	K	Mg	Mn	Na	Ni	P	Pb	S	Si	V	Zn
B.02	2390	0.046	5030	0.229	0.375	1.80	12.0	1390	15100	3480	151	2120	2.59	1100	< LOD	976	10900	4.41	35.1
B.04	1290	0.014	2460	0.008	0.072	1.15	1.19	330	1270	743	9.18	248	0.276	174	< LOD	34.2	2350	2.51	2.58
B.06	73.4	0.007	472	0.015	0.056	0.045	0.593	49.8	905	429	96.8	105	0.430	33.2	0.010	69.5	207	0.345	1.60
B.07	362	0.011	521	0.070	0.097	0.224	2.24	447	3400	739	47.8	513	0.691	294	0.039	110	3140	1.25	5.20
B.08	326	0.006	1080	0.093	0.113	0.297	2.92	110	6800	2620	75.3	1750	1.17	496	< LOD	951	2040	2.73	11.5
B.10	1	0.002	2	0.001	0.03	0.07	0.04	9	2	3	3	6	0.01	8	0.005	3	5	0.01	0.02
B.11	529	0.002	1170	0.054	0.029	0.480	0.133	151	789	1130	8.44	120	0.524	70.9	0.036	75.3	200	0.698	1.78
B.17	1510	0.017	1890	< LOD	0.362	0.769	2.09	1370	2400	477	528	366	0.770	194	0.078	138	2460	2.19	5.57
B.18	3350	0.039	6390	0.893	0.626	2.41	35.1	1010	1000	5520	125	3450	7.17	1520	0.191	1810	8280	11.4	76.5
B.21	1060	0.001	1830	0.002	0.062	1.61	1.90	131	3410	1830	156	542	6.69	255	0.155	110	3350	0.693	4.21
B.23	1	0.002	2	0.001	0.03	0.07	0.04	9	2	3	3	6	0.01	8	0.005	3	5	0.01	0.02
B.25	910	0.024	3370	0.361	0.234	0.528	3.39	390	3880	3080	253	2380	0.844	705	0.080	690	3660	1.66	11.7
C.03	78.8	0.008	1170	0.199	0.003	0.491	0.176	16.5	878	836	1.27	57.0	2.56	21.8	< LOD	14.4	201	0.565	4.56

Table A.5: PTE concentrations (mean) in *M. aquatica* from the Bussento river in 2016. Units are in $\mu g\ g^{-1}$ d.w., unless otherwise specified.

Site	Al	As	Ca	Cd	Co	Cr	Cu	Fe	K	Mg	Mn	Na	Ni	P	Pb	S	Si	V	Zn
B.01	3175.5	0.12	5742	0.501	2.806	2.885	19.817	2413.2	31709	4045.8	1376.7	8242.9	6.765	1625.4	1.6	3228.1	9058	25.08	63.45
B.02	2204.8	0.278	6932	0.453	5.901	2.659	15.714	11353	20476	5201.7	643.8	3514.3	4.272	1030.6	1.31	2671.3	7798	27.658	35.22
B.03	3421.8	0.13	6504	0.539	2.278	3.12	20.831	2579.1	23331	4124.9	1044	4641	5.279	1165.9	0.998	2426.7	10806	25.752	30.395
B.04	825.3	0.077	4076	0.254	1.364	1.065	16.218	1468	14237	3486	534	5122	2.639	944	0.69	2304	3213	17.527	34.14
B.05	2220.2	0.021	5483	0.337	0.776	1.944	21.031	1047.99	26464	4448.7	146.99	3535.3	3.464	1576.6	0.776	2327.6	6890.8	23.739	45.962
B.06	4736	0.163	8422	0.316	3.834	3.731	9.363	4888	32940	3446	1567	5950	5.608	1596.5	1.436	4052	15285	25.62	31.66
B.07	2513.8	0.134	5577	0.647	2.288	2.664	12.444	1909.4	30981	4161.4	1179	4303.9	8.314	1448.8	1.807	3146.7	21053	25.834	53.26
B.08	3070.4	0.112	7314	0.588	1.267	2.668	8.792	1507.5	30010	4615	187.84	4514.6	10.231	1441.3	0.953	2910.2	12778	27.749	39.02
B.09	1775.3	0.127	6046.2	0.511	2.775	2.799	12.716	2747	42052	3841.2	1372.4	3971.2	10.851	2476.1	1.204	4026	14805	23.292	37.87
B.10	6780.6	0.205	10386.4	1.061	4.695	6.093	10.587	4488.5	40211	5118.2	1736.2	4072.5	20.003	2041.4	1.414	3882.1	28461	37.545	41.962
B.11	1525.1	0.073	5900	1.122	0.683	2.244	6.416	872.1	50904	5908.1	54.5	2562.2	44.01	2865.8	0.144	4272.9	11088	31.524	30.75
B.12	2088.4	0.069	7150.9	0.257	0.73	1.958	17.652	953.9	19109	3602.5	46.85	2579	3.232	1764.7	1.099	2521.1	7895	20.452	38.88
B.13	1676	0.01	5378	0.364	0.721	2.096	16.248	853.7	20047	5751.3	47.851	4236.8	3.871	1665.7	0.499	2934.4	5527	29.288	32.96
B.14	5240	0.141	10274	0.366	2.011	3.894	16.888	2850	32565	3968	387.7	3367.2	3.491	1662.8	1.657	3891.9	23350	27.68	79.82
B.15	349.3	0.054	8748	0.421	1.528	1.409	12.119	920.4	22189	2745.4	611.8	4029.2	4.371	1065.9	0.305	2471	4615.8	15.212	17.524
B.16	2188.6	0.039	5197	0.115	0.677	1.817	10.694	1039.2	8647	2388	100.21	3156	1.32	1420.2	0.206	1320.8	6445	14.4	19.425
B.17	5700	0.245	14322	0.554	4.986	5.151	11.265	6355	34570	4983	3685	3551	5.835	1559	1.279	3901	25620	34.43	29.74
B.18	3889	0.46	10710	0.814	11.48	4.466	7.166	18880	26026	4566	993.9	6539	10.138	1444.7	2.06	3897	22930	34.49	32.813
B.19	5529	0.137	10230	0.463	1.99	4.17	22.462	2664	17715	5842	320.3	5530	5.661	1351.5	1.859	2411.8	17750	35.55	45.01
B.20	2917	0.06	7244	0.813	1.192	2.831	17.75	1346.1	24368	4288.9	202.1	4022.4	9.519	1314.4	0.916	2881.4	8320	25.348	47.06
B.21	4973	0.298	11667	0.896	4.815	5.983	22.596	7547	26897	6956.3	1950.1	3180.12	14.315	1394.13	1.69	3140	24983	60.85	31.666

Table A.6: PTE concentrations (s.e.m.) in *M. aquatica* from the Bussento river in 2016. Units are in μg g^{-1} d.w., unless otherwise specified.

Site	Al	As	Ca	Cd	Co	Cr	Cu	Fe	K	Mg	Mn	Na	Ni	P	Pb	S	Si	V	Zn
B.01	81.6	0.001	179	0.017	0.135	0.096	0.282	84.1	311	46.3	49.6	80.1	0.181	14.8	0.126	70.5	210	0.524	2.61
B.02	60.9	0.009	259	0.009	0.134	0.121	0.334	218	168	35.6	16.1	39.9	0.113	13.4	0.096	32.7	120	0.616	1.67
B.03	65.8	0.012	292	0.017	0.074	0.061	0.454	39.8	256	57.9	32.3	86.1	0.116	10.3	0.041	16.5	114	0.357	0.409
B.04	23.6	0.031	209	0.024	0.122	0.090	0.561	124	428	194	30.0	199	0.357	33.2	0.108	106	217	0.821	1.32
B.05	23.8	0.011	321	0.002	0.015	0.029	0.454	3.88	288	91.9	4.17	65.2	0.095	24.8	0.184	44.6	86.5	0.253	0.795
B.06	378	0.016	382	0.036	0.381	0.293	0.356	462	1290	240	160	352	0.398	36.4	0.233	217	855	1.83	1.30
B.07	31.1	0.010	208	0.024	0.093	0.046	0.369	33.9	321	56.4	53.4	36.9	0.178	21.8	0.093	42.5	692	0.161	1.50
B.08	96.6	0.014	426	0.012	0.036	0.015	0.274	51.1	491	120	8.15	84.7	0.310	46.5	0.051	29.8	393	0.398	1.26
B.09	34.4	0.006	57.7	0.026	0.045	0.034	0.315	101	646	79.1	27.6	65.7	0.346	55.2	0.194	114	174	0.390	1.63
B.10	40.3	0.014	65.7	0.015	0.051	0.072	0.091	47.3	226	28.6	26.6	37.2	0.116	11.4	0.053	52.8	392	0.596	0.510
B.11	48.4	0.015	372	0.038	0.020	0.056	0.054	15.2	311	71.4	0.770	20.3	1.01	28.6	0.076	41.8	120	0.506	0.402
B.12	43.0	0.006	87.4	0.014	0.022	0.054	0.398	23.8	498	71.8	1.18	45.6	0.163	46.4	0.138	51.6	208	0.467	2.02
B.13	130	0.005	365	0.008	0.027	0.094	0.241	65.4	250	70.9	0.819	60.9	0.126	11.0	0.064	31.0	640	0.923	1.46
B.14	648	0.014	459	0.010	0.188	0.408	0.336	265	936	119	15.1	54.6	0.301	17.0	0.047	62.7	1960	2.02	1.79
B.15	24.0	0.008	533	0.022	0.020	0.008	0.184	26.8	172	92.0	13.3	32.7	0.107	12.8	0.128	20.1	30.2	0.347	0.111
B.16	83.7	0.007	270	0.011	0.024	0.072	0.329	46.6	223	108	5.16	102	0.109	29.5	0.169	25.0	280	0.765	0.588
B.17	387	0.016	992	0.032	0.247	0.390	0.644	383	2390	359	250	243	0.427	109	0.652	273	1560	2.46	2.20
B.18	138	0.040	235	0.047	0.418	0.192	0.120	1010	538	125	52.5	118	0.242	30.7	0.096	103	1390	1.17	0.248
B.19	522	0.013	1290	0.037	0.125	0.269	0.656	188	798	295	22.5	235	0.406	28.1	0.008	70.8	1200	2.18	2.02
B.20	110	0.023	271	0.052	0.082	0.113	0.356	66.7	271	87.3	10.7	15.0	0.490	25.2	0.505	42.1	122	0.675	1.61
B.21	132	0.016	463	0.016	0.115	0.170	0.373	154	377	46.8	48.5	7.35	0.184	8.16	0.064	31.2	529	0.792	0.703

Table A.7: PTE concentrations (mean) in *M. aquatica* from the Bussento river in 2017. Units are in $\mu g\ g^{-1}$ d.w., unless otherwise specified.

Site	Al	As	Ca	Cd	Co	Cr	Cu	Fe	K	Mg	Mn	Na	Ni	P	Pb	S	Si	V	Zn
B.02	2322.4	0.111	5112	0.291	0.728	2.047	14.4	1428.9	22814	4711	166.7	7558.4	3.384	1306.1	0.26	2040	7437	34.037	26.195
B.04	3694	0.337	6987	0.499	1.131	3.742	10.12	1827.3	46647	4235.6	478.37	2739	5.107	2083.5	0.551	3277.8	27522	33.781	25.533
B.06	354.1	0.447	9427	0.487	3.619	3.144	6.095	6650.4	27431	3585.4	3710.5	4505.5	5.056	1371.1	0.787	3532	31820	26.934	15.679
B.07	1149.2	0.101	4123	0.364	0.572	1.68	10.035	647.5	21701	3545.1	632.42	4579.4	5.085	1491.8	0.259	2301.5	4035	25.772	29.68
B.08	362.3	0.163	8045	0.342	0.431	1.572	4.779	382.5	33950	2535	269.93	2689	8.375	1417.9	0.248	2718.1	13514	18.113	27.152
B.10	2372	0.517	9687	1.222	6.291	5.268	10.733	13062	34430	4926	3572.8	2102.4	23.219	2828.2	0.795	4369	31458	40.146	41.338
B.11	5390	0.232	9694	3.314	1.287	6.985	7.619	2451.2	45152	5231.6	211.1	1523.83	144.61	3066.6	0.381	3128.7	17678	45.58	129.44
B.12	892.7	0.033	4105	0.194	0.242	1.548	3.906	378.1	14533	2336.5	36.461	3072	1.911	1315.9	0.157	2513.5	3233	16.716	34.76
B.13	1384.6	0.16	5614	0.447	2.086	3.37	9.842	3774.2	32446	4077.8	1423.5	3120.8	7.651	1733.3	0.379	2854.7	9336	30.891	53.892
B.14	1110.7	0.244	5838	0.641	4.031	2.467	12.141	5855	35968	4779.9	1517.5	3739.9	5.94	1867.4	0.75	3707	14861	35.024	49.46
B.15	33.32	0.176	5869	0.398	0.346	0.674	4.854	102.35	18228	1310	111.31	3357.3	7.296	883.8	0.314	1911.6	13396.7	11.223	14.291
B.17	3478.7	0.193	11868	0.32	4.538	4.973	8.59	9772	23520	3910	5799	5124	4.91	1712	0.531	3381	13288	35.01	24.08
B.18	3298	0.215	8013	0.461	1.336	3.602	6.487	2112	21143	3298	487.6	1611	9.375	936.3	0.419	2301.2	17590	28.46	26.65
B.19	3456	0.071	7781	0.098	0.684	2.72	12.74	1639	11174	2862	69.08	4942	2.02	760	0.206	1319	9079	24.52	14.97
B.20	761	0.064	2900	0.511	0.536	1	7.09	573	17350	2166	411	1683	6.23	540	0.149	1160	2413	15.68	27.85
B.23	1213.8	0.159	4008.4	1.608	0.41	2.741	5.242	635.1	43210	5414	79.53	1910.9	98.72	1384.9	0.305	2400	7969	38.736	36.91
B.24	7755	0.251	15938	0.442	1.719	6.202	15.204	3464	17251	4019.6	302.24	2705.3	4.536	814.1	0.436	1807.5	21390	40.81	28.635
B.25	2573	0.372	5685	0.469	1.029	2.333	5.665	1005	47310	3610	108.06	3165	4.017	1837	0.566	2529	28260	26.48	16.563

Table A.8: PTE concentrations (s.e.m.) in *M. aquatica* from the Bussento river in 2017. Units are in $\mu g\ g^{-1}$ d.w., unless otherwise specified.

Site	Al	As	Ca	Cd	Co	Cr	Cu	Fe	K	Mg	Mn	Na	Ni	P	Pb	S	Si	V	Zn
B.02	42.5	0.013	138	0.025	0.014	0.056	0.310	32.6	310	106	1.78	97.7	0.590	23.8	0.019	56.0	214	0.636	0.486
B.04	70.9	0.021	328	0.062	0.026	0.044	0.085	74.1	591	92.9	7.31	13.1	0.377	55.8	0.116	59.3	248	0.755	0.993
B.06	18.5	0.020	184	0.089	0.045	0.092	0.568	86.9	554	21.0	61.8	69.3	0.598	25.1	0.073	105	1030	0.445	0.255
B.07	56.2	0.029	156	0.071	0.035	0.119	0.173	41.6	299	22.7	6.55	36.8	0.599	43.8	0.100	71.7	122	0.049	0.549
B.08	51.2	0.010	151	0.063	0.034	0.123	0.164	12.6	1120	157	8.90	119	0.563	14.9	0.081	66.0	326	0.660	0.590
B.10	27.3	0.014	149	0.071	0.053	0.087	0.111	110	734	131	29.0	41.5	0.746	68.2	0.014	87.7	425	0.791	0.485
B.11	121	0.011	241	0.042	0.052	0.226	0.097	90.7	296	50.9	4.34	8.17	2.65	33.6	0.029	52.9	376	1.11	3.22
B.12	10.3	0.017	143	0.062	0.003	0.024	0.029	4.36	330	73.3	0.715	163	0.262	64.3	0.024	45.3	154	0.218	2.27
B.13	16.5	0.017	289	0.022	0.032	0.017	0.112	37.9	191	20.3	26.8	25.6	0.363	42.3	0.015	63.4	228	0.238	0.979
B.14	28.9	0.007	145	0.014	0.080	0.077	0.352	102	692	94.4	25.3	71.3	0.288	49.5	0.033	124	447	0.511	1.62
B.15	2.34	0.019	272	0.026	0.008	0.058	0.198	7.65	339	181	1.38	62.4	0.191	18.6	0.028	21.7	97.8	0.936	0.541
B.17	56.4	0.009	309	0.035	0.201	0.192	0.439	290	1380	182	215	326	0.639	97.4	0.039	197	376	1.48	2.50
B.18	292	0.019	882	0.038	0.097	0.155	0.494	174	871	214	27.0	116	0.632	44.9	0.064	50.0	1140	1.26	1.84
B.19	1	0.002	2	0.001	0.03	0.07	0.04	9	2	3	3	6	0.01	8	0.005	3	5	0.01	0.02
B.20	267	0.028	946	0.191	0.190	0.360	2.56	205	6080	770	145	590	2.30	190	0.072	397	849	5.57	9.98
B.23	38.8	0.020	77.8	0.042	0.008	0.178	0.211	43.4	1490	109	2.27	55.3	2.39	53.3	0.029	111	355	0.734	1.73
B.24	141	0.032	388	0.013	0.046	0.221	0.578	118	440	59.8	1.90	36.6	0.349	14.9	0.042	30.5	1560	0.274	0.158
B.25	951	0.205	204	0.174	0.510	0.971	0.386	336	2810	115	7.15	152	0.889	115	0.225	204	15800	1.42	0.652

Table A.9: PTE concentrations (mean) in *M. aquatica* from the Calore Salernitano river in 2016. Units are in μg g^{-1} d.w., unless otherwise specified.

Site	Al	As	Ca	Cd	Co	Cr	Cu	Fe	K	Mg	Mn	Na	Ni	P	Pb	S	Si	V	Zn
C.01	3046	0.293	7943	0.432	3.534	3.39	14.2	4933	20421	4365.5	1225.4	4242	8.173	1207.4	1.65	2859.52	26769	28.326	23.31
C.02	1997.1	0.101	5851	0.294	1.221	1.728	13.736	1257.8	19110	3443.5	352.52	2012.9	4.634	1003.51	0.697	2032	11183	20.529	18.912
C.03	1187.9	0.316	4900.8	12.238	0.86	7.025	7.286	771.2	52596	4768.3	57.577	1293.3	103.508	2346.27	0.321	3327.7	5740	26.033	197.94
C.04	4871	0.153	9564	0.957	2.661	4.616	27.95	4446	20330	4238	302.9	3817	10.75	1128	1.26	2278	17240	30	37.4
C.05	5754	0.224	10791	0.413	2.778	5.056	24.527	4661.9	21284	4311.7	602.78	3373.1	6.175	1259.59	1.447	2720.8	23209	32.07	32.405
C.06	1395.2	0.09	4358	2.208	0.799	1.581	7.419	777.5	33271	2447.8	195.79	2715	3.626	1482.5	0.345	2837.1	8317	17.201	15.481
C.07	2000.5	0.067	5528.1	0.183	0.676	1.788	24.284	884.3	18530	3274	81.026	1578.94	1.794	537.98	0.562	1412.35	6116.6	18.446	25.947
C.08	3370.5	0.093	7113	0.698	1.344	3.25	19.979	1649.8	28054	3992.3	81.65	3712.6	6.817	734	0.914	2476	15092	25.232	36.992
C.09	10180	0.691	19763	0.618	9.935	8.496	16.012	16171	20488	4245.6	2738.1	3446.7	11.101	1246.6	3.5	2937.6	43951	43.32	41.416
C.10	3433	0.133	7367	0.402	1.533	2.532	19.16	1749.8	19410	4044	238.6	3763	5.179	1115.8	0.964	2123	15961	25.643	67.87
C.11	1514	0.072	6640	0.142	0.611	1.573	27.38	835.4	15620	2891	40.3	2375	1.612	986.2	0.754	1609	5038	16.21	25.03
C.12	1665.7	0.116	5514	0.756	2.011	1.858	19.02	2143	26744	4049	815.2	2558.3	8.76	1011.7	1.149	2149.4	6487	21.178	41.505
C.13	5544	0.196	9756	0.437	2.073	4.847	17.696	3259	27003	3966	220.26	3485	7.836	1706.8	1.37	2834	25158	31.81	35.042
C.14	622.2	0.043	4207.3	0.161	0.513	1.008	10.757	681.9	15399	2478.2	103.95	1974.2	1.345	976.5	0.456	1213.2	2544	12.084	37.97
C.15	2695.9	0.145	5399	2.425	1.365	2.989	17.255	2208	24962	4219	143.02	3824.7	6.863	1189.3	1.339	2371.7	13690	29.491	29.798
C.16	1693	0.077	6233	0.42	1.192	1.644	19.391	832.7	23145	3758	439	3092.9	5.211	1533.4	0.999	2839.1	8090	20.647	86.21
C.17	368.2	0.061	4907	0.446	0.936	1.017	27.042	543.3	26984	3718	302.22	3568.9	6.789	1203	1.369	2467.8	1955.9	17.163	55.582
C.18	3836	0.084	7352	0.458	1.164	2.93	15.893	1656.6	20639	5428	96.69	4479	3.523	1162.4	0.405	2342.7	11574	32.59	27.431

Table A.10: PTE concentrations (s.e.m.) in *M. aquatica* from the Calore Salernitano river in 2016. Units are in $\mu g\ g^{-1}$ d.w., unless otherwise specified.

Site	Al	As	Ca	Cd	Co	Cr	Cu	Fe	K	Mg	Mn	Na	Ni	P	Pb	S	Si	V	Zn
C.01	101	0.012	330	0.011	0.028	0.054	0.271	38.8	168	55.9	41.7	76.9	0.135	17.0	0.003	9.85	343	0.327	1.06
C.02	25.7	0.008	219	0.007	0.007	0.032	0.373	12.3	325	19.7	5.22	32.3	0.050	7.85	0.141	25.6	136	0.140	0.097
C.03	63.3	0.012	42.2	0.059	0.041	0.014	0.140	46.7	868	30.8	0.599	19.0	0.184	6.36	0.108	46.4	247	0.140	2.05
C.04	469	0.022	625	0.682	0.237	0.571	1.70	416	3140	416	23.8	233	5.53	110	0.112	214	1480	2.88	10.7
C.05	116	0.012	165	0.003	0.030	0.047	0.369	48.3	458	48.0	9.00	96.6	0.178	7.28	0.025	34.4	461	0.684	0.935
C.06	40.5	0.008	141	0.062	0.043	0.092	0.082	63.7	418	42.8	4.34	43.6	0.204	28.2	0.128	66.6	321	0.483	0.575
C.07	20.8	0.006	98.4	0.018	0.029	0.099	0.414	59.9	84.7	112	0.921	5.82	0.068	2.67	0.248	2.64	84.0	0.334	0.995
C.08	49.0	0.009	148	0.023	0.003	0.020	0.085	29.5	156	52.6	3.71	39.3	0.135	354	0.025	11.1	199	0.341	0.597
C.09	138	0.012	237	0.030	0.131	0.147	0.412	139	114	62.4	50.3	43.8	0.243	10.4	0.063	57.7	997	0.344	0.554
C.10	153	0.008	161	0.012	0.063	0.059	0.392	58.8	824	119	11.7	102	0.100	16.3	0.145	67.1	814	0.659	2.51
C.11	156	0.016	1590	0.045	0.067	0.071	2.73	78.3	1270	432	3.96	254	0.580	64.8	0.169	219	543	2.21	4.58
C.12	74.3	0.002	370	0.033	0.061	0.061	0.364	93.6	139	103	16.4	44.9	0.298	11.2	0.056	62.6	321	0.498	0.522
C.13	270	0.003D	272	0.019	0.063	0.186	0.311	151	442	126	4.53	142	0.236	33.0	0.063	142	681	1.62	0.847
C.14	10.1	0.012	99.8	0.020	0.020	0.024	0.208	22.6	701	50.1	3.93	56.2	0.096	13.2	0.192	31.6	117	0.339	2.30
C.15	38.7	0.015	281	0.065	0.019	0.046	0.252	37.0	392	67.4	1.13	59.6	0.146	20.8	0.042	17.4	166	0.376	0.168
C.16	99.3	0.003	252	0.007	0.056	0.085	0.578	41.4	288	188	16.2	74.9	0.206	44.9	0.101	66.3	541	0.968	3.25
C.17	20.1	0.006	538	0.015	0.029	0.021	0.357	13.7	311	80.9	6.53	49.1	0.200	15.8	0.133	21.6	22.8	0.414	0.280
C.18	249	0.004	307	0.019	0.076	0.031	0.707	84.0	554	282	5.81	234	0.203	46.2	0.089	83.1	536	1.95	0.805

Table A.11: PTE concentrations (mean) in *M. aquatica* from the Calore Salernitano river in 2017. Units are in μg g^{-1} d.w., unless otherwise specified.

Site	Al	As	Ca	Cd	Co	Cr	Cu	Fe	K	Mg	Mn	Na	Ni	P	Pb	S	Si	V	Zn
C.01	124.9	0.341	11355	0.465	1.874	2.235	5.25	1676	22350	1023.3	3153	1838	11.83	711	0.454	2381.9	23170	10.556	16.78
C.02	6.48	0.063	4044	0.226	0.109	0.113	3.293	46.6	16514.2	1347.4	115.27	993.65	4.329	549.21	0.102	1415.3	1873.7	9.042	12.832
C.03	475	0.112	3707	5.635	0.173	2.785	2.783	308.03	42499	1996.3	32.273	1143	50.85	1713.9	0.177	2239.1	1502.7	14.56	137.43
C.04	295.9	0.079	5228	0.252	0.493	1.157	8.125	392.27	14938	1868.3	903.5	1863.2	3.176	474.69	0.262	1548.1	4968.7	12.435	12.571
C.05	2788.8	0.434	11209	0.585	3.886	4.44	8.639	9869	17348	2957.7	2047.6	2329.8	5.366	749.9	0.934	2253.8	28332	24.699	19.019
C.06	523.4	0.091	3113	2.038	0.72	1.743	4.33	862.1	25067	1896.9	494.58	2365.64	3.26	706.54	0.304	1855.7	4618.6	14.119	9.767
C.07	3345	0.177	8960	0.559	0.93	3.716	18.688	1776	17232	2510.6	161.26	2309.4	6.92	548	0.906	1564.9	10297	24.093	42.231
C.08	2121.8	0.137	4982	0.58	0.638	2.486	15.336	1068.2	17905	2812.2	71.03	2081	3.77	717.97	0.252	1695.81	7719	23.049	42.39
C.09	3093	0.53	17915	0.52	8.435	5.191	7.951	21921	13971	2355	2898.5	2627	5.713	1048.7	0.745	2691.4	15051	24.24	27.99
C.10	1319	0.111	5629	0.502	0.54	1.603	9.124	865.3	15762	2267	129.93	2185.2	3.259	604	0.275	1511.1	5875	17.452	20.401
C.12	3601	0.287	11191.1	0.902	4.242	4.449	14.774	9703.8	25345	3312.1	1605.5	2115.15	7.943	1075.23	0.551	2135.04	4320	30.217	39.854
C.13	1341.9	0.174	5068	0.487	3.401	2.819	6.413	4769	24703	3066	2395.6	3484	7.485	1390.1	0.451	2261.1	11492	24.09	26.84
C.14	321.77	0.196	4337	0.362	0.383	0.807	5.332	238.75	20346	1719.47	99.76	1198.4	2.24	868.8	0.438	1911.91	12495	12.417	11.648
C.15	1166.2	0.183	4911	1.914	1.106	2.635	9.19	2924	26810	3302	244.9	2635.2	6.41	961.6	0.464	1927.4	9274	24.48	32.5
C.20	4493	0.198	10340	0.67	1.447	4.325	17.023	3401	17595	2760	508.4	2677.6	4.418	741.2	0.404	1657.7	12675	27.944	48.41

Table A.12: PTE concentrations (s.e.m.) in *M. aquatica* from the Calore Salernitano river in 2017. Units are in μg g^{-1} d.w., unless otherwise specified.

Site	Al	As	Ca	Cd	Co	Cr	Cu	Fe	K	Mg	Mn	Na	Ni	P	Pb	S	Si	V	Zn
C.01	21.6	0.026	930	0.073	0.110	0.165	0.652	123	1920	84.1	177	112	0.809	25.9	0.063	25.7	1110	0.629	2.42
C.02	1.53	0.010	280	0.018	0.006	0.045	0.077	4.70	67.8	73.4	1.28	7.84	0.382	1.83	0.048	12.5	31.6	0.396	0.524
C.03	21.6	0.008	256	0.059	0.015	0.090	0.131	2.62	222	39.6	0.457	5.65	1.03	22.0	0.080	34.4	57.6	0.449	2.16
C.04	14.7	0.003	569	0.038	0.027	0.090	0.069	2.64	133	63.8	10.1	27.4	0.205	1.84	0.012	25.6	62.4	0.191	0.221
C.05	15.1	0.016	398	0.045	0.023	0.171	0.612	332	473	89.6	51.5	90.5	0.311	19.3	0.078	15.9	263	0.256	0.972
C.06	18.5	0.009	123	0.041	0.026	0.168	0.054	25.8	150	57.7	3.66	2.78	0.088	3.39	0.022	15.4	85.3	0.311	0.163
C.07	103	0.010	324	0.052	0.037	0.085	0.666	35.4	814	45.5	1.35	47.7	0.406	16.3	0.082	22.5	332	0.289	0.944
C.08	51.0	0.008	160	0.025	0.029	0.163	0.494	57.2	123	86.1	2.67	35.1	0.117	9.35	0.017	6.84	214	0.351	1.27
C.09	304	0.030	514	0.023	0.250	0.171	0.853	888	787	100	97.0	112	0.454	49.9	0.084	87.8	269	1.98	1.82
C.10	10.7	0.011	278	0.028	0.025	0.061	0.394	31.6	136	12.2	1.23	14.2	0.305	10.7	0.028	17.9	239	0.350	0.639
C.12	128	0.024	83.7	0.018	0.024	0.365	0.038	82.8	333	44.0	17.2	5.19	0.385	8.65	0.002	6.43	4140	0.921	0.281
C.13	85.1	0.011	248	0.027	0.157	0.104	0.626	179	700	123	86.4	103	0.389	66.3	0.016	66.8	698	1.38	1.56
C.14	3.23	0.001	520	0.013	0.034	0.054	0.150	2.92	389	8.85	3.96	15.1	0.014	19.1	0.065	8.49	203	0.132	0.757
C.15	86.1	0.006	208	0.115	0.055	0.117	0.147	201	1080	135	10.3	56.5	0.267	29.3	0.008	17.4	670	1.10	0.669
C.20	173	0.003	567	0.022	0.052	0.198	0.827	127	989	142	4.00	65.1	0.089	27.7	0.016	19.6	712	0.808	6.19

Appendix B

PTE concentrations in active biomonitors

Table B.1: PTE concentrations (mean) in *F. antipyretica* from the Bussento river. Units are in μg g^{-1} d.w., unless otherwise specified.

Site	Al	As	Ca	Cd	Co	Cr	Cu	Fe	K	Mg	Mn	Na	Ni	P	Pb	S	Si	V	Zn
B.02	168.9	0.545	3471	0.975	0.753	1.289	3.748	296.6	3232.4	451.6	303.28	10.288	5.678	762.6	< LOD	1179.4	31350	14.558	0.743
B.04	6270	0.427	5910	0.819	1.619	3.82	8.51	1284	6439	1456	943.3	61.7	8.82	1534	< LOD	1439.7	27400	30.41	1.828
B.06	4250	0.635	4575	1.093	1.483	2.802	8.685	889	5077	1161	442.4	67.91	10.055	807	< LOD	883.7	39540	32.53	1.446
B.07	689	0.345	2598	0.793	0.834	1.043	5.61	272.3	5853	747	526.3	26.612	8.596	1939	< LOD	1226.5	20078	15.57	1.258
B.08	6934	0.654	8253	1.181	1.842	4.987	8.073	1379.3	7008	1293	746.5	42.88	18.629	1508.3	< LOD	1165.8	42020	38.281	1.867
B.10	2092	0.186	3075	0.557	1.273	1.691	7.056	559.8	6779	911	970.4	34.95	11.523	2055.3	< LOD	1355.7	11566	24.28	1.395
B.11	6850	0.516	8160	0.995	1.966	4.934	12.11	1493	6801	1116	432.9	36.18	20.95	1699.1	< LOD	1027.3	31170	42.4	1.906
B.12	1799	0.434	4714	0.793	1.172	3.008	6.515	709.2	4302	764.4	239.1	14.93	10.21	1322	< LOD	990	26345	28.75	1.534
B.13	995	0.516	2830	0.909	1.203	1.056	7.672	273.1	4632	774	982	20.94	10.331	2163	< LOD	1349.9	28280	15.837	2.231
B.14	8007	0.742	17100	1.474	2.123	3.654	15.507	2581	7430	2585	1445	432.09	34.46	3219.8	1.072	1108.6	9340	23.68	57.96
B.15	29.33	0.295	8387	0.68	0.573	0.755	4.505	151.9	2705	343.5	308.6	73.09	17.63	1468.2	< LOD	573.3	13080	6.81	17.133
B.16	4880	0.285	5333	0.716	1.652	3.259	12.74	1172	5256	1218	629.4	14.84	8.429	2005	0.017	1354	21940	30.97	1.431
B.17	1094	0.581	10392	1.468	1.908	1.796	12.56	806	7319	945	3104	157.9	35.2	4093	0.303	1211.9	24940	14.59	48.84
B.18	16120	0.762	32810	1.429	2.665	8.08	22.38	6670	12601	3287	1466.5	586.4	54.01	3152	2.798	1341.5	34590	45.17	64.66
B.19	9420	0.566	19720	1.011	2.15	5.08	20.51	3980	10050	2421	1932	394.3	35.22	3314.4	1.774	1243.8	25740	27.04	63.07
B.20	24720	0.872	34424	1.548	3.304	11.1	26.31	9560	14746	4409	1320.5	871	57.74	3722	4.061	1212.2	43940	50.25	67.2
B.21	38260	1.571	28476	2.519	4.729	16.59	25.801	16046	13929	4504.1	1184.3	670.35	107.42	2987.9	6.065	1147.4	71792	106.65	66.84
B.22	2275	0.375	3214	0.853	1.145	1.851	6.246	545.9	5766	892.8	1029	12.833	15.738	1569.2	< LOD	1013.9	20585	27.73	1.574
B.23	556	0.385	2886	0.924	1.951	1.156	6.409	323.6	5237	681	1713	15.25	19.26	2162.5	< LOD	1250	21281	20.626	1.745
B.24	341	0.204	2404	0.57	1.093	0.751	4.296	194.3	4160	511.1	756	10.45	6.39	1409	< LOD	1001.7	11185	14.49	1.27
B.25	4448	0.954	17170	2.209	2.088	3.021	16.79	1623	8682	1271	1691	398.5	34.67	4193	0.845	1356.2	39241	15.72	55.86
B.26	24160	0.946	35200	1.619	3.641	12.28	31.48	10970	16867	4659	2179.1	893.9	50.44	4298	4.518	1407.9	46860	50.84	85.36
B.27	12100	0.673	30550	1.201	1.786	5.967	19.04	4792	10939	2524	575.1	361.8	62.6	3325	1.994	1174.2	31330	34.14	49.18
B.28	4224	0.636	16260	1.452	1.264	2.919	17.9	1935	10995	1675	935	394.3	24.37	4105	0.739	1306.5	23530	17.282	46.92
B.29	17010	1.282	41770	2.385	3.176	7.606	20.03	6251	12159	3105	1428	522.3	62.6	4069	2.757	1296.2	57920	33.8	64.36

Table B.2: PTE concentrations (s.e.m.) in *F. antipyretica* from the Bussento river. Units are in $\mu g\ g^{-1}$ d.w., unless otherwise specified.

Site	Al	As	Ca	Cd	Co	Cr	Cu	Fe	K	Mg	Mn	Na	Ni	P	Pb	S	Si	V	Zn
B.02	61.5	0.009	251	0.026	0.015	0.194	0.033	42.9	83.9	52.3	2.10	0.443	0.076	48.3	< LOD	40.8	1090	0.633	0.037
B.04	2730	0.128	1810	0.144	0.520	1.46	1.81	518	824	350	75.5	18.7	2.35	103	< LOD	78.4	9070	9.98	0.220
B.06	1010	0.036	451	0.030	0.190	0.508	0.447	181	349	154	13.3	8.43	0.889	29.6	< LOD	41.5	2610	4.28	0.131
B.07	306	0.012	125	0.019	0.026	0.052	0.134	27.7	524	112	27.7	0.864	0.376	152	< LOD	42.2	247	1.13	0.080
B.08	212	0.044	295	0.049	0.037	0.129	0.093	34.0	54.1	26.2	43.2	1.07	0.244	41.8	< LOD	19.2	2210	0.682	0.026
B.10	486	0.011	288	0.026	0.072	0.226	0.244	92.7	467	133	63.8	2.28	0.633	84.6	< LOD	34.7	528	1.88	0.092
B.11	1570	0.043	1250	0.029	0.211	0.717	0.955	256	523	144	41.9	3.18	1.26	40.7	< LOD	26.2	3150	4.84	0.117
B.12	501	0.011	191	0.021	0.045	0.163	0.290	44.8	148	34.0	10.5	1.61	0.302	42.9	< LOD	29.3	661	1.35	0.067
B.13	186	0.038	105	0.038	0.076	0.052	0.853	23.6	251	66.9	162	3.37	0.574	156	< LOD	45.5	1870	0.253	0.195
B.14	892	0.026	1180	0.044	0.181	0.317	0.682	243	131	179	240	7.45	2.42	51.1	0.125	45.3	1200	1.16	3.55
B.15	5.13	0.054	393	0.098	0.049	0.068	0.381	16.3	179	26.5	28.7	6.80	1.43	98.5	< LOD	37.6	1880	0.697	0.828
B.16	1180	0.048	603	0.061	0.200	0.569	1.34	252	443	192	72.0	4.35	0.639	239	0.016	102	2300	3.76	0.154
B.17	425	0.031	455	0.067	0.197	0.206	1.19	167	518	191	514	19.6	1.31	239	0.056	51.4	1340	0.979	2.77
B.18	2660	0.053	3350	0.063	0.258	1.19	3.43	1230	805	554	93.8	85.3	4.94	108	0.490	27.2	3070	5.27	3.87
B.19	2370	0.064	3440	0.109	0.262	1.11	2.16	1060	686	419	142	80.9	3.81	70.5	0.437	41.4	4000	3.37	5.09
B.20	2890	0.092	875	0.132	0.294	1.20	1.18	1030	476	367	45.8	77.8	3.60	210	0.472	47.1	4160	4.92	2.99
B.21	1910	0.075	451	0.098	0.060	0.520	0.506	119	195	41.8	30.2	2.35	1.60	16.8	0.205	20.5	416	1.75	1.06
B.22	450	0.010	204	0.020	0.061	0.188	0.238	61.0	317	73.0	110	0.723	0.560	65.9	< LOD	35.7	646	1.84	0.050
B.23	106	0.010	189	0.013	0.223	0.071	0.329	17.7	120	32.6	276	1.11	1.66	38.6	< LOD	14.7	788	0.469	0.195
B.24	172	0.012	192	0.023	0.163	0.154	0.534	44.4	287	86.6	140	1.44	1.03	180	< LOD	66.2	523	2.27	0.211
B.25	944	0.033	1070	0.090	0.190	0.258	1.55	200	244	127	231	27.9	2.14	169	0.102	32.6	897	1.13	3.66
B.26	2070	0.081	1820	0.122	0.304	1.34	1.34	1220	520	320	85.1	93.5	2.77	169	0.501	35.7	4460	4.69	3.82
B.27	1090	0.056	3260	0.090	0.138	0.535	1.12	491	304	146	37.6	30.7	3.40	127	0.211	13.1	3060	2.28	1.96
B.28	730	0.073	1380	0.153	0.101	0.257	0.656	190	394	189	88.3	17.0	1.73	149	0.100	69.1	3580	0.880	2.05
B.29	1230	0.229	2420	0.475	0.313	0.862	1.77	426	800	174	232	25.8	8.55	434	0.336	56.1	5950	5.69	4.73

Table B.3: PTE concentrations (mean) in *F. antipyretica* from the Calore Salernitano river. Units are in $\mu g\ g^{-1}$ d.w., unless otherwise specified.

Site	Al	As	Ca	Cd	Co	Cr	Cu	Fe	K	Mg	Mn	Na	Ni	P	Pb	S	Si	V	Zn
C.01	17.97	0.032	1525	0.439	0.556	1.569	1.26	623	2594	177	236.4	< LOD	10.25	339.4	< LOD	606.6	10728	9.625	0.598
C.03	6263	0.165	5787	1.472	2.74	12.35	7.991	3394	8643	1962	1261.4	22.11	45.12	2132.6	< LOD	1832	32740	35.87	26.49
C.04	1045	0.061	3491	0.502	1.259	5.81	5.273	2167	3527	507.7	743.2	< LOD	9.57	622.7	< LOD	630.3	20840	15.55	9.244
C.05	625	0.033	2765	0.442	0.829	3.34	4.211	1501	3611	488	518.9	< LOD	8.6	426.4	< LOD	396.8	16900	10.43	7.267
C.06	75.9	0.033	1451	1.047	0.478	0.816	1.511	569.4	3173	111.4	248.7	< LOD	8.727	766.9	< LOD	723.7	9424	7.537	2.374
C.07	4360	0.115	4790	0.643	1.926	11.41	6.034	1074.6	4196	1409	369.2	2.02	21.56	398.5	< LOD	539.8	31370	29.51	12.86
C.08	4279	0.065	4206	0.97	1.943	9.277	5.774	4276	7537	1363.4	1462	< LOD	29.07	1314.3	< LOD	1117.7	22710	23.694	16.172
C.09	2061	0.038	2681	0.52	1.04	2.144	5.548	2449.4	4959	408.3	836.7	2.2	14.746	1259.2	< LOD	1409.1	13330	11.504	13.799
C.10	282	0.017	2298	0.425	0.578	2.007	4.362	497.1	3381	216.3	174.5	< LOD	11.16	691.3	< LOD	832.6	14550	13.46	11.3
C.11	38.68	0.052	2956	0.611	0.374	1.597	1.683	258.1	2031.3	217.3	91.7	< LOD	7.411	378.2	< LOD	489.7	16600	7.281	7.09
C.12	1240	0.12	2958	0.83	1.14	5.057	5.526	1304	4176	578.2	447.8	2.9	19.259	797.2	< LOD	958	31088	19.83	15.253
C.13	663	0.112	2484	0.954	0.943	3.283	4.355	1788	5615	557.4	628.7	< LOD	20.4	1593.6	< LOD	1207.6	25557	15.11	12.589
C.14	128.8	0.041	2110	0.664	0.73	2.063	4.1	846.9	4472	256.8	344.3	< LOD	14.418	994.3	< LOD	890.4	14920	13.29	10.586
C.15	8350	0.153	6983	1.381	2.995	17.82	8.884	2905.8	8510	1743	992	22.3	32.09	1631.3	< LOD	1551.3	40320	43.95	18.73
C.19	5980	0.18	7702	0.777	3.047	18.32	10.166	2548	7285	2219	871.8	37.8	28.24	777.9	< LOD	873.9	46190	37.51	18.597
C.20	3867	0.057	4266	0.515	2.563	7.894	6.687	5513	5725	961.6	1882.9	< LOD	25.23	1112.6	< LOD	874.9	22610	16.651	10.389

Table B.4: PTE concentrations (s.e.m.) in *F. antipyretica* from the Calore Salernitano river. Units are in $\mu g\ g^{-1}$ d.w., unless otherwise specified.

Site	Al	As	Ca	Cd	Co	Cr	Cu	Fe	K	Mg	Mn	Na	Ni	P	Pb	S	Si	V	Zn
C.01	2.72	0.004	240	0.037	0.043	0.152	0.176	42.7	158	29.9	15.0	< LOD	0.647	35.7	< LOD	27.3	690	0.421	0.598
C.03	647	0.034	507	0.156	0.209	1.22	0.274	169	186	128	57.4	3.90	1.15	45.7	< LOD	39.3	6170	1.20	2.39
C.04	413	0.023	449	0.063	0.173	1.32	0.662	292	200	89.2	99.3	< LOD	1.82	27.4	< LOD	27.6	3340	2.02	0.955
C.05	295	0.015	239	0.068	0.173	1.04	0.705	282	269	108	95.8	< LOD	1.82	13.7	< LOD	23.3	3080	2.06	0.997
C.06	37.0	0.008	199	0.058	0.029	0.232	0.170	76.2	301	42.0	15.0	< LOD	0.597	56.1	< LOD	63.4	532	0.339	0.962
C.07	1430	0.023	702	0.039	0.301	2.90	0.794	45.0	534	301	15.4	1.53	2.67	17.6	< LOD	17.1	4850	4.66	1.71
C.08	208	0.007	195	0.053	0.064	0.436	0.290	516	363	48.3	176	< LOD	2.15	30.0	< LOD	99.5	1250	0.360	0.405
C.09	968	0.007	145	0.021	0.041	0.202	0.375	68.6	229	44.9	23.4	1.46	0.405	90.5	< LOD	30.3	1070	0.893	0.460
C.10	104	0.009	209	0.040	0.054	0.424	0.384	34.7	117	40.8	11.9	< LOD	1.02	35.2	< LOD	40.7	1860	1.30	1.03
C.11	7.07	0.011	183	0.035	0.038	0.303	0.182	32.9	69.2	26.0	11.0	< LOD	0.487	40.5	< LOD	37.5	1510	0.518	0.397
C.12	241	0.004	119	0.025	0.086	0.541	0.321	148	161	83.3	49.9	1.19	0.815	88.7	< LOD	66.7	552	1.16	0.957
C.13	182	0.008	153	0.031	0.083	0.357	0.124	202	149	51.1	73.7	< LOD	1.36	50.3	< LOD	30.9	902	1.08	0.500
C.14	43.0	0.008	269	0.066	0.040	0.508	0.568	94.8	249	43.4	30.3	< LOD	0.898	78.2	< LOD	68.5	1700	1.07	0.754
C.15	1620	0.043	793	0.210	0.349	2.98	0.909	93.3	318	193	31.8	5.01	3.17	85.9	< LOD	28.4	8150	4.67	1.66
C.19	1460	0.009	308	0.033	0.215	1.29	0.464	210	322	133	71.7	9.64	1.49	70.4	< LOD	27.4	2230	1.46	0.830
C.20	333	0.006	463	0.022	0.124	0.800	0.314	248	282	57.7	84.5	< LOD	1.08	47.1	< LOD	67.6	1100	0.846	0.756

Table B.5: PTE concentrations (mean) in *Ch. gymnophylla* from the Bussento river. Units are in $\mu g\ g^{-1}$ d.w., unless otherwise specified.

Site	Al	As	Ca	Cd	Co	Cr	Cu	Fe	K	Mg	Mn	Na	Ni	P	Pb	S	Si	V	Zn
B.02	1055	0.391	15048	0.288	1.498	2.317	2.995	1170.6	3500	1657	268.2	205.3	7.672	549.2	0.004	1428.6	58160	17.137	18.41
B.04	1777	0.332	12199	0.356	1.629	2.042	3.7	983.7	9859	2243	359.9	765.3	9.766	800	< LOD	2126.7	55160	19.408	24.45
B.06	1148	0.265	10750	0.254	0.866	1.033	2.25	505	7224	1255	210.2	210.3	5.37	532.9	< LOD	1679.2	41130	9.2	14.06
B.07	95.8	0.108	8280	0.187	0.672	0.617	1.822	268.2	12780	895.7	355.7	183.8	7.263	586.6	0.036	1874	17410	7.677	14.69
B.08	332.2	0.322	13235	0.285	0.916	1.516	2.477	592.5	7175	1164	225.95	176.1	12.538	966.7	< LOD	1717	49330	12.369	18.145
B.10	12.94	0.108	6528	0.21	0.256	0.15	1.461	43.81	10650	548	89.67	197.4	5.454	694.3	0.011	2348.6	13593	2.396	10.394
B.11	5610	0.309	17020	0.386	2.121	3.865	5.013	2014	22965	3660	263.9	576.8	20.88	1971.6	< LOD	2610.7	51970	26.97	29.21
B.12	69.1	0.154	8757	0.14	0.326	0.354	1.299	95.4	6194	550	83.5	133.06	3.74	817.6	0.006	1125	21639	4.507	104.7
B.13	39.4	0.116	10873	0.196	0.431	0.482	2.591	152.6	15910	988	111.25	503	4.937	1093	0.148	2251	20020	4.634	24.59
B.14	1533	0.295	12060	0.244	1.168	1.589	1.158	828	19458	2457	242	553.4	6.69	1053.8	0.621	2548.1	30410	11.85	35.28
B.15	28	0.06	6230	0.128	0.095	0.035	0.506	10.93	8998	474	32.18	231.7	2.754	405.9	0.285	1556	6031	0.776	6.954
B.16	12.73	0.175	7940	0.256	0.356	0.299	5.377	76.28	1237	338.1	133.1	94.33	3.234	1042.8	0.019	2072.8	25228	3.149	13.25
B.17	268	0.142	9330	0.221	0.639	0.54	2.027	257.6	18800	1234	923	463.4	3.75	1192	0.046	2956	18660	5.18	15.12
B.18	5580	0.335	19060	0.357	2.244	4.225	5.632	2017	15652	3026	303.2	433.8	16.23	894	< LOD	2283.3	53910	28.16	30.13
B.19	3260	0.159	16310	0.228	1.807	1.752	3.964	1007	19956	1405	311.1	395.8	8.49	901.6	0.595	2278.4	28940	12.37	29.02
B.20	349.1	0.169	14398	0.284	1.011	1.302	4.33	590.7	13129	1226	234.12	201.8	6.32	450.9	0.089	1836.9	23330	11.923	20.29
B.21	36320	0.888	36200	0.825	7	12.87	11.65	8660	27060	7229	929	842.6	51.5	2141	< LOD	3134	135860	88.1	57.41
B.22	408	0.147	10545	0.225	0.798	0.995	2.179	460	15490	1440	519.8	254.4	9.209	680.2	0.045	1985.8	20060	10.79	16.72
B.23	15.54	0.116	7229	0.203	0.288	0.261	1.433	74.8	4004	281.2	54	51.98	6.288	526.6	< LOD	1858.7	14340	3.678	12.1
B.24	3.066	0.11	6495	0.153	0.154	0.129	0.725	28.16	5648	479.9	41.979	96.4	1.541	359.4	0.004	1733.2	16857	1.525	7.536
B.25	78.7	0.175	10570	0.321	0.659	0.695	2.101	313.1	22670	1482	138.41	872	3.396	1354	0.138	2634.5	24210	6.345	14.026
B.26	3570	0.683	18060	0.263	1.437	2.675	4.309	1167	17050	1420.7	429.4	395.2	8.79	1005.3	0.553	3050	32470	17.36	35.82
B.27	130.3	0.139	12720	0.262	0.889	1.194	3.51	521.1	13819	1140.4	128.51	166.05	10.426	576.8	0.102	1902.3	19424	10.965	20.49
B.28	4920	0.247	16870	0.298	1.793	3.153	5.173	1572	20930	2866	358.2	584.5	8.4	833.6	0.015	2790.3	35910	18.05	27.79
B.29	14.71	0.071	9463	0.179	0.361	0.386	1.345	117.6	17339	708.6	77.4	270	3.466	595.6	0.301	2217	6958	3.453	11.483

Table B.6: PTE concentrations (s.e.m.) in *Ch. gymnophylla* from the Bussento river. Units are in μg g^{-1} d.w., unless otherwise specified.

Site	Al	As	Ca	Cd	Co	Cr	Cu	Fe	K	Mg	Mn	Na	Ni	P	Pb	S	Si	V	Zn
B.02	216	0.005	640	0.031	0.043	0.064	0.107	81.2	54.0	100	15.7	31.4	0.455	20.1	0.004	26.6	1570	0.650	1.09
B.04	342	0.024	247	0.015	0.027	0.098	0.040	47.6	197	106	20.6	20.4	0.255	14.9	< LOD	74.8	1100	0.455	1.24
B.06	561	0.039	1040	0.027	0.245	0.377	0.477	217	466	333	27.4	35.6	1.13	17.5	< LOD	46.3	6820	2.87	2.67
B.07	17.4	0.008	1750	0.021	0.026	0.068	0.086	20.8	1020	94.6	58.8	19.0	0.360	20.6	0.024	103	1410	0.356	0.706
B.08	44.7	0.017	427	0.020	0.032	0.097	0.058	40.7	206	101	6.42	15.0	0.300	26.2	< LOD	35.4	2200	0.458	0.551
B.10	8.60	0.008	497	0.009	0.012	0.020	0.063	4.04	1140	44.2	3.41	24.1	0.199	30.0	0.007	85.6	174	0.164	0.298
B.11	1330	0.029	2450	0.026	0.266	0.703	0.437	339	372	253	23.9	16.3	1.93	51.2	< LOD	37.1	5110	3.28	1.97
B.12	12.8	0.008	236	0.013	0.020	0.032	0.072	15.6	179	38.0	11.5	5.43	0.212	91.5	0.006	149	460	0.372	94.1
B.13	13.2	0.023	407	0.013	0.025	0.064	0.176	19.7	3810	109	8.39	107	0.141	119	0.080	269	3540	0.541	1.66
B.14	705	0.032	1050	0.019	0.169	0.504	0.382	255	871	471	13.9	16.1	1.01	18.4	0.110	51.2	5820	2.71	3.91
B.15	9.42	0.020	1450	0.013	0.008	0.016	0.109	2.32	824	50.8	4.36	31.2	0.183	36.3	0.145	151	283	0.056	0.388
B.16	4.90	0.010	463	0.012	0.012	0.013	0.503	2.82	125	11.4	13.4	4.25	0.235	93.0	0.012	84.9	311	0.241	0.954
B.17	121	0.016	1160	0.017	0.124	0.113	0.286	95.1	1750	208	215	42.1	0.420	103	0.028	195	1120	1.26	2.83
B.18	1470	0.032	1660	0.017	0.313	0.731	0.689	356	776	444	38.6	35.3	1.56	25.1	< LOD	56.4	5750	3.47	2.63
B.19	1410	0.037	3340	0.029	0.696	0.637	0.959	314	760	261	56.9	36.3	2.24	57.9	0.475	44.4	7240	3.31	5.63
B.20	70.1	0.007	709	0.016	0.065	0.144	2.09	70.7	608	128	9.51	15.4	0.244	18.0	0.059	61.0	1330	0.727	2.46
B.21	8850	0.137	1160	0.056	1.47	2.64	1.68	1890	1240	640	143	20.1	7.63	192	< LOD	430	24000	16.8	7.80
B.22	166	0.012	364	0.024	0.123	0.214	0.219	128	1790	327	91.3	39.8	0.732	38.8	0.045	74.5	1350	1.85	1.36
B.23	2.51	0.012	382	0.018	0.029	0.048	0.149	19.1	880	66.0	1.83	5.21	0.325	24.2	< LOD	86.4	2070	0.711	1.82
B.24	0.542	0.013	474	0.021	0.018	0.019	0.115	2.28	289	35.8	0.988	12.5	0.184	22.5	0.004	36.8	953	0.226	0.674
B.25	39.1	0.025	1060	0.033	0.069	0.096	0.309	56.6	1180	112	5.29	109	0.381	130	0.076	41.6	3520	0.923	0.563
B.26	1530	0.298	2500	0.025	0.293	0.791	0.865	332	1820	49.3	83.2	32.8	1.66	28.9	0.365	280	6540	3.24	8.79
B.27	26.6	0.008	760	0.014	0.060	0.124	0.249	57.4	366	82.4	3.87	6.82	0.390	12.7	0.022	80.6	948	0.835	1.86
B.28	1280	0.042	1590	0.028	0.352	0.711	0.880	372	1320	432	53.2	64.2	1.46	75.4	0.011	27.3	6970	3.87	3.55
B.29	3.45	0.004	509	0.018	0.025	0.054	0.082	15.7	506	51.3	6.25	32.0	0.262	46.0	0.096	141	931	0.360	0.795

Table B.7: PTE concentrations (mean) in *Ch. gymnophylla* from the Calore Salernitano river. Units are in $\mu g\ g^{-1}$ d.w., unless otherwise specified.

Site	Al	As	Ca	Cd	Co	Cr	Cu	Fe	K	Mg	Mn	Na	Ni	P	Pb	S	Si	V	Zn
C.01	14.53	3.739	9832	0.179	0.518	0.585	2.817	324.7	2934	485.2	167.51	261.5	5.999	424.1	0.24	1459.4	17381	4.819	7.47
C.03	2620	14.18	17380	0.914	1.886	3.11	6.58	2309	20920	2601	201.8	1111.4	14.2	2634	0.096	3899.2	66140	13.18	33.78
C.04	312	4.662	14550	0.246	1.434	2.215	7.491	1470	3582	954	567.5	292.2	7.033	557.1	< LOD	1722.1	28430	10.01	16.85
C.05	148.9	5.155	13382	0.273	1.065	1.421	5.145	993	7153	959.7	363.8	458	5.663	507.4	< LOD	2151.7	29030	7.81	13.62
C.06	10.34	1.725	7450	0.46	0.215	0.074	1.158	91.6	4168	232.9	74.09	150.6	2.17	658.8	0.115	1244.2	8090	1.548	6.877
C.07	6960	8.58	17065	0.342	3.112	6.757	9.288	4730	5778	2716	146.5	529.5	13.89	521.4	< LOD	1348.5	49700	29.61	26.54
C.08	15.95	4.322	12099	0.354	0.895	1.33	5.139	715	9193	906.1	183.8	397.9	7.721	1462.1	0.377	3189	23290	7.33	18.19
C.09	5.67	3.981	8513	0.224	0.579	0.443	4.441	226.9	12444	635	290.4	578.6	3.063	803.4	0.059	2391.4	16110	3.222	13.02
C.10	41.3	3.89	9113	0.21	0.512	0.493	3.494	333	6738	503.1	123.5	277.5	3.722	570.6	0.342	1588	17230	4.25	11.16
C.11	34.37	5.805	10710	0.244	0.795	1.05	3.882	638.9	2311	473.2	107.08	421.6	5.198	631.6	0.156	1411.4	27910	6.728	18.9
C.12	24.02	5.212	9472	0.242	0.792	0.69	3.784	470	6547	533	215.2	379.2	5.176	745.2	0.212	1731	22766	5.775	13.447
C.13	8.1	4.558	8885	0.408	0.596	0.601	4.337	309.9	12937	716.9	191.33	461.3	5.956	1170.5	1.02	2362.1	19940	4.325	15.141
C.14	28.59	3.084	9747	0.284	0.65	0.774	5.013	416.3	7508	436	139.6	291.1	5.606	717.2	0.3	1516	14810	5.91	14.31
C.15	1387	11.31	12650	0.838	1.467	2.193	5.988	1421	9021	1050	199.3	414.5	9.67	1347	0.032	2701.4	57200	14.59	18.1
C.19	8487	11.244	19675	0.364	4.476	9.202	11.823	7492	7559	3290.6	611.8	1039.4	15.413	743.3	< LOD	1322.6	66880	31.761	31.57
C.20	3090	10.114	15814	0.45	2.57	4.091	9.35	3292	14777	2247	447.9	1196.4	9.999	1034.7	< LOD	3846.5	66470	16.44	27.82

Table B.8: PTE concentrations (s.e.m.) in *Ch. gymnophylla* from the Calore Salernitano river. Units are in $\mu g\ g^{-1}$ d.w., unless otherwise specified.

Site	Al	As	Ca	Cd	Co	Cr	Cu	Fe	K	Mg	Mn	Na	Ni	P	Pb	S	Si	V	Zn
C.01	5.75	0.150	548	0.012	0.031	0.070	0.231	32.7	181	32.5	8.64	34.7	0.370	46.8	0.099	94.1	355	0.363	0.722
C.03	1170	4.30	3160	0.198	0.611	1.18	0.821	874	1380	591	24.7	32.0	3.09	175	0.069	67.1	23600	3.61	8.15
C.04	150	0.515	1560	0.018	0.241	0.506	0.808	410	313	191	68.2	54.4	0.943	40.1	< LOD	45.4	3870	1.87	2.14
C.05	68.6	0.523	926	0.022	0.222	0.440	0.510	292	429	87.0	78.8	125	0.821	48.4	< LOD	41.8	3560	1.86	1.85
C.06	7.58	0.235	534	0.024	0.013	0.038	0.076	10.2	376	22.5	3.89	28.7	0.113	16.3	0.049	51.8	1140	0.155	0.685
C.07	1530	0.674	983	0.015	0.317	0.838	0.868	675	325	291	12.3	94.6	1.08	29.6	< LOD	14.3	4360	2.86	3.21
C.08	4.14	0.341	978	0.027	0.109	0.266	0.357	155	379	77.6	17.2	12.3	0.834	83.2	0.086	111	1520	1.03	1.87
C.09	1.25	0.180	657	0.019	0.065	0.076	0.445	38.0	335	31.3	31.9	26.6	0.456	35.2	0.048	76.7	1010	0.474	1.32
C.10	19.5	0.403	966	0.015	0.106	0.167	0.604	111	551	33.5	16.6	30.9	0.637	24.2	0.189	116	1770	1.15	1.24
C.11	6.84	0.259	709	0.012	0.053	0.127	0.191	84.3	119	34.3	5.48	70.1	0.370	30.2	0.109	60.9	1610	0.602	1.68
C.12	6.16	0.103	426	0.006	0.040	0.108	0.199	55.5	203	56.1	10.9	31.6	0.232	19.4	0.098	58.5	758	0.320	0.723
C.13	2.75	0.380	685	0.012	0.088	0.162	0.590	88.0	711	41.9	9.91	20.3	0.468	31.3	0.121	23.6	2120	0.810	0.839
C.14	5.38	0.100	350	0.022	0.070	0.179	0.410	79.7	898	21.1	11.2	21.9	0.567	16.1	0.151	128	411	0.836	1.01
C.15	684	1.66	1020	0.097	0.255	0.504	0.771	348	666	190	17.2	46.9	1.39	117	0.032	71.7	8480	2.52	1.80
C.19	589	0.138	751	0.009	0.130	0.248	0.277	322	152	73.7	14.9	55.5	0.403	24.9	< LOD	39.4	1620	0.633	1.08
C.20	1250	0.746	643	0.021	0.332	0.750	0.885	606	196	254	30.9	55.6	0.909	38.6	< LOD	60.4	3930	2.24	1.27

Appendix C

PTE concentrations in sediments

Table C.1: Total PTE concentrations (mean) in sediments from the Bussento and Calore Salernitano. Units are in $\mu g\ g^{-1}$ d.w., except for Al, Ca, Fe, Mg, expressed in $mg\ g^{-1}$ d.w..

Site	Al	As	Ca	Cd	Co	Cr	Cu	Fe	K	Mg	Mn	Na	Ni	P	Pb	S	Si	V	Zn
B.02	8.347	1.603	125	0.159	35.273	29.69	27.831	24.912	557.4	6.861	973	50.4	37.65	288.4	7.556	282.5	1498	22.545	82.21
B.08	6.595	1.264	182.9	0.223	32.49	28.73	29.74	23.95	913.9	13.54	703	77.3	33.13	279.9	16.84	611	743.3	22.383	80.2
B.11	8.493	1.596	146.8	0.274	46.86	41.35	38.01	31.72	1138	9.33	789	67.1	45.16	358.6	18.57	190.1	1412	34.14	103.89
B.15	5.427	1.403	239.5	0.276	23.555	26.63	19.378	16.907	1203.6	13.5	633.1	88.53	23.31	336	5.68	524.3	808.5	24.4	78.6
B.16	6.47	0.799	137.5	0.13	32.22	23.98	30.3	21.43	1063	12.467	1225	68.5	32.11	618	6.739	599	1836	21.39	79.9
B.18	5.016	1.01	102.53	0.131	23.07	17.34	19.15	14.892	516.7	6.628	594.4	91.5	24.89	266.4	7.225	559.4	1964	20.63	66.6
B.21	2.541	0.316	278.76	0.155	20.04	13.256	13.82	13.1	1228	41.23	837.2	107.19	23.71	202.4	5.88	142.8	541	22.867	40.31
B.22	3.754	1.193	221.5	0.167	22.05	17.62	15.48	15.35	1548.7	24.95	603	78.3	23.46	225.11	5.9	858	591.7	15.969	47.06
B.27	2.342	0.411	328.73	0.196	14.9	9.26	9.71	11.55	978.1	11.888	830	85.9	14.2	142.8	1.815	447.7	487.6	16.69	27.09
B.29	4.78	0.347	232.7	0.182	28.89	18.87	20.72	20.53	366	6.722	861	82.9	27	251.2	9.16	511	1089	22.37	67.02
C.01	6.232	0.553	84.15	0.102	26.508	25.44	24.33	18.235	438.7	4.435	1171.2	143.4	29.88	997.6	< LOD	525.4	1888.1	19.602	70.12
C.03	6.772	0.703	119.8	0.277	29.88	29.64	26.21	21.56	443	5.61	960	118.3	37.05	1090.5	< LOD	1239	1208	25.44	77.9
C.06	3.115	0.656	73.9	0.293	25.36	17.26	10.16	15.8	291.7	2.217	734	176.9	23.85	938	< LOD	77	1036	18.88	39.84
C.09	6.081	0.511	102.34	0.252	26.906	20.827	20.941	17.678	371	4.117	940.8	66.7	27.88	1016.3	< LOD	263.18	990.4	19.159	68.74
C.10	6.077	0.349	123.1	0.144	23.4	19.736	18.65	18.157	276.7	4.911	763.4	56.07	27.33	956.6	< LOD	549	817	16.977	69.11
C.15	3.645	0.695	213.57	0.299	16.793	19.448	12.598	12.343	322.9	7.616	701.3	110.4	22.79	1115	< LOD	838	559.7	19.963	46.19
C.16	4.024	16.5	228.1	0.477	38.1	24.37	15.02	16	496	32.2	734.6	290	52.5	1122.4	< LOD	2436	675.2	16.22	47.34
C.17	2.924	0.295	302.41	0.333	10.46	10.18	7.389	8.472	157.1	5.63	762	65.78	13.85	899.2	< LOD	470	385.5	12.19	65.6

Table C.2: Total PTE concentrations (s.e.m.) in sediments from the Bussento and Calore Salernitano. Units are in μg g^{-1} d.w., unless otherwise specified.

Site	Al	As	Ca	Cd	Co	Cr	Cu	Fe	K	Mg	Mn	Na	Ni	P	Pb	S	Si	V	Zn
B.02	0.317	0.327	8.64	0.008	0.732	0.286	0.780	0.994	10.5	0.291	101	20.9	1.81	15.8	0.370	29.5	199	0.920	3.83
B.08	0.366	0.433	10.6	0.027	1.73	1.67	2.43	1.22	21.1	1.91	177	14.1	1.62	17.8	0.883	109	68.5	0.869	8.58
B.11	0.995	0.243	22.9	0.041	2.36	3.31	3.47	1.66	127	2.06	163	21.5	3.24	63.8	2.83	40.1	311	1.90	9.86
B.15	0.323	0.040	9.09	0.012	0.957	1.59	0.422	0.719	74.3	2.41	59.8	3.50	1.45	10.9	1.29	64.7	20.2	1.21	22.2
B.16	1.43	0.070	31.2	0.008	5.57	5.17	6.77	4.54	251	0.144	314	14.5	6.98	181	0.689	128	344	2.50	14.6
B.18	0.355	0.332	3.01	0.012	1.48	1.74	1.08	0.694	67.3	0.689	31.8	18.3	0.845	15.3	0.276	43.3	113	1.55	12.6
B.21	0.204	0.052	8.58	0.011	2.00	0.993	1.73	1.93	118	1.70	68.4	4.13	2.49	45.0	2.42	16.3	34.9	0.842	5.76
B.22	0.229	0.291	10.3	0.005	2.21	1.05	2.25	1.66	67.1	1.98	146	17.5	3.26	8.25	1.35	390	52.9	0.890	3.44
B.27	0.279	0.192	9.56	0.014	2.65	1.39	2.67	1.94	52.4	0.727	222	15.3	1.58	14.6	0.662	51.2	82.5	1.73	5.58
B.29	1.03	0.108	13.9	0.033	3.35	3.30	3.35	3.29	21.7	0.963	311	24.8	3.04	27.9	4.89	131	173	2.37	7.52
C.01	0.332	0.055	1.88	0.013	0.686	1.47	1.30	0.612	19.6	0.099	94.9	60.5	1.07	19.1	< LOD	39.6	50.9	0.730	2.95
C.03	0.754	0.069	14.4	0.052	4.21	2.06	2.67	3.34	39.0	1.34	130	41.2	4.63	36.0	< LOD	824	135	2.90	8.38
C.06	0.371	0.345	11.3	0.045	4.76	2.54	1.54	2.53	37.5	0.248	103	75.3	4.22	61.1	< LOD	2.69	225	4.79	4.78
C.09	0.128	0.192	4.24	0.081	0.876	0.866	0.389	0.369	16.5	0.113	67.4	15.2	0.797	12.2	< LOD	8.60	84.9	0.275	2.76
C.10	0.130	0.123	16.7	0.009	1.09	0.531	2.13	0.605	37.8	0.042	87.0	4.88	1.34	27.8	< LOD	160	228	0.361	3.08
C.15	0.176	0.195	7.56	0.016	0.437	0.963	0.823	0.358	17.0	0.316	35.1	33.2	0.787	40.8	< LOD	27.8	12.5	0.176	4.05
C.16	0.631	12.4	19.6	0.208	13.8	7.09	1.79	3.29	126	23.8	53.3	197	10.9	90.1	< LOD	666	69.1	1.03	3.22
C.17	0.330	0.025	9.77	0.066	1.20	1.32	0.482	0.961	16.6	1.04	173	7.76	1.93	28.4	< LOD	161	38.3	1.10	35.5

Table C.3: PTE concentrations (mean) in the exchangeable fraction in sediments from the Bussento and Calore Salernitano. Units are in $\mu g\ g^{-1}$ d.w., unless otherwise specified.

Site	Al	As	Ca	Cd	Co	Cr	Cu	Fe	K	Mg	Mn	Na	Ni	P	Pb	S	Si	V	Zn
B.02	3.82	0.566	95050	0.066	0.798	0.061	0.043	16.64	47.9	696.8	330.4	3.209	0.241	1.125	0.433	39.27	53.08	0.092	0.014
B.08	5.624	0.538	99154	0.054	0.438	0.066	0.082	8.71	64.1	887	154.4	7.25	0.211	1.749	0.418	57.33	69.19	0.273	0.076
B.11	7.155	0.548	93550	0.072	0.282	0.039	0.024	2.166	117.84	881.1	110.8	7.73	0.739	3.434	0.425	44.44	119.34	0.284	0
B.15	1.02	0.596	91529.1	0.061	0.313	0.034	0.064	< LOD	73.05	601.3	137	6.99	0.142	2.433	0.391	57.12	85.37	0.233	0
B.16	12.67	0.631	80000	0.079	0.921	0.211	0.626	17.88	116.9	2195	421.7	17.25	0.667	19.7	0.544	47.841	116.84	0.272	3.814
B.18	12.84	0.489	90820	0.072	0.863	0.083	0.134	6.779	94.21	1292	262.8	7.96	0.452	2.309	0.355	71.16	119.81	0.142	0.75
B.21	21.2	0.316	90820	0.069	0.467	0.071	0.097	12.57	74.2	1779	261.6	19.06	0.842	5.93	0.293	45.22	112	0.382	0.212
B.22	5.352	0.472	96340	0.055	0.511	0.053	0.048	4.62	68.98	1237.5	188.3	7.27	0.377	2.793	0.396	67.98	63.68	0.201	0.025
B.27	7.596	0.392	91040	0.065	0.191	0.027	0.101	2.436	52.15	623.2	71.57	27.5	0.134	12.39	0.272	96.3	76	0.671	0.044
B.29	9.347	0.292	86161	0.058	0.225	0.003	0.053	2.561	84.78	666.9	119.15	25.69	0.234	1.276	0.149	54.08	112	0.23	0
C.01	10.02	0.553	66992	0.08	1.06	0.108	0.121	15.86	92.46	452.94	573.1	43.82	0.753	< LOD	0	44.47	79.8	0.122	0
C.03	2.3	0.487	64234	0.098	0.985	0.065	0.111	9.8	61.91	460.8	405.6	26.68	1.044	< LOD	0	62.91	66.83	0.102	0
C.06	13.94	0.155	62390	0.128	0.61	0.231	0.093	37.5	62.33	501.7	273.9	88.8	0.498	5.4	< LOD	30.22	85.1	0.113	0
C.09	0.752	0.282	70190	0.075	0.573	0.048	0.059	4.19	62.63	458.1	302.65	20.49	0.361	< LOD	0	60.14	50.18	0.099	0
C.10	3.92	0.26	71403	0.066	0.594	0.05	0.053	34.37	55.28	411.64	288.7	24.82	0.354	< LOD	0	57.84	40.1	0.13	0
C.15	2.17	0.299	72688	0.079	0.409	0.027	0.118	4.19	67.48	407.08	160.89	28.93	0.299	< LOD	0	64.31	46	0.206	0
C.16	1.29	3.18	44930	0.259	17.7	0.105	0.082	4.04	175	23800	95	41.7	17.6	< LOD	0	56.8	25.7	0.107	0.81
C.17	< LOD	0.226	68360	0.064	0.139	0.033	0.026	11.28	20.09	323.19	96.7	19.99	0.039	< LOD	0	48.07	12.34	0.236	0

Table C.4: PTE concentrations (s.e.m.) in the exchangeable fraction in sediments from the Bussento and Calore Salernitano. Units are in $\mu g\ g^{-1}$ d.w., unless otherwise specified.

Site	Al	As	Ca	Cd	Co	Cr	Cu	Fe	K	Mg	Mn	Na	Ni	P	Pb	S	Si	V	Zn
B.02	1.41	0.168	2300	0.004	0.041	0.005	0.017	1.33	1.59	24.5	11.7	0.286	0.023	0.134	0.050	2.55	3.06	0.015	0.014
B.08	0.466	0.114	921	0.002	0.038	0.030	0.023	6.14	6.63	61.8	21.3	2.31	0.072	0.393	0.014	1.85	4.68	0.022	0.058
B.11	0.646	0.122	1100	0.006	0.030	0.004	0.003	0.483	8.48	25.5	13.5	2.92	0.173	0.536	0.031	7.90	7.31	0.020	0.000
B.15	0.510	0.077	43.4	0.005	0.037	0.003	0.013	< LOD	2.25	24.6	15.6	5.42	0.037	0.468	0.015	1.54	2.15	0.018	0.000
B.16	4.74	0.083	5170	0.005	0.085	0.046	0.222	1.59	3.34	470	77.6	3.17	0.061	14.9	0.015	0.699	9.87	0.093	0.186
B.18	1.80	0.109	1340	0.003	0.038	0.009	0.007	0.852	5.18	147	16.7	2.50	0.058	0.286	0.004	4.79	3.27	0.008	0.140
B.21	10.3	0.052	1150	0.002	0.230	0.012	0.027	6.32	8.19	145	19.5	7.31	0.238	2.48	0.032	8.48	20.0	0.131	0.212
B.22	0.972	0.055	1870	0.004	0.058	0.019	0.015	2.91	4.58	68.8	29.1	2.17	0.110	0.570	0.037	4.23	1.92	0.029	0.025
B.27	0.376	0.207	467	0.005	0.033	0.015	0.067	0.483	6.81	15.0	2.01	16.2	0.071	9.96	0.084	39.1	17.6	0.116	0.043
B.29	0.990	0.092	801	0.001	0.021	0.003	0.014	0.524	8.64	42.6	7.33	4.48	0.014	0.135	0.037	2.82	13.2	0.008	0.000
C.01	5.12	0.055	283	0.006	0.022	0.008	0.012	3.40	2.21	2.29	1.77	3.05	0.016	< LOD	0.000	3.12	10.0	0.003	0.000
C.03	1.25	0.029	483	0.008	0.041	0.006	0.020	1.21	6.85	20.3	13.9	2.15	0.048	< LOD	0.000	4.97	8.29	0.007	0.000
C.06	6.97	0.051	4060	0.005	0.093	0.079	0.040	19.8	6.00	78.5	62.0	58.8	0.116	5.40	< LOD	3.91	13.1	0.002	0.000
C.09	0.752	0.043	3200	0.001	0.029	0.002	0.009	2.13	3.40	11.9	6.86	7.28	0.004	< LOD	0.000	4.25	1.12	0.010	0.000
C.10	2.53	0.035	390	0.005	0.071	0.007	0.015	6.78	5.96	1.70	21.8	4.88	0.083	< LOD	0.000	8.27	7.78	0.008	0.000
C.15	1.16	0.055	533	0.003	0.014	0.006	0.009	1.06	3.51	3.99	4.06	4.39	0.015	< LOD	0.000	3.11	5.48	0.014	0.000
C.16	1.29	2.41	22500	0.212	17.3	0.086	0.082	1.63	126	23400	44.6	15.4	17.3	< LOD	0.000	28.9	13.6	0.103	0.479
C.17	< LOD	0.028	1170	0.004	0.015	0.001	0.004	1.81	2.59	9.26	13.6	4.33	0.020	< LOD	0.000	6.05	2.96	0.044	0.000

Table C.5: PTE concentrations (mean) in the fraction bound to Fe-Mn oxides in sediments from the Bussento and Calore Salernitano. Units are in $\mu g\ g^{-1}$ d.w., unless otherwise specified.

Site	Al	As	Ca	Cd	Co	Cr	Cu	Fe	K	Mg	Mn	Na	Ni	P	Pb	S	Si	V	Zn
B.02	684.6	< LOD	28220	0.031	5.016	1.158	3.76	1746	23.85	1506	530	15.04	2.319	154	5.209	22.12	410.9	3.759	8.113
B.08	96.6	< LOD	73930	0.069	3.038	< LOD	0.13	733	29.2	5700	411	25.42	1.648	36.6	1.368	53.43	158.5	4.133	4.714
B.11	546	0.017	44560	0.104	6.51	0.564	0.783	691	40.34	2355	511	12.97	3.29	43.4	3.02	14.73	302	4.43	6.19
B.15	25.64	0.203	126270	0.12	1.319	< LOD	0.036	434.9	39.35	2227	392.9	27.38	0.993	18.67	0.298	77.72	151.4	4.773	3.283
B.16	1095	< LOD	23270	< LOD	7.139	2.074	6.89	3069	48.71	5751	618	20.13	3.313	340	3.799	20.65	749	4.678	18.44
B.18	1076.9	< LOD	11180	0.006	5.863	1.732	4.091	2353.6	37.832	2818	253.2	20.19	3.56	161	5.328	18.92	754.9	6.423	11.582
B.21	24.64	< LOD	75540	0.086	1.764	< LOD	0.03	279.6	19.28	10250	459.2	24.45	2.41	36.8	0.024	34.04	89.81	5.121	2.043
B.22	20.009	< LOD	78300	0.038	1.337	< LOD	0	434	23.07	5390	281.5	21.73	0.804	13.29	0.095	50.12	85.47	3.222	2.607
B.27	20.26	0.019	124070	0.092	0.565	< LOD	0	117.44	20.04	1255	477	28.01	0.46	6.837	0.088	77.19	54.33	4.491	1.139
B.29	23.75	0.055	133660	0.119	1.385	< LOD	0.191	241.6	37.3	1761	543	46.9	1.128	11	0.185	86.95	154	5.17	2.825
C.01	781.7	< LOD	16370	0.017	5.803	1.95	8.303	2368	42.89	928.9	513.9	2	4.741	210.5	< LOD	17.85	578.8	3.122	15.619
C.03	219	< LOD	51060	0.142	2.695	0.658	3.555	1034	44.7	754.3	432.6	5.25	3.408	66.3	< LOD	31.26	264.8	3.037	7.14
C.06	462	0.427	11160	0.16	6.76	1.342	2.86	1208	43.7	352.8	301	51.3	6.25	78.7	< LOD	7.13	381	3.906	6.93
C.09	376	< LOD	30640	0.144	6.09	0.885	2.956	1063	23.72	585	528.3	4.58	3.198	84	< LOD	34.45	209.4	2.713	7.94
C.10	243	< LOD	49200	0.062	2.356	0.77	2.369	1055	22.12	1155	388.8	1.67	1.737	66.3	< LOD	56.7	172.5	2.526	6.32
C.15	25.69	0.091	108300	0.159	0.701	0.335	1.304	349.8	33.87	799.51	309.9	6.12	0.827	8.844	< LOD	89.08	79.3	3.186	4.605
C.16	12.92	0.03	106330	0.172	0.425	0.342	1.167	280.4	20.67	862	238.8	3.07	0.818	13.44	< LOD	97.6	61.2	2.993	4.547
C.17	14.69	0.069	120150	0.182	0.373	0.529	0.37	233	14.84	762.1	219.7	2.299	0.098	11.106	< LOD	106.12	31.72	2.691	1.397

Table C.6: PTE concentrations (s.e.m.) in the fraction bound to Fe-Mn oxides in sediments from the Bussento and Calore Salernitano. Units are in $\mu g\ g^{-1}$ d.w., unless otherwise specified.

Site	Al	As	Ca	Cd	Co	Cr	Cu	Fe	K	Mg	Mn	Na	Ni	P	Pb	S	Si	V	Zn
B.02	15.4	< LOD	8070	0.014	0.844	0.021	0.246	200	1.59	350	110	4.14	0.155	16.4	0.372	3.96	75.3	0.156	0.974
B.08	29.2	< LOD	9040	0.009	0.711	< LOD	0.130	136	1.10	1460	157	2.21	0.227	13.8	0.171	3.10	27.6	0.338	0.786
B.11	361	0.016	15200	0.034	2.09	0.417	0.757	304	6.52	660	130	1.59	1.60	20.5	1.78	6.96	133	0.922	2.27
B.15	3.58	0.203	10900	0.012	0.107	< LOD	0.020	68.5	2.38	360	48.3	1.44	0.086	2.11	0.057	5.33	14.4	0.125	0.279
B.16	128	< LOD	3920	< LOD	0.687	0.220	1.58	423	6.70	396	264	3.51	0.356	115	0.335	3.30	135	0.367	1.07
B.18	30.9	< LOD	2210	0.006	0.258	0.072	0.142	43.7	0.454	360	37.1	4.78	0.143	10.7	0.210	4.22	11.2	0.091	0.585
B.21	2.88	< LOD	1440	0.010	0.303	< LOD	0.030	59.0	3.13	1090	46.0	2.73	0.156	23.3	0.019	3.13	9.49	0.454	0.443
B.22	0.461	< LOD	2300	0.007	0.317	< LOD	0.000	44.8	2.75	264	84.4	0.847	0.188	1.13	0.038	1.89	5.68	0.153	0.128
B.27	4.51	0.019	8230	0.013	0.133	< LOD	0.000	4.47	4.11	100	173	4.34	0.234	0.918	0.034	2.84	7.29	0.726	0.275
B.29	3.64	0.055	8100	0.030	0.300	< LOD	0.086	32.7	7.89	391	240	22.2	0.433	2.45	0.038	7.53	22.6	0.755	0.540
C.01	42.1	< LOD	2020	0.005	0.174	0.136	0.512	162	4.57	76.8	98.2	1.01	0.331	10.4	< LOD	5.47	24.4	0.215	0.332
C.03	173	< LOD	11500	0.043	0.552	0.342	0.477	296	10.6	70.2	94.5	5.25	0.335	42.1	< LOD	7.01	90.2	0.319	1.95
C.06	122	0.427	7230	0.049	1.99	0.155	0.979	273	18.6	71.2	171	23.9	2.32	25.6	< LOD	3.17	148	0.807	2.29
C.09	111	< LOD	2450	0.076	1.34	0.173	0.517	154	3.35	106	70.0	4.58	0.320	19.0	< LOD	6.17	47.0	0.174	0.935
C.10	125	< LOD	15900	0.009	0.689	0.255	0.870	257	1.25	142	67.2	1.67	0.729	29.2	< LOD	24.5	59.8	0.054	2.14
C.15	5.93	0.012	1740	0.011	0.068	0.011	0.159	20.3	4.62	9.26	10.1	1.65	0.058	0.567	< LOD	1.79	10.5	0.096	0.337
C.16	1.88	0.013	3620	0.030	0.009	0.016	0.047	28.8	2.17	29.7	13.0	1.73	0.082	1.61	< LOD	5.50	10.8	0.101	0.227
C.17	2.93	0.035	5520	0.015	0.045	0.064	0.009	22.5	1.22	27.7	51.2	0.635	0.090	0.877	< LOD	8.45	3.57	0.096	0.173

Table C.7: PTE concentrations (mean) in the fraction bound to organic fraction in sediments from the Bussento and Calore Salernitano. Units are in $\mu g\ g^{-1}$ d.w., unless otherwise specified.

Site	Al	As	Ca	Cd	Co	Cr	Cu	Fe	K	Mg	Mn	Na	Ni	P	Pb	S	Si	V	Zn
B.02	438	1.036	1437	0.063	1.677	1.4	1.338	613.9	292.6	546.96	25.38	17.69	2.761	7.53	1.913	221.1	578.5	2.216	4.12
B.08	309.2	0.725	9520	0.1	1.783	2.002	2.279	545.5	646.7	3618	37.03	31.2	1.746	66.42	4.358	494	287.9	3.206	0.655
B.11	782	1.032	8660	0.098	3.48	3.146	1.156	627	590	3270	51.86	19.13	3.325	29.5	3.88	131	662	5.291	2.47
B.15	500.9	0.604	21600	0.095	2.453	3.065	1.722	615.9	971.6	8070	38.33	42.86	1.579	139.4	3.865	389.4	375.1	5.201	1.455
B.16	665	0.169	34010	0.05	3.197	2.288	1.746	1341	662	1930	113.2	18.23	3.42	54.6	1.838	524	613	1.813	2.28
B.18	690.1	0.521	508	0.053	2.454	1.968	1.115	1044	226.9	607.4	24.96	30.9	4.164	12.92	1.467	469.3	811.8	2.264	2.539
B.21	187.1	< LOD	112340	< LOD	1.243	1.661	1.022	196.15	1080	28157	23.712	63.68	0.982	77.2	0.909	63.58	174.1	6.243	0
B.22	277.3	0.721	46680	0.074	2.113	2.156	1.768	550.7	1345.8	16510	42.2	28.15	1.325	75.25	3.079	397.8	268.53	1.724	0.767
B.27	219.2	< LOD	113550	0.039	1.172	1.259	1.238	367.35	866.5	9023	140.2	30.34	0.505	49.02	0.88	274.2	194.3	2.031	0
B.29	476.9	< LOD	12810	0.005	2.653	1.626	1.427	729	64.4	2218	59.1	10.33	1.984	53.9	2.08	359	460	1.738	1.711
C.01	760.1	< LOD	682.83	0.005	2.168	2.523	0.828	867	50.95	747.5	27.01	33.69	5.074	368.2	< LOD	463.1	878.3	4.38	5.474
C.03	644	0.216	4400	0.037	2.214	2.473	1.06	526.8	61.86	1530	41	30.01	4.173	513.4	< LOD	460	482.3	5.065	3.853
C.06	283.5	0.074	383.3	0.005	1.43	2.193	0.204	196.9	23.18	290.6	47.5	19.49	2.97	508.1	< LOD	39.65	388.8	3.049	2.355
C.09	512.2	0.229	1377	0.033	1.321	1.856	0.569	380.1	37.15	519.2	41.43	28.01	3.284	491.5	< LOD	168.59	423.16	3.224	4.346
C.10	363.4	0.089	2096	0.015	1.248	1.477	0.529	425	30.69	559.7	24.46	20.12	2.804	454.8	< LOD	435	361	2.285	4.514
C.15	290.9	0.305	32250	0.061	1.339	1.93	1.815	377.4	60.24	4313	162.6	27.966	1.378	739.3	< LOD	684.6	241.5	3.423	7.74
C.16	229	0.07	76210	0.045	2.055	1.804	3.729	798	75	4882	327.9	30.1	3.126	608	< LOD	2021	254.4	2.873	5.141
C.17	113.1	< LOD	113440	0.088	0.864	1.201	1.128	450.3	43.59	2777	393.7	28.79	0.455	714.9	< LOD	316	173	2.571	32.4

Table C.8: PTE concentrations (s.e.m.) in the fraction bound to organic fraction in sediments from the Bussento and Calore Salernitano. Units are in $\mu g\ g^{-1}$ d.w., unless otherwise specified.

Site	Al	As	Ca	Cd	Co	Cr	Cu	Fe	K	Mg	Mn	Na	Ni	P	Pb	S	Si	V	Zn
B.02	16.8	0.180	378	0.012	0.054	0.067	0.098	26.4	20.1	5.19	1.34	4.93	0.107	1.55	0.056	30.9	43.5	0.482	0.368
B.08	32.6	0.398	1490	0.021	0.167	0.181	0.897	88.7	27.0	923	6.99	11.8	0.515	2.40	0.223	102	39.2	0.551	0.573
B.11	191	0.137	6750	0.001	1.13	0.318	0.056	140	142	2530	4.34	4.53	0.760	12.7	1.27	26.3	180	0.582	1.15
B.15	26.2	0.103	3760	0.014	0.098	0.071	0.060	43.1	46.2	2030	5.79	9.21	0.090	10.3	0.286	59.8	10.2	0.317	0.313
B.16	144	0.091	31900	0.003	0.288	0.157	0.284	150	324	999	50.5	3.03	1.27	11.1	0.260	134	144	0.336	1.04
B.18	27.7	0.358	69.8	0.011	0.142	0.053	0.078	122	69.6	31.9	2.12	6.31	0.208	1.60	0.018	40.0	75.1	0.248	0.117
B.21	12.9	< LOD	7450	< LOD	0.088	0.093	0.067	7.86	131	858	0.957	5.73	0.028	12.7	0.082	5.33	19.1	0.345	0.000
B.22	13.0	0.243	7210	0.007	0.295	0.108	0.103	46.0	99.6	1830	11.7	2.59	0.278	6.53	0.079	87.5	9.23	0.702	0.767
B.27	41.0	< LOD	8100	0.006	0.166	0.087	0.176	9.06	51.7	633	55.5	3.82	0.100	5.13	0.363	22.8	26.2	0.496	0.000
B.29	21.0	< LOD	5550	0.004	0.267	0.077	0.216	52.6	32.9	865	12.7	1.69	0.553	13.9	0.760	110	119	0.703	0.877
C.01	19.4	< LOD	2.96	0.004	0.152	0.076	0.056	78.5	5.37	67.3	1.31	7.38	0.323	28.1	< LOD	39.1	53.8	0.246	0.042
C.03	54.7	0.079	2660	0.002	0.486	0.080	0.201	62.0	7.26	979	14.9	2.56	0.126	31.7	< LOD	128	29.1	0.620	0.418
C.06	31.0	0.074	38.9	0.005	0.183	0.384	0.017	11.4	2.33	21.3	15.2	3.10	0.195	35.9	< LOD	9.55	51.3	0.808	0.230
C.09	24.8	0.158	179	0.005	0.028	0.101	0.081	19.4	2.22	36.8	2.72	5.06	0.082	29.7	< LOD	9.84	5.24	0.147	0.379
C.10	96.2	0.089	849	0.012	0.269	0.203	0.050	131	6.98	20.9	2.66	4.28	0.655	29.1	< LOD	178	118	0.437	0.932
C.15	14.4	0.155	6360	0.016	0.053	0.057	0.160	12.4	4.58	383	38.4	0.845	0.129	20.0	< LOD	24.5	12.7	0.136	1.68
C.16	13.1	0.060	12200	0.008	0.260	0.032	0.603	108	15.0	642	68.7	2.45	0.897	67.0	< LOD	507	11.7	0.453	0.744
C.17	19.3	< LOD	5460	0.058	0.096	0.064	0.358	19.1	7.16	858	95.6	3.82	0.128	43.7	< LOD	147	34.3	0.077	30.3

Table C.9: PTE concentrations (mean) in the residual fraction in sediments from the Bussento and Calore Salernitano. Units are in μg g^{-1} d.w., unless otherwise specified.

Site	Al	As	Ca	Cd	Co	Cr	Cu	Fe	K	Mg	Mn	Na	Ni	P	Pb	S	Si	V	Zn
B.02	7220	< LOD	293.4	< LOD	27.78	27.071	22.69	22540	193.09	4111	87.73	14.5	32.32	125.7	< LOD	0	456	16.478	69.97
B.08	6184	< LOD	267	< LOD	27.23	26.67	27.25	22660	173.9	3334.6	100.64	13.4	29.52	175.11	10.696	6.47	227.68	14.771	74.75
B.11	7158	< LOD	77.3	< LOD	36.595	37.6	36.05	30400	389.3	2824	115.5	27.3	37.8	282.4	11.25	< LOD	328.7	24.14	95.23
B.15	4899	< LOD	104	< LOD	19.47	23.53	17.556	15856	119.7	2608	64.9	11.3	20.6	175.51	1.12	< LOD	196.7	14.19	73.8
B.16	4700	< LOD	206.4	< LOD	20.96	19.4	21.04	17000	235.1	2591	72.1	12.9	24.71	203.3	0.559	6.24	357.7	14.63	55.4
B.18	3236	< LOD	25.1	< LOD	13.89	13.56	13.81	11488	157.7	1910	53.45	32.44	16.71	90.16	0.075	< LOD	277.9	11.8	51.7
B.21	2308	< LOD	54	< LOD	16.56	11.524	12.68	12610	54.3	1039.8	92.8	< LOD	19.48	82.54	4.65	< LOD	165	11.121	38.05
B.22	3452	< LOD	164.6	< LOD	18.09	15.41	13.66	14360	110.8	1816.1	91	21.1	20.95	133.78	2.33	342	174	10.821	43.66
B.27	2095	< LOD	71.9	< LOD	12.97	7.98	8.37	11060	39.4	987	141.5	< LOD	13.1	74.5	0.574	< LOD	163	9.496	25.91
B.29	4270	< LOD	60	< LOD	24.62	17.24	19.05	19550	179.6	2077	139.8	< LOD	23.65	185.1	6.75	11.5	363	15.23	62.49
C.01	4681	< LOD	100	< LOD	17.477	20.86	15.08	14984	252.4	2305	57.2	63.9	19.31	418.93	< LOD	0	351.2	11.977	49.03
C.03	5906	< LOD	140	< LOD	23.98	26.44	21.49	19990	274.5	2861	81.3	56.3	28.43	510.8	< LOD	685	393.9	17.24	66.9
C.06	2355	< LOD	10.5	< LOD	16.56	13.49	7.007	14360	162.5	1072.4	111.3	17.27	14.13	345.8	< LOD	0	181	11.81	30.55
C.09	5192	< LOD	142.4	< LOD	18.919	18.039	17.356	16230	247.5	2555.2	68.42	13.6	21.037	440.9	< LOD	0	307.6	13.124	56.45
C.10	5467	< LOD	434	< LOD	19.205	17.44	15.7	16642	168.6	2784	61.42	9.46	22.436	435.5	< LOD	0	243.7	12.035	58.281
C.15	3327	< LOD	331	< LOD	14.344	17.156	9.361	11612	161.34	2096	67.91	47.4	20.286	366.9	< LOD	0	192.9	13.147	33.84
C.16	3781	13.2	602	< LOD	17.95	22.12	10.04	14910	224.7	2631	72.84	215	30.95	501	< LOD	261	333.8	10.25	36.84
C.17	2796	< LOD	459	< LOD	9.08	8.41	5.864	7777	78.53	1772	52.2	14.7	13.26	173.2	< LOD	0	168.4	6.7	31.81

Table C.10: PTE concentrations (s.e.m.) in the residual fraction in sediments from the Bussento and Calore Salernitano. Units are in $\mu g\ g^{-1}$ d.w., unless otherwise specified.

Site	Al	As	Ca	Cd	Co	Cr	Cu	Fe	K	Mg	Mn	Na	Ni	P	Pb	S	Si	V	Zn
B.02	342	< LOD	86.9	< LOD	1.58	0.322	0.840	1210	9.00	111	4.53	14.5	1.77	12.9	< LOD	0.000	191	0.610	4.42
B.08	349	< LOD	141	< LOD	1.04	1.53	1.92	1020	17.2	92.9	3.37	13.4	1.03	7.89	0.962	3.25	4.12	0.684	7.37
B.11	485	< LOD	38.6	< LOD	0.562	2.82	3.09	1230	61.9	232	25.5	15.3	1.01	55.6	3.11	< LOD	10.4	2.00	7.33
B.15	303	< LOD	64.6	< LOD	1.00	1.59	0.440	763	26.4	169	10.9	11.3	1.63	4.40	1.12	< LOD	21.2	1.02	21.8
B.16	1230	< LOD	48.5	< LOD	5.00	4.88	5.79	4190	64.3	730	14.4	12.9	5.54	59.0	0.457	5.91	78.8	2.15	12.5
B.18	360	< LOD	13.0	< LOD	1.42	1.73	1.00	783	12.6	214	4.05	6.92	1.14	7.11	0.075	< LOD	31.4	1.29	13.4
B.21	204	< LOD	54.0	< LOD	2.07	0.920	1.81	1870	26.1	80.5	14.7	< LOD	2.50	6.73	2.34	< LOD	35.3	0.229	5.83
B.22	237	< LOD	86.1	< LOD	1.98	1.16	2.26	1680	28.7	51.5	29.6	21.1	3.00	9.06	1.27	342	39.2	0.536	4.24
B.27	235	< LOD	37.0	< LOD	2.41	1.32	2.57	1920	22.3	106	16.7	< LOD	1.31	17.4	0.438	< LOD	68.6	0.953	5.35
B.29	1030	< LOD	34.8	< LOD	3.64	3.36	3.63	3260	41.4	522	56.5	< LOD	2.74	43.6	4.11	11.5	86.5	1.70	8.38
C.01	340	< LOD	100	< LOD	0.912	1.40	1.22	746	23.6	193	3.68	53.0	1.17	9.01	< LOD	0.000	72.9	0.851	2.91
C.03	831	< LOD	104	< LOD	3.93	2.29	2.37	3450	22.6	388	12.6	44.8	4.62	27.8	< LOD	685	47.3	2.22	8.41
C.06	245	< LOD	10.5	< LOD	2.54	1.99	0.532	2300	22.1	98.4	16.4	8.00	1.67	19.3	< LOD	0.000	16.9	3.23	2.89
C.09	130	< LOD	32.2	< LOD	0.507	0.699	0.320	366	14.8	42.2	8.16	5.79	0.637	6.44	< LOD	0.000	46.9	0.565	2.94
C.10	257	< LOD	104	< LOD	0.117	0.149	1.54	254	24.8	117	4.19	1.64	0.560	27.5	< LOD	0.000	56.4	0.193	0.523
C.15	175	< LOD	266	< LOD	0.320	0.920	0.559	345	6.36	114	1.35	36.5	0.653	20.5	< LOD	0.000	10.1	0.357	2.34
C.16	634	13.2	108	< LOD	3.63	7.17	1.20	3150	13.5	303	8.85	203	7.44	108	< LOD	234	61.0	1.42	4.15
C.17	314	< LOD	110	< LOD	1.15	1.23	0.160	955	7.68	185	13.0	3.79	1.93	24.1	< LOD	0.000	12.9	1.16	5.23

Appendix D

Analytes in water

Table D.1: PTE concentrations in water from the Bussento and Calore Salernitano rivers in 2016. Units are in μg L^{-1} d.w., unless otherwise specified.

Site	Ca	Cd	Co	Cr	Cu	Fe	K	Mg	Mn	Na	P	Pb	S	Si	V	Zn
B.1	129568.65	< LOD	0.65	0.21	< LOD	0.2	6116.96	31752.96	6.45	119182.66	95.72	< LOD	15030.8	5128.72	0.99	5.29
B.2	131961.76	< LOD	0.31	0.4	< LOD	0.55	2129.97	20686.53	0.36	10830.42	61.9	0.13	4855.02	4690.13	0.37	2.46
B.3	132466.84	< LOD	0.12	0.13	< LOD	0.39	2216.39	20071.36	4.39	11060.17	71.29	0.26	4818.03	4947.33	1.5	1.78
B.4	138268.66	< LOD	0.84	0.12	< LOD	0.3	2183.43	20773.62	3.99	11842.59	57.79	0.03	5374.08	5119.71	1.48	1.46
B.5	122664.68	< LOD	0.15	0.45	< LOD	0.6	1898.22	19143.71	3.31	8099.22	52.95	< LOD	2944.03	4801.44	2.73	0.84
B.6	130984.57	0.01	0.23	0.13	< LOD	0.03	2142.18	21627.15	3.85	10713.04	59.72	0.13	4657.12	5122.69	1.94	2.3
B.7	124938.78	< LOD	0.26	0.2	< LOD	< LOD	1991.38	22559.5	1.88	9578.38	66.92	0.04	3764.74	5412.31	0.77	0.11
B.8	125184.07	< LOD	0.64	0.44	< LOD	< LOD	2026.65	23173.58	1.7	9601.29	66.7	0.2	3715.83	5450.45	0.9	1.19
B.9	105615.04	< LOD	0.19	0.13	< LOD	< LOD	1704.09	20201.16	1.34	8006.13	60	0.12	3421.4	4940.45	2.07	0.05
B.10	98477.2	< LOD	0.4	0.12	< LOD	< LOD	1714.54	22101.4	0.04	7765.7	81.44	< LOD	3651.41	5562.84	1.55	< LOD
B.11	106600.84	< LOD	0.52	0.08	< LOD	0.01	2083.91	20046.81	1.13	8299.19	78.01	0.03	3327.69	5368.31	3.37	1.07
B.12	110556.15	< LOD	0.12	0.13	< LOD	< LOD	1340.83	17630.91	0.19	7661.33	55.88	0.27	3369.43	3840.09	1.14	< LOD
B.13	94024.97	< LOD	0.99	0.4	< LOD	2.75	3859.23	19085.8	2.25	9434.2	227.07	12.15	3742.47	3873.69	1.03	65.76
B.14	104607.08	< LOD	0.16	0.82	1.77	0.16	4395.01	15611.18	2.66	15310.11	40.07	0.07	8399.94	8630.75	0.91	8.61
B.15	105880.9	< LOD	0.08	0.06	< LOD	< LOD	1158.69	14652.56	0.54	6677.45	63.21	0.03	2608.73	4214.76	0.96	0.08
B.16	113341.41	< LOD	0.68	0.11	< LOD	0.57	6366.02	16241.11	5.63	27132.61	192.69	0.14	10229.6	3992.62	1.75	0.25
B.17	132441.82	< LOD	0.15	0.15	< LOD	1.24	2227.17	19218.08	15.67	11505.86	63.47	< LOD	4661.03	5340.47	1.56	< LOD
B.18	93748.26	< LOD	0.29	0.19	< LOD	< LOD	1351.49	14872.82	0.4	5920.54	50.66	< LOD	2277.68	3907.17	1.91	0.47
B.19	52058.83	< LOD	0.14	0.34	< LOD	0.04	585.64	5729.97	4.75	2904.27	22.51	0.21	1257.42	1857.31	< LOD	< LOD
B.20	123421.19	< LOD	0.34	0.1	< LOD	26.84	1625.82	14261.72	7.04	7026.91	66.15	< LOD	2670.95	133.94	3.42	0.05
B.21	107804.65	< LOD	0.18	0.17	< LOD	< LOD	1390.71	15247.7	2.11	5551.31	48.22	0.09	1756.73	4159.53	3.64	1.49
C.1	155742.98	< LOD	0.19	0.35	< LOD	< LOD	3872.22	26265.23	5.15	18587.44	72.17	0.19	9456.4	7951.62	0.52	1.43
C.2	130682.99	< LOD	1.06	0.23	< LOD	0.01	2931.31	21029.91	0.29	14500.87	67.09	0.13	8484.18	7779.26	< LOD	11.48
C.3	195263.72	< LOD	0.71	0.77	< LOD	0.12	4746.22	42529.07	0.14	21722.51	91.68	0.05	10680.82	9087.67	1.49	0.42
C.4	120771.73	0.11	0.47	0.21	< LOD	0.19	3505.69	14729	3.57	18263.46	57.93	0.14	9081.97	6668.17	< LOD	1.67
C.5	96215.44	< LOD	0.23	0.09	< LOD	0.23	2543.49	11056.3	3.86	13326.59	49.46	0.15	7880.45	5014.41	0.26	2.91
C.6	137322.85	< LOD	0.5	0.5	< LOD	7.21	2436.22	9058.32	3.06	10259.2	57.48	0.03	3191.31	< LOD	0.36	2.31
C.7	113106.47	< LOD	0.45	0.23	< LOD	< LOD	2925.86	16206.11	1.31	14932.41	47.84	0.06	8575.47	5026.03	0.16	1.63
C.8	125506.74	< LOD	0.13	0.54	< LOD	0.19	2377.29	15776.92	1.81	10055.48	52.98	1.05	4610.47	3981.96	0.23	1.55
C.9	122162.88	< LOD	0.08	0.2	< LOD	0.3	2497.56	10551.82	5.77	10463.61	28.09	0.14	3694.37	4273.52	1.23	2.35
C.10	79427.13	0.18	0.22	0.16	< LOD	0.02	1360.11	6373.85	1.29	5603.32	46.76	0.25	2472.15	3691.68	0.68	2.29
C.11	121711.71	< LOD	0.39	0.48	< LOD	0.1	2263.28	9567.57	0.46	8816.91	50.45	0.27	2892.22	4567.11	< LOD	2.13
C.12	126455	< LOD	0.32	0.31	< LOD	0.33	2493.66	9568.07	4.99	8915.91	56.69	0.14	2897.78	4250.08	0.76	4.92
C.13	123001.71	< LOD	0.24	0.25	< LOD	0.19	2182.6	9589.36	1.72	7944.66	45.28	0.21	2338.68	4068.9	0.69	2.35
C.14	118896.58	< LOD	0.08	0.32	< LOD	0.78	2072.01	6666.2	1.89	7115.44	65.6	0.25	1913.25	4993.73	1.51	3.56
C.15	113365.7	< LOD	0.48	0.22	< LOD	0.37	1872.27	6649.46	0.07	6607.5	35.83	0.15	1756.2	4605.05	2.03	0.27
C.16	122262.36	< LOD	0.78	0.83	1.38	23.94	10439.19	15082.32	66.1	37253.03	1857.32	0.28	9194.39	4343.62	1.12	23.82
C.17	77429.24	< LOD	0.63	0.23	< LOD	11.49	1699.04	7738.74	6.76	6622.61	52.73	0.16	3651.32	936.71	0.26	4.38
C.18	140942.59	< LOD	0.68	0.09	< LOD	0.14	1895.31	7224.25	4.7	9294.3	28.85	0.31	4738.12	3988.97	0.13	1.39

Table D.2: Dissolved O_2, electrical conductivity, pH, and concentration of anions, photosynthetic pigments, TC, IC, TOC, and TN in water from the Bussento and Calore Salernitano rivers.

Site	O_2	e^-	pH	F^-	Cl^-	Br^-	NO_2^-	NO_3^-	PO_4^{3-}	SO_4^{2-}	TC	IC	TOC	TN	Chl a	Chl b	Pheo a	Pheo b	Car
	%	μS		mg L^{-1}	mg L^{-1}	mg L^{-1}	mg L^{-1}	mg L^{-1}	mg L^{-1}	mg L^{-1}	mg L^{-1}	mg L^{-1}	mg L^{-1}	mg L^{-1}	μg L^{-1}	μg L^{-1}	μg L^{-1}	μg L^{-1}	μg L^{-1}
B.1	100	745	8.17	0.06	134.46	< LOD	0.57	1.43	< LOD	20.37	33.27	31.43	1.84	0.44	584.33	152.93	319.43	141.03	404.07
B.10	72.5	477	8.01	0.07	6	< LOD	< LOD	1.63	< LOD	4.25	18.87	18.16	0.71	0.21	87.01	36.06	216.25	62.45	125.34
B.11	83	494	8.16	0.07	6.97	< LOD	< LOD	3.22	< LOD	4.09	23.24	22.69	0.55	0.65	87.53	37.59	168.76	59.18	85.98
B.12	99.2	458	7.78	0.05	6.14	< LOD	< LOD	1.87	< LOD	4.34	25.79	25.2	0.59	0.44	192.07	59.28	495.98	151.83	279.06
B.13	139.6	470	8.07	0.04	5.87	< LOD	< LOD	1.93	< LOD	3.94	20.11	19.2	0.91	0.43	89.92	34.41	172.75	49.65	87.37
B.14	91.8	477	7.87	0.04	7.5	< LOD	< LOD	1.2	< LOD	11.7	18.56	17.65	0.92	0.21	26.46	13.46	217.04	79.47	98.71
B.15	96.4	473	7.82	0.04	6.4	< LOD	< LOD	1.65	< LOD	3.83	20.47	18.86	1.61	0.4	69.55	16.93	174.31	45.24	89.97
B.16	109.3	514	8.16	0.09	10.03	0.13	< LOD	1.19	< LOD	12.91	24.92	22.69	2.24	0.51	6796.23	1018.94	3175	1511.83	3594.68
B.17	89.9	507	8.08	0.03	4.47	< LOD	< LOD	0.86	< LOD	4.07	16.75	16.23	0.53	0.14	769.07	204.61	660.88	200.37	522.67
B.18	82.4	468	7.99	0.03	5.52	< LOD	< LOD	1.71	< LOD	3.01	20.37	20.18	0.2	0.33	58.32	24.09	210.46	71.26	120.25
B.19	89.4	464	7.87	0.03	4.93	< LOD	< LOD	1.38	< LOD	3.09	22.46	21.68	0.78	0.31	244.37	91.62	403.88	121.19	313.74
B.2	96.7	493	8.22	0.05	5.78	< LOD	< LOD	1.21	< LOD	5.14	28.97	28.1	0.87	0.52	849.47	242.69	337.88	161.01	524.22
B.20	94.2	460	8.15	0.03	4.76	< LOD	< LOD	1.18	< LOD	2.79	22.16	20.78	1.38	0.37	198.17	75.01	398.78	118.44	293.76
B.21	89.9	482	7.91	0.04	3.68	< LOD	< LOD	1.9	< LOD	2.02	16.11	15.91	0.2	0.31	< LOD	< LOD	< LOD	< LOD	< LOD
B.3	104	497	7.96	0.04	6.18	< LOD	< LOD	1.32	< LOD	5.67	21.84	20.81	1.03	0.84	628.16	186.49	307.39	134.88	434.26
B.4	104.5	506	7.76	0.05	6.85	< LOD	< LOD	1.41	< LOD	6.62	36.94	35.31	1.63	0.32	369.31	113.52	257.01	117.73	265.17
B.5	107.2	473	7.5	0.03	4.97	< LOD	< LOD	1.47	< LOD	3.07	26.74	26.9	0.48	0.38	2586.5	761.36	450.08	78.15	1517.48
B.6	97	500	7.59	0.06	6.15	< LOD	< LOD	1.08	< LOD	5.79	26.77	25.87	0.9	0.36	159.99	43	306.44	95.53	210.79
B.7	103.1	499	7.69	0.06	6.53	< LOD	< LOD	1.82	< LOD	5.08	32.06	30.77	1.29	0.37	292.25	94.72	315.37	103.22	250.31
B.8	103.6	496	7.76	0.09	6.56	< LOD	< LOD	1.73	< LOD	5.19	29.53	28.39	1.14	0.39	141.07	35.01	302.44	79.57	173.46
B.9	95.9	493	8.14	0.08	6.79	< LOD	< LOD	2.11	< LOD	4.62	16.68	16.3	0.38	0.3	84.92	19.5	261.1	90.13	138.79
C.1	99.6	575	8.11	0.11	9.48	< LOD	0.05	0.69	< LOD	10.69	22.99	22.14	0.85	0.28	252.48	66.61	254.24	131.47	271.44
C.10	94.4	452	7.81	0.03	5.9	< LOD	< LOD	1.62	< LOD	3.42	26.16	24.88	1.28	0.59	55.99	0.65	324.83	95.81	214.8
C.11	98.4	457	7.92	0.03	6	< LOD	< LOD	1.66	< LOD	3.34	28.35	25.07	3.28	0.6	82.89	16.8	320.49	82.6	175.49
C.12	100.6	464	7.86	0.03	6.18	< LOD	< LOD	1.59	< LOD	3.19	28.09	25.71	2.38	0.71	107.64	23.92	283.79	94.43	191.75
C.13	77.4	449	7.92	0.03	5.3	< LOD	< LOD	2	< LOD	2.47	45.14	21.42	23.72	0.51	127.94	24.18	269.31	70.83	218.26
C.14	91.2	454	7.88	0.03	5.23	< LOD	< LOD	2.41	< LOD	2.04	27	22.85	4.16	0.73	119.55	23.86	110	20.48	103.55
C.15	100	454	8.04	0.02	4.97	< LOD	< LOD	2.4	< LOD	1.86	27.26	24.92	2.34	0.6	44.1	15.3	53.7	21.84	34.89
C.16	55.4	541	8.2	0.12	20.88	0.56	< LOD	34.6	1.45	14.74	39.85	32.13	7.72	8.17	638.29	78.46	1452.1	488.12	1990.16
C.17	87.2	438	7.88	0.08	17.77	< LOD	< LOD	0.75	< LOD	5.32	27.33	23.28	4.05	0.54	89.44	19.5	295.25	95.66	223.16
C.18	100	371	7.84	0.03	3.57	< LOD	< LOD	0.7	< LOD	5.86	32.07	31.48	0.59	0.3	76.66	34.8	303.07	114.85	173.24
C.2	106.4	580	7.77	0.14	11.53	< LOD	0.06	0.91	< LOD	12.8	46.33	45.69	0.64	0.41	244.07	80.62	419.77	160.84	325.44
C.3	60	697	7.74	0.3	17.22	< LOD	0.08	1.49	< LOD	15.93	60.82	60.04	0.77	0.41	< LOD	< LOD	< LOD	< LOD	< LOD
C.4	92.7	486	7.96	0.06	8.42	< LOD	< LOD	0.51	< LOD	13.17	30.75	29.55	1.2	0.28	285.58	60.87	167.49	73.17	265.51
C.5	95.2	484	7.93	0.07	7.51	< LOD	< LOD	0.56	< LOD	11.52	30.43	28.62	1.81	0.38	240.42	55.86	187.19	90.42	224.4
C.6	85.9	487	8	0.04	7.14	< LOD	< LOD	1.28	< LOD	3.88	33.05	32.54	0.51	0.39	189.04	69.16	304.85	120.68	182.71
C.7	72.1	468	8.01	0.06	6.92	< LOD	< LOD	0.77	< LOD	11.59	31.88	31.06	0.82	0.32	< LOD	< LOD	< LOD	< LOD	< LOD
C.8	90	466	7.93	0.04	5.71	< LOD	< LOD	1.01	< LOD	5.17	32.43	32.55	0.06	0.41	248.28	88.51	396.55	154.69	325.24
C.9	90.5	459	7.91	0.05	6.26	< LOD	< LOD	1.14	< LOD	4.42	26.45	25.11	1.34	0.52	300.89	80.7	339.62	142.75	260.58

Table D.3: PTE concentrations in water from the Bussento and Calore Salernitano rivers in 2017. Units are in μg L^{-1} d.w., unless otherwise specified.

Site	Al	As	Ca	Cd	Co	Cr	Cu	Fe	K	Mg	Mn	Na	Ni	P	Pb	S	Si	V	Zn
B.02	2.15	< LOD	22256.06	0.53	0.34	1.51	1.7	< LOD	1637.78	4728.98	< LOD	2721.42	< LOD	< LOD	< LOD	1572.97	357.02	< LOD	< LOD
B.04	8.67	< LOD	38743.47	0.46	0.33	1.76	1.74	< LOD	1853.86	7968.45	< LOD	3312.47	< LOD	< LOD	< LOD	1717.39	525.18	< LOD	< LOD
B.06	< LOD	< LOD	13469.62	0.68	0.52	1.21	1.77	< LOD	1437.16	2085.97	< LOD	885.64	< LOD	< LOD	< LOD	729.79	25.13	< LOD	< LOD
B.07	< LOD	< LOD	15760.84	0.56	0.55	1.23	1.69	< LOD	1620.37	4762.56	< LOD	2019.08	< LOD	< LOD	< LOD	1131.82	815.87	< LOD	< LOD
B.08	6.76	< LOD	26081.05	0.72	0.41	1.54	1.82	< LOD	1927.32	8566.4	< LOD	3194.76	< LOD	< LOD	< LOD	1600.54	822.04	< LOD	< LOD
B.10	13.37	< LOD	53666.96	0.66	0.57	1.99	1.86	< LOD	2375.51	14564.62	< LOD	5196.35	< LOD	< LOD	< LOD	2385.83	470.45	< LOD	< LOD
B.11	< LOD	< LOD	13185.55	0.67	0.7	1.45	1.52	< LOD	1503.39	3659.53	< LOD	1300.4	< LOD	< LOD	< LOD	890.9	1237.21	< LOD	< LOD
B.12	1.94	< LOD	24192.89	0.67	0.55	1.02	1.53	< LOD	1537.43	4432.48	< LOD	1790.69	< LOD	< LOD	< LOD	1087.19	423.39	< LOD	< LOD
B.13	14.62	< LOD	59335.89	0.66	0.48	1.61	1.62	< LOD	2362.25	14839.78	< LOD	6286.1	< LOD	< LOD	< LOD	2592.84	380.43	< LOD	< LOD
B.14	8.86	< LOD	30879.32	0.59	0.66	1.99	1.7	< LOD	1708.02	4964.25	< LOD	2528.07	< LOD	< LOD	< LOD	1932.27	563.96	< LOD	< LOD
B.15	9.24	< LOD	19667.83	0.72	< LOD	1.93	1.67	< LOD	1899.78	10512.88	< LOD	4073.18	< LOD	< LOD	< LOD	2107.73	856	< LOD	< LOD
B.16	< LOD	< LOD	18019.73	0.55	0.51	1.51	2.9	< LOD	2125.38	2453.09	0.35	6273.9	< LOD	< LOD	< LOD	2064.54	928.85	< LOD	< LOD
B.17	10.81	< LOD	34360.63	0.33	0.46	1.68	1.87	< LOD	2083.12	8910.76	0.95	4450.97	< LOD	< LOD	< LOD	2230.35	710.96	< LOD	< LOD
B.18	< LOD	< LOD	11262.06	0.52	0.45	1.45	1.61	< LOD	1367.42	1622.75	< LOD	601.08	< LOD	< LOD	< LOD	592.33	265.11	< LOD	< LOD
B.19	10.96	< LOD	30168.74	0.41	0.19	2.02	1.67	< LOD	1810.36	5250.38	< LOD	2946.47	< LOD	< LOD	< LOD	1302.06	1380.64	< LOD	< LOD
B.20	11.55	< LOD	37655.65	0.41	0.53	1.82	1.99	< LOD	2002.6	6628.98	< LOD	3430.01	< LOD	< LOD	< LOD	1675.72	623.39	< LOD	< LOD
B.21	9.26	< LOD	32829.2	0.52	0.57	1.43	2.07	< LOD	2207	6934.95	< LOD	2601.34	< LOD	< LOD	< LOD	1564.73	1408.62	< LOD	< LOD
B.22	< LOD	< LOD	18469.86	0.61	0.59	1.52	1.6	< LOD	1533.23	4469.72	< LOD	1604.68	< LOD	< LOD	< LOD	1087.68	56.5	< LOD	< LOD
B.23	< LOD	< LOD	9829.96	0.57	0.17	1.34	1.52	< LOD	1348.94	1441.23	< LOD	515.74	< LOD	< LOD	< LOD	599.69	839.86	< LOD	< LOD
B.24	14.82	< LOD	61741.61	0.66	0.43	1.59	2.21	< LOD	2371.24	14228.14	< LOD	6009.2	< LOD	< LOD	< LOD	2447.39	223.2	0.45	2.03
B.25	11.6	< LOD	24223.75	0.93	1.07	1.27	1.89	< LOD	2055.81	3227.31	< LOD	5166.24	< LOD	< LOD	< LOD	1883.79	3393.93	< LOD	19.01
B.26	16.95	< LOD	22427.88	0.54	0.24	1.88	1.49	< LOD	1578.51	3506.26	< LOD	1902.04	< LOD	< LOD	< LOD	1096.53	585.91	< LOD	< LOD
B.27	7.61	< LOD	26312.27	0.47	0.32	1.4	1.69	< LOD	2023.72	4892.33	< LOD	2283.68	< LOD	< LOD	< LOD	983.68	986.87	< LOD	< LOD
B.28	4.81	< LOD	20947.95	0.53	0.3	1.43	1.88	< LOD	2002.04	5314.26	< LOD	4916.64	< LOD	< LOD	< LOD	1539.19	2985.61	< LOD	< LOD
B.29	24.38	< LOD	15257.91	0.5	0.3	4.36	1.57	< LOD	1494.63	1410.32	< LOD	803.51	< LOD	< LOD	< LOD	574.15	1104.9	< LOD	< LOD
C.01	0.92	< LOD	25537.66	0.61	0.51	1.81	1.73	< LOD	2137.34	8179.13	< LOD	5258.37	< LOD	< LOD	< LOD	3090.72	1456.33	< LOD	< LOD
C.02	6.37	< LOD	40983.53	0.53	0.41	1.34	1.74	< LOD	2738.38	13337.93	< LOD	8354.58	< LOD	< LOD	< LOD	4938.32	624.8	< LOD	< LOD
C.03	5.64	< LOD	32397.67	0.55	0.35	1.43	1.85	< LOD	2234.54	11138.58	< LOD	5610.96	< LOD	< LOD	< LOD	3444.46	1038.78	< LOD	< LOD
C.04	3.18	< LOD	30469.3	0.71	0.12	1.65	1.78	< LOD	2171.31	4736.12	0.28	5930.56	< LOD	< LOD	< LOD	3619.76	1227.7	< LOD	< LOD
C.05	6.34	< LOD	44015.98	0.56	0.06	1.41	1.99	< LOD	2615.77	6478.19	1.31	7995.4	< LOD	< LOD	< LOD	4830.03	658.1	< LOD	< LOD
C.06	< LOD	< LOD	16079.41	0.48	0.37	1.97	1.75	< LOD	1453.1	1249.8	< LOD	1165.55	< LOD	< LOD	< LOD	840.79	533.38	< LOD	< LOD
C.07	< LOD	< LOD	17443.51	0.42	0.07	2.28	1.7	< LOD	1511.65	2264.64	< LOD	1571.21	< LOD	< LOD	< LOD	1242.66	1133.22	< LOD	< LOD
C.08	< LOD	< LOD	22961.3	0.54	0.26	1.91	1.77	< LOD	1793.47	4931.4	< LOD	2844.15	< LOD	< LOD	< LOD	1590.34	92.06	< LOD	< LOD
C.09	12.64	< LOD	47509.6	0.49	0.17	0.99	1.98	< LOD	2326.95	6115.06	< LOD	5672.85	< LOD	< LOD	< LOD	2558.72	64.45	< LOD	< LOD
C.10	< LOD	< LOD	14404.98	0.62	0.64	1.86	1.69	< LOD	1499.85	1435.43	< LOD	1305.24	< LOD	< LOD	< LOD	832.75	359.05	< LOD	< LOD
C.11	< LOD	< LOD	16369.59	0.64	0.36	1.58	1.71	< LOD	1513.67	1573.73	< LOD	1354.07	< LOD	< LOD	< LOD	798.1	595.59	< LOD	< LOD
C.12	< LOD	< LOD	15507.15	0.62	0.31	1.83	1.67	< LOD	1454.86	1275.32	< LOD	1091.67	< LOD	< LOD	< LOD	721.83	839.21	< LOD	< LOD
C.13	< LOD	< LOD	13676.94	0.62	0.11	1.81	1.47	< LOD	1409.38	649.38	< LOD	755.7	< LOD	< LOD	< LOD	626.55	469.31	< LOD	< LOD
C.14	< LOD	< LOD	16005.04	0.64	0.6	1.78	1.56	< LOD	1504.82	1533.66	< LOD	1178.88	< LOD	< LOD	< LOD	733.37	426.45	< LOD	< LOD
C.15	< LOD	< LOD	16149.13	0.74	0.09	2.91	1.62	< LOD	1408.03	725	< LOD	776.83	< LOD	< LOD	< LOD	607.75	1314.31	< LOD	< LOD
C.19	11.82	< LOD	45616.22	0.59	0.36	1.27	1.76	< LOD	2423.78	6447.31	0.12	6785.8	< LOD	< LOD	< LOD	3606.96	133.21	< LOD	< LOD
C.20	8.05	< LOD	36386.05	0.65	0.58	1.74	1.64	< LOD	2228.86	6274.25	< LOD	7614.84	< LOD	< LOD	< LOD	4889.79	428.52	< LOD	< LOD

Table D.4: ORP, dissolved O_2, electrical conductivity, pH, and concentration of anions, photosynthetic pigments, TC, IC, TOC, and TN in water from the Bussento and Calore Salernitano rivers.

Site	ORP	O_2	e^-	pH	F^-	Cl^-	Br^-	NO_2^-	NO_3^-	PO_4^{3-}	SO_4^{2-}	TC	IC	TOC	TN	Chl a	Chl b	Pheo a	Pheo b	Car
	mV	%	μS		$mg\ L^{-1}$	$mg\ L^{-1}$	$mg\ L^{-1}$	$mg\ L^{-1}$	$mg\ L^{-1}$	$mg\ L^{-1}$	$mg\ L^{-1}$	$mg\ L^{-1}$	$mg\ L^{-1}$	$mg\ L^{-1}$	$mg\ L^{-1}$	$\mu g\ L^{-1}$	$\mu g\ L^{-1}$	$\mu g\ L^{-1}$	$\mu g\ L^{-1}$	$\mu g\ L^{-1}$
B.02	149.31	101.9	353	7.91	0.07	7	< LOD	< LOD	1.09	< LOD	6.56	21.01	18.97	2.04	0.38	0.43	0.16	0.86	0.3	0.44
B.04	138.47	107.4	312	8.18	0.05	5.63	< LOD	< LOD	1.6	< LOD	3.68	21.36	19.26	2.1	0.41	2.87	0.91	1.64	0.96	2.04
B.06	158.52	97.9	310	7.86	0.06	5.43	< LOD	< LOD	1.49	< LOD	3.18	19.12	17.21	1.91	0.31	2.96	0.98	1.33	1	2.05
B.07	172.43	107.1	326	8.27	0.11	6.9	< LOD	< LOD	1.46	< LOD	5.04	19.91	17.73	2.18	0.6	0.63	0.22	0.9	0.2	0.92
B.08	173.31	88.9	324	8.23	0.12	6.31	< LOD	< LOD	1.42	< LOD	4.36	26	23.51	2.5	0.46	0.44	0.14	0.84	0.27	0.56
B.10	205	45.7	337	7.75	0.1	6.24	< LOD	< LOD	1.65	< LOD	4.17	16.02	14.17	1.85	0.31	0.83	0.35	1.64	0.45	0.88
B.11	171.29	80.6	339	7.61	0.1	6.37	< LOD	< LOD	2.43	< LOD	4.17	23.1	20.7	2.4	0.56	0.24	0.1	0.44	0.05	0.46
B.12	132.98	99.7	294	8.31	0.06	5.66	< LOD	< LOD	1.68	< LOD	3.64	16.24	14.47	1.77	0.3	0.77	0.21	1.06	0.29	1.46
B.13	184.54	82.3	314	7.98	0.05	5.68	< LOD	< LOD	2.05	< LOD	3.45	14.24	12.48	1.76	0.45	1.12	0.27	1.21	0.51	0.84
B.14	171.74	66.6	317	8.07	0.04	5.71	< LOD	< LOD	1.47	< LOD	4.38	15.73	13.88	1.85	0.52	0.7	0.3	2.04	0.71	1.13
B.15	146.28	79.2	316	8.25	0.04	5.39	< LOD	< LOD	1.56	< LOD	3.46	9.72	8.02	1.7	20.69	0.21	0.09	0.49	0.14	0.52
B.16	192.21	46.1	531	7.58	0.09	24.2	< LOD	< LOD	4.34	0.19	21.71	27.05	24.55	2.5	1.13	0.76	0.18	0.72	0.28	0.6
B.17	171.2	71.3	336	7.88	0.07	5.46	< LOD	< LOD	1.39	< LOD	4.53	15.72	13.83	1.89	0.39	1.2	0.34	1.2	0.47	0.9
B.18	175.37	79.1	313	7.92	0.06	3.28	< LOD	< LOD	0.87	< LOD	1.83	19.3	17.19	2.11	0.43	0.21	0.1	0.54	0.16	0.53
B.19	118.65	51.6	313	8.09	0.03	3.51	< LOD	< LOD	0.67	< LOD	2.36	17	14.95	2.06	0.32	0.45	0.16	0.79	0.19	0.77
B.20	158.31	77.6	312	8.13	0.04	2.2	< LOD	< LOD	0.71	< LOD	1.63	13.07	11.19	1.88	0.31	0.32	0.13	0.54	0.18	0.56
B.21	178.01	69.2	343	7.03	0.05	4.52	< LOD	< LOD	10.91	< LOD	3.4	18.61	16.4	2.22	3.24	0.41	0.24	0.65	0.13	1.04
B.22	183.3	90.1	325	8.02	0.09	5.63	< LOD	< LOD	1.34	< LOD	3.79	17.49	15.46	2.04	0.35	0.37	0.1	0.61	0.04	0.83
B.23	87.65	66.5	337	7.65	0.08	5.36	< LOD	< LOD	1.58	< LOD	3.71	17.49	15.35	2.14	0.42	0.2	0.15	0.38	0.14	0.54
B.24	176.43	60.7	286	8.25	0.05	5.63	< LOD	< LOD	1.36	< LOD	3.36	13.03	11.37	1.66	0.44	0.17	0.11	0.42	0.18	0.42
B.25	177.52	65.6	298	7.97	0.06	8.09	< LOD	< LOD	5.85	< LOD	4.18	12.94	11.31	1.63	1.06	0.54	0.16	0.9	0.12	0.82
B.26	164.32	75.9	313	7.97	0.05	5.11	< LOD	< LOD	0.89	< LOD	3.27	20.84	18.49	2.35	0.41	0.76	0.24	1.37	0.44	1.09
B.27	161.18	70.8	306	8	0.03	7.12	< LOD	< LOD	1.27	< LOD	2.23	15.39	13.48	1.92	0.36	0.19	0.1	0.41	0.12	0.47
B.28	187.9	74.5	320	6.6	0.05	5.9	< LOD	< LOD	0.6	< LOD	3.76	21.1	18.64	2.46	0.32	0.38	0.17	0.66	0.15	0.7
B.29	180	75	249	7	0.02	2.77	< LOD	< LOD	1.25	< LOD	1.41	14.91	12.98	1.93	0.59	0.38	0.17	0.66	0.12	0.65
C.01	167.12	114.2	462	8.03	0.21	10.71	< LOD	< LOD	0.35	< LOD	11.63	36.03	33.02	3.01	0.31	117.99	47.54	14.01	2.07	39.08
C.02	199.95	105.8	473	7.92	0.21	11.25	< LOD	0.04	0.7	< LOD	11.66	28.63	26.08	2.55	0.29	1.55	0.44	1.71	0.66	1.02
C.03	190.3	35.1	592	7.06	0.66	15.16	< LOD	0.05	1.36	< LOD	14.69	46.77	43.1	3.67	0.45	0.29	0.13	0.26	0.15	0.34
C.04	194.36	94.1	320	8.05	0.12	7.37	< LOD	< LOD	0.02	< LOD	10.98	18.28	16.4	1.87	0.19	0.66	0.21	0.9	0.32	0.84
C.05	210.48	82.5	329	7.91	0.11	7.09	< LOD	< LOD	0.15	< LOD	10.59	25.15	22.85	2.3	0.16	1.26	0.34	0.52	0.19	0.74
C.06	218.95	33.1	334	6.98	0.13	6.79	< LOD	< LOD	1.05	< LOD	4.69	16.69	14.82	1.87	0.38	0.86	0.25	0.51	0.16	0.48
C.07	145.69	100.4	297	8.18	0.09	6.05	< LOD	< LOD	0.54	< LOD	6.71	16.55	14.81	1.75	0.22	0.47	0.09	0.89	0.16	0.74
C.08	156.8	99.7	307	7.99	0.05	5.32	< LOD	< LOD	1.07	< LOD	3.93	11.64	10.16	1.48	0.38	0.22	0.12	0.63	0.22	0.6
C.09	234.43	60	293	7.82	0.04	3.48	< LOD	< LOD	0.25	< LOD	2.63	16.11	14.33	1.78	0.2	0.87	0.25	1.24	0.44	0.76
C.10	140	95.7	262	8.22	0.04	4.17	< LOD	< LOD	0.63	< LOD	2.55	13.54	11.96	1.57	0.28	0.33	0.15	0.65	0.26	0.65
C.11	139.66	104.6	281	8.31	0.05	5.46	< LOD	< LOD	1.03	< LOD	3.13	10.52	9.18	1.34	0.26	3.93	1.3	0.58	0.25	2
C.12	147.78	110.8	293	8.28	0.05	4.5	< LOD	< LOD	0.75	< LOD	2.5	11.89	10.48	1.41	0.32	0.46	0.08	1.33	0.52	0.94
C.13	142	101.7	283	8.38	0.02	3.2	< LOD	< LOD	1.01	< LOD	1.26	11.68	10.25	1.43	0.41	0.6	0.11	0.9	0.13	0.99
C.14	140.39	98.5	283	8.4	0.03	3.75	< LOD	< LOD	1.36	< LOD	1.34	12.24	10.8	1.45	0.6	1.03	0.61	2.68	1.28	1.4
C.15	206.51	87.4	290	8.04	0.05	4.75	< LOD	< LOD	2.01	< LOD	1.96	11.72	10.27	1.45	0.53	0.22	0.14	0.4	0.17	0.6
C.19	126.04	49.6	304	8.02	0.07	6.14	< LOD	< LOD	0.25	< LOD	6.64	12.7	11.21	1.49	0.18	5.07	1.63	1.31	0.54	2.39
C.20	79.76	46.6	414	7.4	0.07	8.82	< LOD	< LOD	0.05	< LOD	14.11	14.96	13.31	1.66	0.11	0.97	0.31	0.66	0.35	0.91

Appendix E

MEM maps based on passive and active biomonitors

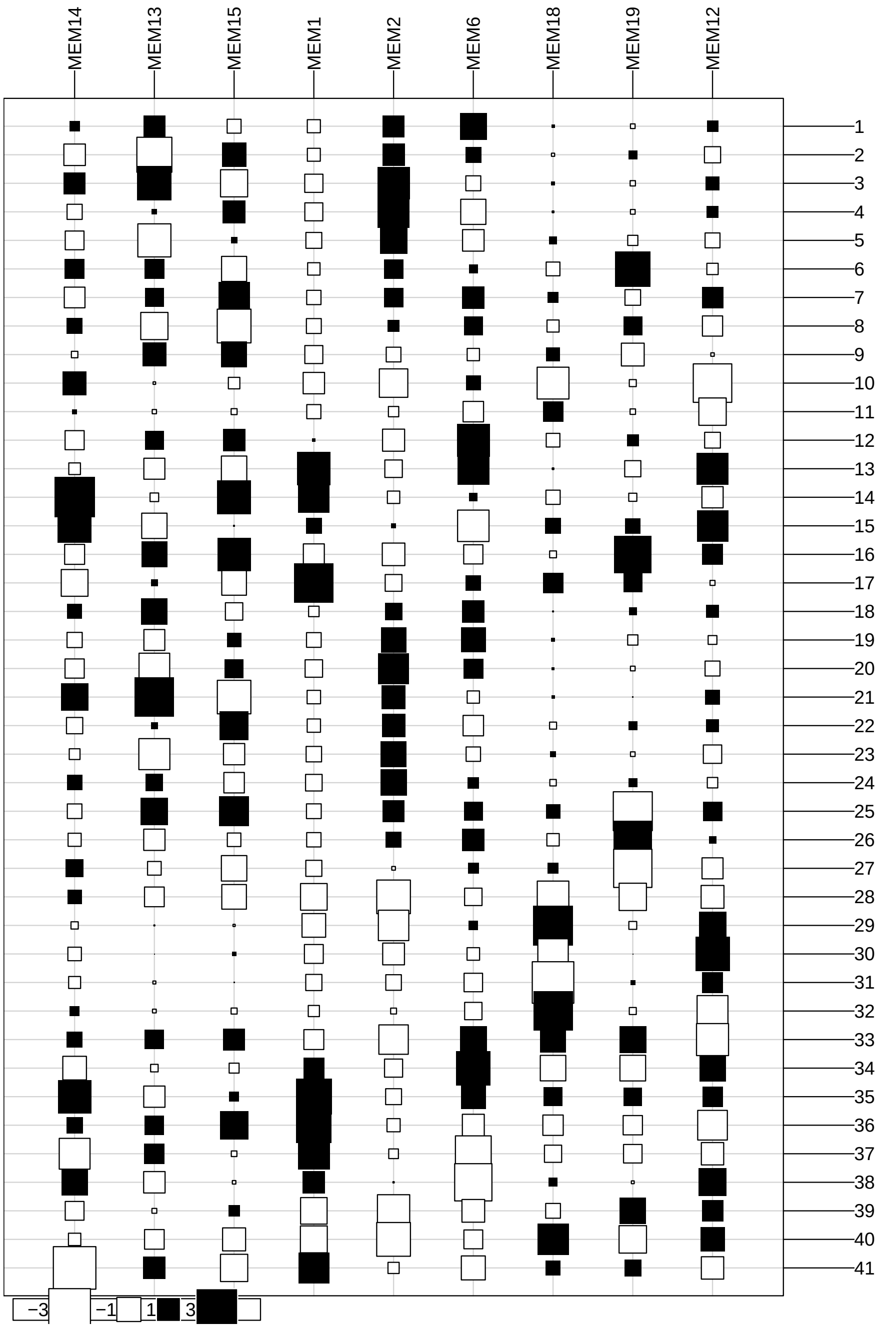

Figure E.1: MEM map based on passive biomonitoring data, relative to the Bussento-Bussentino river system. MEMs are ordered from left to right in relation to their importance in the relative RDA. Square size indicate the relative strength of spatial autocorrelation (■: positive; □: negative).

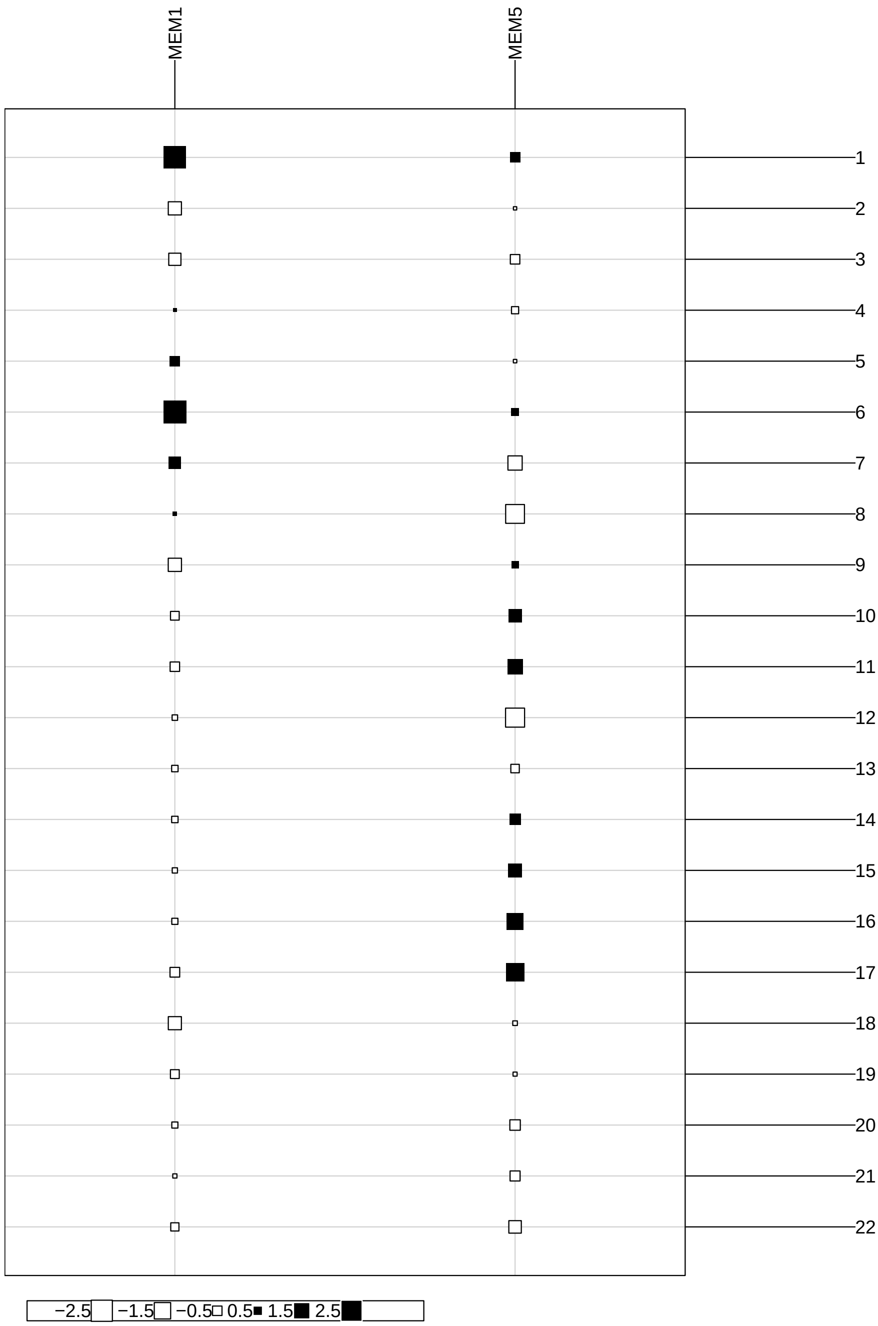

Figure E.2: MEM map based on passive biomonitoring data, relative to the Calore Salernitano-Rio Pietra-Fasanella river system. MEMs are ordered from left to right in relation to their importance in the relative RDA. Square size indicate the relative strength of spatial autocorrelation (■: positive; □: negative).

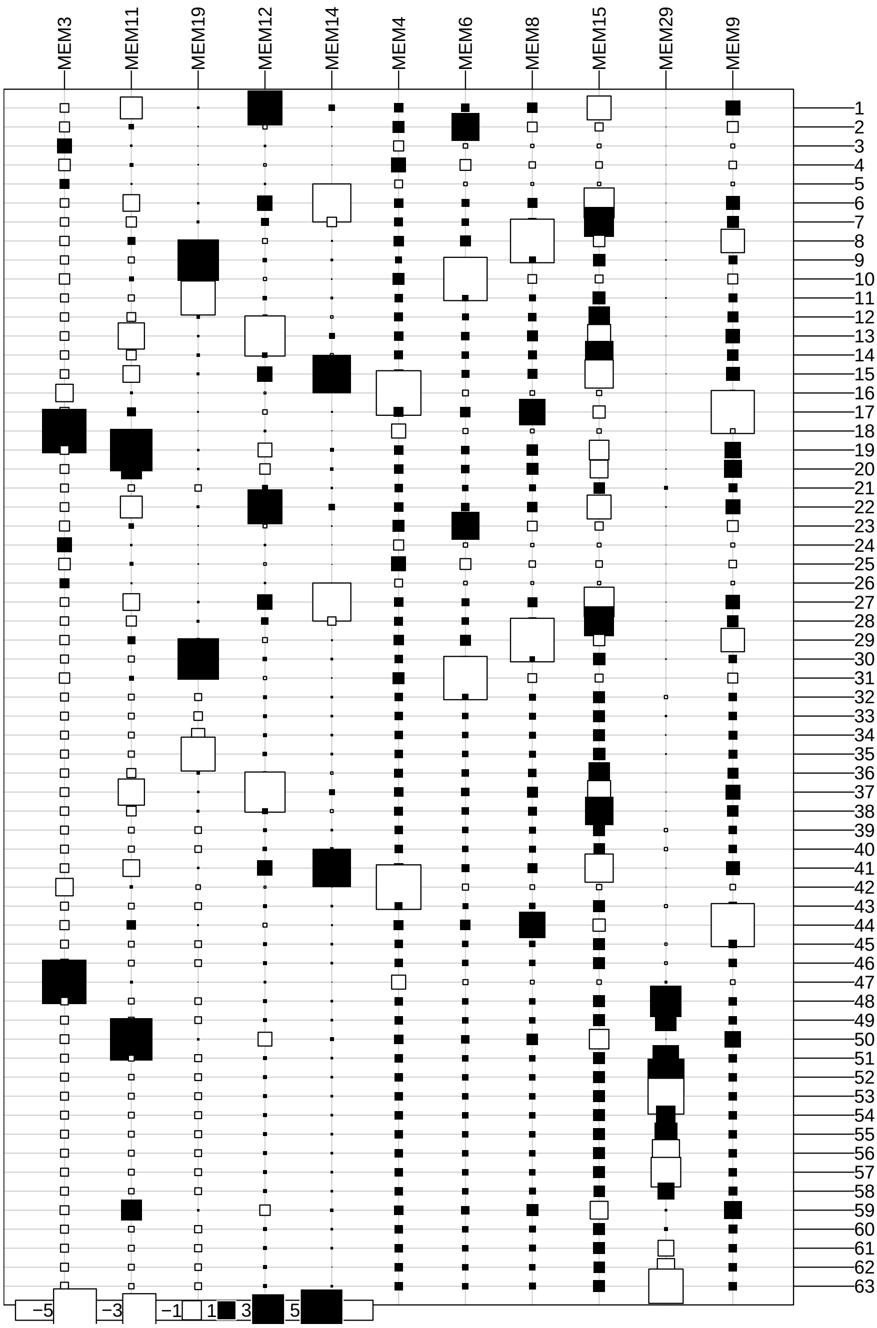

Figure E.3: MEM map based on passive biomonitoring data, relative to the joint river system. MEMs are ordered from left to right in relation to their importance in the relative RDA. Square size indicate the relative strength of spatial autocorrelation (■: positive; □: negative).

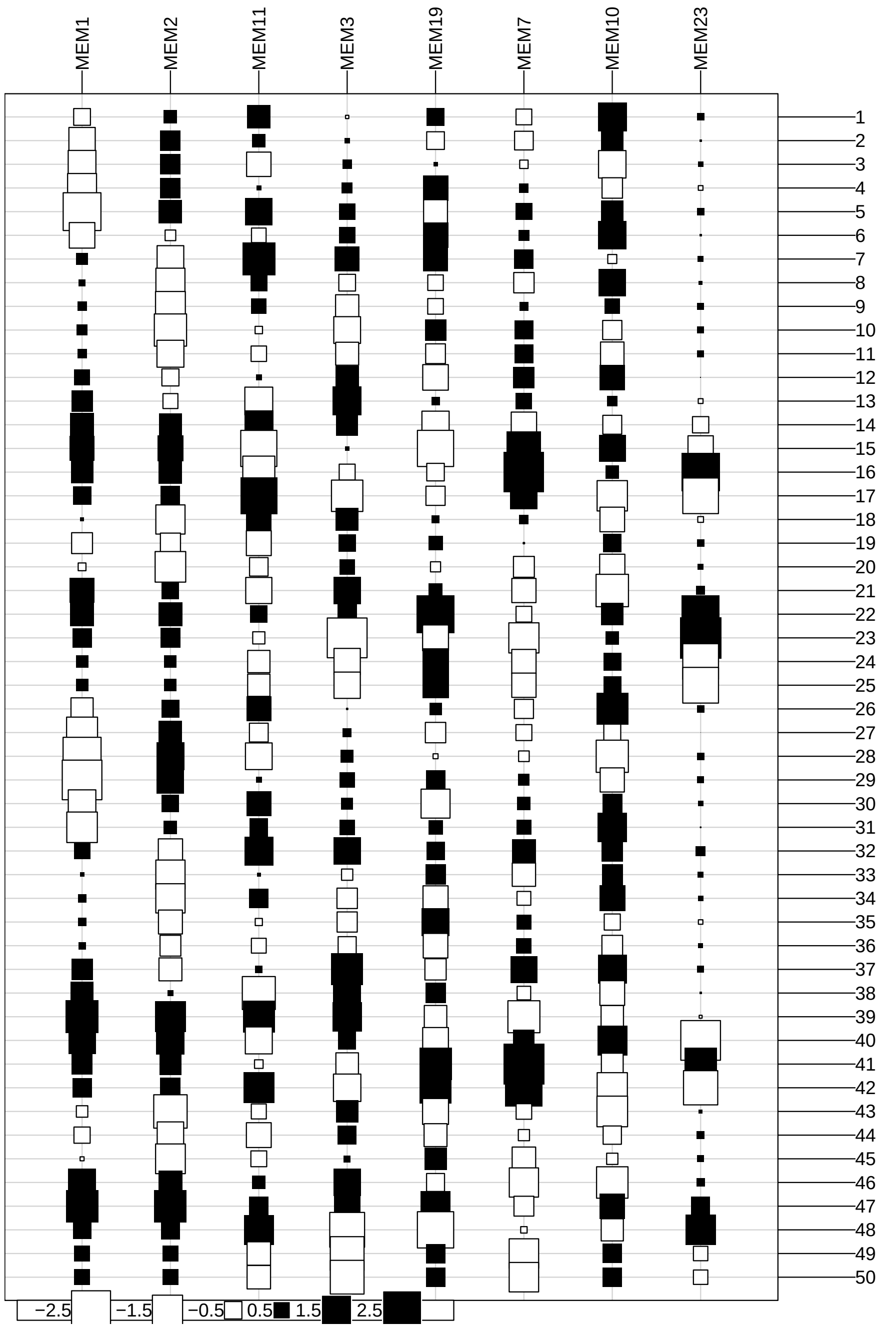

Figure E.4: MEM map based on active biomonitoring data, relative to the Bussento-Bussentino river system. MEMs are ordered from left to right in relation to their importance in the relative RDA. Square size indicate the relative strength of spatial autocorrelation (■: positive; □: negative).

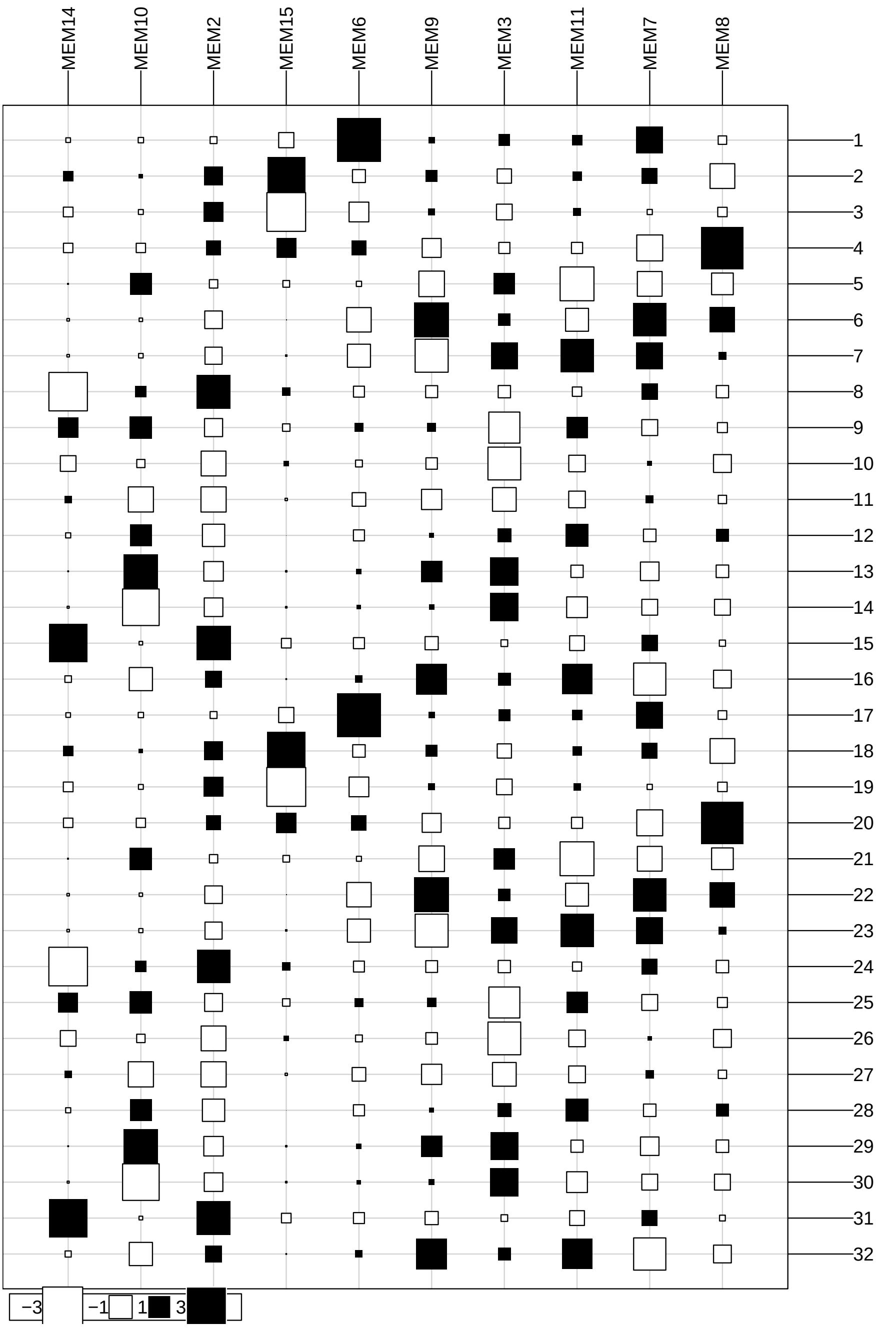

Figure E.5: MEM map based on active biomonitoring data, relative to the Calore Salernitano-Rio Pietra-Fasanella river system. MEMs are ordered from left to right in relation to their importance in the relative RDA. Square size indicate the relative strength of spatial autocorrelation (■: positive; □: negative).

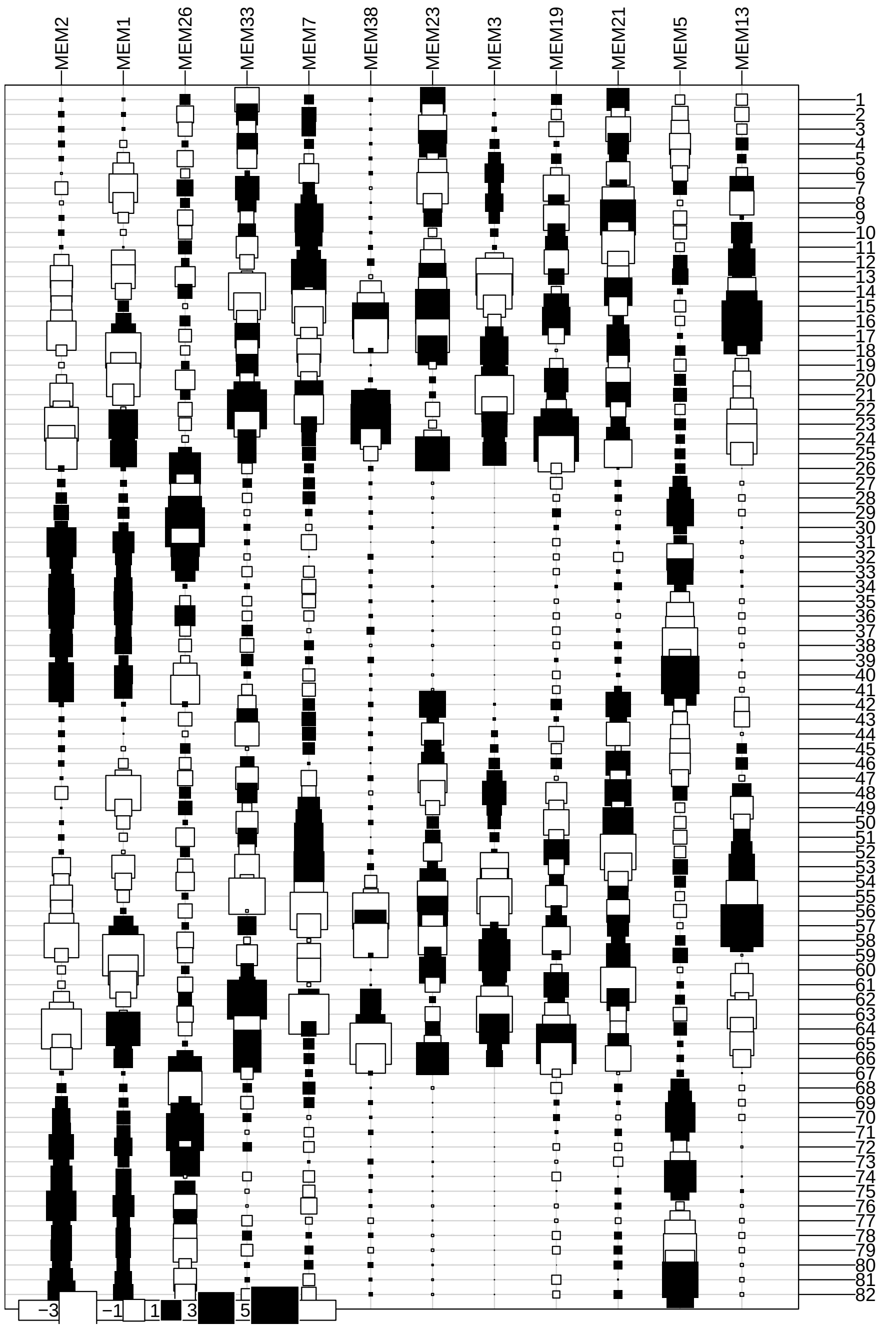

Figure E.6: MEM map based on active biomonitoring data, relative to the joint river system. MEMs are ordered from left to right in relation to their importance in the relative RDA. Square size indicate the relative strength of spatial autocorrelation (■: positive; □: negative).

References

Aguirre-Rubí J, Ortiz-Zarragoitia M, Izagirre U, Etxebarria N, Espinoza F, Marigómez I (2019) Prospective biomonitor and sentinel bivalve species for pollution monitoring and ecosystem health disturbance assessment in mangrove–lined Nicaraguan coasts. Science of the Total Environment 649:186–200. doi:10.1016/j.scitotenv.2018.08.269

Ahmadi A, Riahi H, Sheidai M, Van Raam J (2012) Some Charophytes (Characeae, Charophyta) from Central and Western of Iran including *Chara kohrangiana* species nova. Cryptogamie, Algologie 33:359–390. doi:10.7872/crya.v33.iss4.2012.359

Alam A (2018) Biotic and abiotic stress tolerance in plants, chap. Bryomonitoring of environmental pollution. Springer Netherland, pp. 349–366. doi:10.1007/978-981-10-9029-5_13

Albanese S, De Vivo B, Lima A, Cicchella D (2007) Geochemical background and baseline values of toxic elements in stream sediments of Campania region (Italy). Journal of Geochemical Exploration 93(1):21 – 34. doi:https://doi.org/10.1016/j.gexplo.2006.07.006

Allan I, Vrana B, Greenwood R, Mills G, Roig B, Gonzalez C (2006) A "toolbox" for biological and chemical monitoring requirements for the European Union's Water Framework Directive. Talanta 69(2 SPEC. ISS.):302–322. doi:10.1016/j.talanta.2005.09.043

Arthington AH (2015) Environmental flows: a scientific resource and policy framework for river conservation and restoration. Aquatic

Conservation: Marine and Freshwater Ecosystems 25(2):155–161. doi:10.1002/aqc.2560. https://onlinelibrary.wiley.com/doi/pdf/10.1002/aqc.2560

Atherton ID, Bosanquet SDS, Llawley M (eds.) (2010) Mosses and liverworts of Britain and Ireland: A field guide. British Bryological Society

Augusto S, Gonzalez C, Vieira R, Máguas C, Branquinho C (2011) Evaluating sources of PAHs in urban streams based on land use and biomonitors. Environmental Science and Technology 45(8):3731–3738. doi:10.1021/es1036332

Baldantoni D, Alfani A (2016) Usefulness of different vascular plant species for passive biomonitoring of Mediterranean rivers. Environmental Science and Pollution Research 23(14):13907–13917. doi:10.1007/s11356-016-6592-6

Baldantoni D, Bellino A, Lofrano G, Libralato G, Pucci L, Carotenuto M (2018) Biomonitoring of nutrient and toxic element concentrations in the Sarno River through aquatic plants. Ecotoxicology and Environmental Safety 148:520 – 527. doi:https://doi.org/10.1016/j.ecoenv.2017.10.063

Barnosky A, Matzke N, Tomiya S, Wogan G, Swartz B, Quental T, Marshall C, McGuire J, Lindsey E, Maguire K, Mersey B, Ferrer E (2011) Has the Earth's sixth mass extinction already arrived? Nature 471(7336):51–57. doi:10.1038/nature09678. Cited By 1049

Bartram J, Ballance R (1996) Water quality monitoring: a practical guide to the design and implementation of freshwater quality studies and monitoring programmes. E & FN Spon

Bauman D, Vleminckx J, Hardy OJ, Drouet T (2018) Testing and interpreting the shared space-environment fraction in variation partitioning analyses of ecological data. Oikos 1(1). doi:10.

1111/oik.05496. https://onlinelibrary.wiley.com/doi/pdf/10.1111/oik.05496

Bazzichelli G, Abdelahad N (2009) Flora analitica delle Caroficee: alghe d'acqua dolce d'Italia. Ministero dell'Ambiente e della Tutela del Territorio e del Mare

Beilby M, Schneider S, Puckacz A, Martín-Closas C (2018) Towards an integrated understanding of charophyte biology and paleobiology. Botany Letters 165(1):7–10. doi:10.1080/23818107.2017.1415819

Bellino A, Alfani A, Selosse MA, Guerrieri R, Borghetti M, Baldantoni D (2014) Nutritional regulation in mixotrophic plants: new insights from *Limodorum abortivum*. Oecologia 175(3):875–885. doi:10.1007/s00442-014-2940-8

Bellino A, Bellino L, Baldantoni D, Saracino A (2015) Evolution, ecology and systematics of *Soldanella* (Primulaceae) in the southern Apennines (Italy). BMC Evolutionary Biology 15(1):158. doi:10.1186/s12862-015-0433-y

Besse JP, Geffard O, Coquery M (2012) Relevance and applicability of active biomonitoring in continental waters under the Water Framework Directive. TrAC Trends in Analytical Chemistry 36:113 – 127. doi:https://doi.org/10.1016/j.trac.2012.04.004. Chemical Monitoring Activity for the Implementation of the Water Framework Directive

Bivand R, Keitt T, Rowlingson B (2018) rgdal: Bindings for the 'Geospatial' Data Abstraction Library. R package version 1.3-4

Blais J, Rosen M, Smol J (eds.) (2015) Environmental contaminants - using natural archives to track sources and long-term trends of pollution, vol. 18. Springer Netherlands

Bonanno G, Borg JA, Martino VD (2017) Levels of heavy metals in wetland and marine vascular plants and their biomonitoring potential: A comparative assessment. Science of The Total Environment 576:796 – 806. doi:https://doi.org/10.1016/j.scitotenv.2016.10.171

Bonanno G, Vymazal J (2017) Compartmentalization of potentially hazardous elements in macrophytes: Insights into capacity and efficiency of accumulation. Journal of Geochemical Exploration 181:22 – 30. doi:https://doi.org/10.1016/j.gexplo.2017.06.018

Borcard D, Gillet F, Legendre P (2011) Numerical ecology with R. Springer-Verlag

Bovolin V, Cuomo A, Guida D (2015) Monitoring activity at the Middle Bussento Karst System (Cilento geopark, southern Italy). Springer International Publishing. doi:10.1007/978-3-319-09054-2_57

Bovolin V, Cuomo A, Guida D (2017) Hydraulic modeling of flood pulses in the Middle Bussento Karst System (MBSKS), UNESCO Cilento Global Geopark, southern Italy. Hydrological Processes 31(3):639–653. doi:10.1002/hyp.11056

Branković S, Pavlović-Muratspahić D, Topuzović M, Glišić R, Milivojević J, Dekić V (2012) Metals concentration and accumulation in several aquatic macrophytes. Biotechnology and Biotechnological Equipment 26(1):2731–2736. doi:10.5504/bbeq.2011.0086

Branković S, Pavlović-Muratspahić D, Topuzović M, Glišić R, Stanković M (2010) Concentration of some heavy metals in aquatic macrophytes in reservoir near city Kragujevac (Serbia). Biotechnology & Biotechnological Equipment 24(sup1):223–227. doi:10.1080/13102818.2010.10817840. `https://doi.org/10.1080/13102818.2010.10817840`

Bruns I, Friese K, Markert PDB, Krauss GJ (1997) The use of *Fontinalis antipyretica* L. ex Hedw. as a bioindicator for heavy metals. 2. heavy metal accumulation and physiological reaction of *Fontinalis antipyretica* L. ex Hedw. in active biomonitoring in the River Elbe. Science of The Total Environment 204:161–176. doi:10.1016/S0048-9697(97)00174-5

Cardwell R, DeForest D, Brix K, Adams W (2013) Do Cd, Cu, Ni, Pb, and Zn biomagnify in aquatic ecosystems? Reviews of environmental contamination and toxicology 226:101–22. doi: 10.1007/978-1-4614-6898-1_4

Celico PB (1994) Sull'idrogeologia e l'idrogeochimica dei monti Alburni (SA). Geologica Romana

Chapman D (ed.) (1992) Water quality assessments - A guide to use of biota, sediments and water in environmental monitoring. E&FN Spon, second edn.

Chmist J, Hämmerling M, Szoszkiewicz K (2018) Choice of the most useful early warning system , based on AHP and Rembrandt Analysis. Acta Scientiarum Polonorum Hortorum Cultus 17(1):17

Cohen JE (2003) Human population: The next half century. Science 302(5648):1172–1175. doi:10.1126/science.1088665. http://science.sciencemag.org/content/302/5648/1172.full.pdf

Cuomo A, Guida M, Guida D, Villani P, Guadagnuolo D, Longobardi A, Siervo V (2013) Using Radon222 as a Naturally Occurring Tracer to investigate the streamflow-groundwater interactions in a typical Mediterranean fluvial-karst landscape: the interdisciplinary case study of the Bussento river (Campania region, Southern Italy). WSEAS Transactions on Systems 12:5893

Czédli H, Csedreki L, Szíki G, Jolánkai G, Pataki B, Hancz C, Antal L, Nagy S (2014) Investigation of the bioaccumulation of copper in fish. Fresenius Environmental Bulletin 23(7):1547–1552. Cited By 3

De Nicola F, Baldantoni D, Maisto G, Alfani A (2017) Heavy metal and polycyclic aromatic hydrocarbon concentrations in *Quercus ilex* L. leaves fit an a priori subdivision in site typologies based on human management. Environmental Science and Pollution Research 24(13):11911–11918. doi:10.1007/s11356-015-5890-8

De Nicola F, Spagnuolo V, Baldantoni D, Sessa L, Alfani A, Bargagli R, Monaci F, Terracciano S, Giordano S (2013) Improved biomonitoring of airborne contaminants by combined use of holm oak leaves and epiphytic moss. Chemosphere 92(9):1224–1230. doi: 10.1016/j.chemosphere.2013.04.050

Debén S, Fernández J, Carballeira A, Kosior G, Aboal J (2018) Improving active biomonitoring in aquatic environments: The optimal number and position of moss bags. Ecological Indicators 93:753–758. doi:10.1016/j.ecolind.2018.05.058

Debén García S, Fernández J, A c, Aboal J (2016) Using devitalized moss for active biomonitoring of water pollution. Environmental Pollution 210:315–322. doi:10.1016/j.envpol.2016.01.009

Debén García S, Aboal J, A c, Cesa M, Fernández J (2017) Monitoring river water quality with transplanted bryophytes: A methodological review. Ecological Indicators 81:461–470. doi:10.1016/j.ecolind.2017.06.014

Díaz S, Villares R, Carballeira A (2012) Uptake kinetics of As, Hg, Sb, and Se in the aquatic moss *Fontinalis antipyretica* hedw. Water, Air, and Soil Pollution 223(6):3409–3423. doi:10.1007/s11270-012-1120-x

Diviš P, Machát P, Szkandera R, Dočekalová H (2012) In situ measurement of bioavailable metal concentrations at the downstream on the Morava river using transplanted aquatic mosses and DGT technique. International Journal of Environmental Research 6(1):87–94

Doebelin N, Kleeberg R (2015) Profex: A graphical user interface for the rietveld refinement program BGMN. Journal of Applied Crystallography 48:1573–1580. doi:10.1107/S1600576715014685

Dray S, Bauman D, Blanchet G, Borcard D, Clappe S, Guenard G, Jombart T, Larocque G, Legendre P, Madi N, Wagner HH (2018) adespatial: Multivariate Multiscale Spatial Analysis. R package version 0.3-2

Dray S, Legendre P, Peres-Neto P (2006) Spatial modelling: a comprehensive framework for principal coordinate analysis of neighbour matrices (PCNM). Ecological Modelling 196(3-4):483–493. doi: 10.1016/j.ecolmodel.2006.02.015

Ducci D, De Masi G, Delli Priscoli G (2008) Contamination risk of the Alburni Karst System (Southern Italy). Engineering Geology 99(3-4):109–120. doi:10.1016/j.enggeo.2007.11.008

Esposito S, Loppi S, Monaci F, Paoli L, Vannini A, Sorbo S, Maresca V, Fusaro L, Asadi karam E, Lentini M, De Lillo A, Conte B, Cianciullo P, Basile A (2018) In-field and in-vitro study of the moss *Leptodictyum* riparium as bioindicator of toxic metal pollution in the aquatic environment: Ultrastructural damage, oxidative stress and HSP70 induction. PLOS ONE 13(4):1–16. doi:10.1371/journal.pone.0195717

Farago ME (ed.) (2008) Plants and the chemical elements: biochemistry, uptake, tolerance and toxicity. Wiley-Blackwell. doi: 10.1002/9783527615919

Favas P, Pratas J (2013) Uptake of uranium by native aquatic plants: Potential for bioindication and phytoremediation. In: N P (ed.) 16th International Conference on Heavy Metals in the Environment, ICHMET 2012, vol. 1. EDP Sciences. doi:10.1051/e3sconf/20130113007

Favas PJ, Pratas J, Rodrigues N, D'Souza R, Varun M, Paul MS (2018) Metal(loid) accumulation in aquatic plants of a mining area: Potential for water quality biomonitoring and biogeochemical prospecting. Chemosphere 194:158 – 170. doi:https://doi.org/10.1016/j.chemosphere.2017.11.139

Ferreira D, Ciffroy P, Tusseau-Vuillemin MH, Bourgeault A, Garnier JM (2013) DGT as surrogate of biomonitors for predicting the bioavailability of copper in freshwaters: An ex situ validation study. Chemosphere 91(3):241–247. doi:10.1016/j.chemosphere.2012.10.016

Filzmoser P (2005) Identification of multivariate outliers: A performance study. Austrian Journal of Statistics 34(2):127–138

Filzmoser P, Gschwandtner M (2018) mvoutlier: Multivariate Outlier Detection Based on Robust Methods. R package version 2.0.9

Ford D, William P (2013) Karst hydrogeology and geomorphology. Wiley

Gecheva G, Yurukova L (2014) Water pollutant monitoring with aquatic bryophytes: A review. Environmental Chemistry Letters 12(1):49–61. doi:10.1007/s10311-013-0429-z

Geneletti D, Van Duren I (2008) Protected area zoning for conservation and use: a GIS-based integration of multicriteria and multiobjective analysis. Landscape and Urban Planning 85:97–110

Greger M (2004) Metal Availability, Uptake, Transport and Accumulation in Plants. Springer

Guiry MD, Guiry GM (2018) AlgaeBase. World-wide electronic publication. National University of Ireland , Galway

Herbst A, Henningsen L, Schubert H, Blindow I (2018a) Encrustations and element composition of charophytes from fresh or brackish water sites – habitat- or species-specific differences? Aquatic Botany 148:29–34. doi:10.1016/j.aquabot.2018.04.007

Herbst A, von Tümpling W, Schubert H (2018b) The seasonal effects on the encrustation of charophytes in two hard-water lakes. Journal of Phycology 54(5):630–637. doi:10.1111/jpy.12772

Jordan M, Teasdale P, Dunn R, Lee S (2008) Modelling copper uptake by *Saccostrea glomerata* with diffusive gradients in a thin film measurements. Environmental Chemistry 5(4):274–280. doi:10.1071/EN07092

Kilunga PI, Sivalingam P, Laffite A, Grandjean D, Mulaji CK, de Alencastro LF, Mpiana PT, Poté J (2017) Accumulation of toxic metals and organic micro-pollutants in sediments from tropical urban rivers, Kinshasa, Democratic Republic of the Congo. Chemosphere 179:37 – 48. doi:https://doi.org/10.1016/j.chemosphere.2017.03.081

Küpper H, Seibert S, Parameswaran A (2007) Fast, sensitive, and inexpensive alternative to analytical pigment HPLC: Quantification of chlorophylls and carotenoids in crude extracts by fitting with Gauss Peak Spectra. Analytical Chemistry 79(20):7611–7627. doi:10.1021/ac070236m. PMID: 17854156, `https://doi.org/10.1021/ac070236m`

Lafabrie C, Pergent G, Kantin R, Pergent-Martini C, Gonzalez JL (2007) Trace metals assessment in water, sediment, mussel and seagrass species - validation of the use of *Posidonia oceanica* as a metal biomonitor. Chemosphere 68(11):2033–2039. doi:10.1016/j.chemosphere.2007.02.039

Laffont-Schwob I, Triboit F, Prudent P, Soulié-Märsche I, Rabier J, Despréaux M, Thiéry A (2015) Trace metal extraction and biomass production by spontaneous vegetation in temporary Mediterranean stormwater highway retention ponds: Freshwater macroalgae (*Chara* spp.) vs. cattails (*Typha* spp.). Ecological Engineering 81:173–181. doi:10.1016/j.ecoleng.2015.04.052

Le Saout S, Hoffmann M, Shi Y, Hughes A, Bernard C, Brooks TM, Bertzky B, Butchart SHM, Stuart SN, Badman T, Rodrigues ASL (2013) Protected areas and effective biodiversity conservation. Science 342(6160):803–805. doi:10.1126/science.1239268. `http://science.sciencemag.org/content/342/6160/803.full.pdf`

Ledl G, Janauer G, Horak O (1981) Die Anreicherung von Schwermetallen in Wasserpflanzen aus einigen österreichischen Fließgewässern. Acta hydrochimica et hydrobiologica 9(6):651–663. doi:10.1002/aheh.19810090610

Legendre P, Legendre L (2012) Numerical ecology. Elsevier

Leibovici DG (2010) Spatio-temporal multiway decompositions using Principal Tensor Analysis on k-modes: The R package PTAk. Journal of Statistical Software 34(10):1–34

Lenth R (2018) emmeans: Estimated Marginal Means, aka Least-Squares Means. R package version 1.2.4

Les D (2017) Aquatic dicotyledons of North America: ecology, life history, and systematics. CRC Press. doi:10.1201/9781315118116

Liu HY, Bartonova A, Pascal M, Smolders R, Skjetne E, Dusinska M (2012) Approaches to integrated monitoring for environmental health impact assessment. Environmental Health: A Global Access Science Source 11(1). doi:10.1186/1476-069X-11-88

Longobardi A, Cuomo A, Guida D, Villani P (2011) Earth and Environmental Sciences, chap. Water Resources Assessment for Karst Aquifer Conditioned River Basins: Conceptual Balance Model Results and Comparison with Experimental Environmental Tracers Evidences. InTechOpen, pp. 275–300. doi:10.5772/26310

Mackey E, of Standards NI, (US) T (2004) Certification of NIST Standard Reference Material 1575a Pine Needles and Results of an International Laboratory Comparison. NIST special publication. U.S. Department of Commerce, National Institute of Standards and Technology

Maechler M, Rousseeuw P, Struyf A, Hubert M, Hornik K (2018) cluster: Cluster Analysis Basics and Extensions

Maffei M (1998) Environmental factors affecting the oil composition of some *Mentha* species grown in north west Italy. Flavour and Fragrance Journal 3(2):79–84. doi:10.1002/ffj.2730030206. `https://onlinelibrary.wiley.com/doi/pdf/10.1002/ffj.2730030206`

Maione U, Majone-Lehto B, Monti R (2000) New Trends in Water and Environmental Engineering for Safety and Life. Taylor & Francis

Malhi Y (2017) The concept of the Anthropocene. Annual Review of Environment and Resources 42(1):77–104. doi:10.1146/annurev-environ-102016-060854

Mangal V, Zhu Y, Shi Y, Guéguen C (2016) Assessing cadmium and vanadium accumulation using diffusive gradient in thin-films (DGT) and phytoplankton in the Churchill River estuary, Manitoba. Chemosphere 163:90 – 98. doi:https://doi.org/10.1016/j.chemosphere.2016.08.008

Marcelli M, Fusillo R (2009) Assessing range re-expansion and recolonization of human-impacted landscapes by threatened species: a case study of the otter (*Lutra lutra*) in Italy. Biodiversity and Conservation 18(11):2941–2959. doi:10.1007/s10531-009-9618-2

Markert B, Fränzle S, Wünschmann S (2015) Chemical evolution - the biological system of the elements. Springer International Publishing

Markert PDB, Breure A, Zechmeister H (eds.) (2003) Bioindicators and biomonitors: principles, concepts and applications, vol. 6. Elsevier

Matagi S, Swai D, Mugabe R (1998) A review of heavy metal removal mechanisms in wetlands. African Journal of Tropical Hydrobiology and Fisheries 8

Moreira H, Marques AP, Rangel AO, Castro PM (2011) Heavy metal accumulation in plant species indigenous to a contaminated portuguese site: Prospects for phytoremediation. Water, air and soil pollution 221(1-4):377–389

Morozov I, Dueker K (2003) Signal-to-noise ratios of teleseismic receiver functions and effectiveness of stacking for their enhancement. Journal of Geophysical Research: Solid Earth 108(2):ESE 17–1 – 17–8

Mueller P, Thoss H, Kaempf L, Güntner A (2013) A buoy for continuous monitoring of suspended sediment dynamics. Sensors (Switzerland) 13(10):13779–13801. doi:10.3390/s131013779

Naser HM, Sultana S, Mahmud NU, Gomes R, Noor S (2011) Heavy metal levels in vegetables with growth stage and plant species variations. Bangladesh Journal of Agricultural Research

Nowak P, Schubert H, Holzhausen A, Sommer V, Schaible R (2018) Morphological adaptations of *Chara baltica* and *Chara liljebladii* (Characeae) under different light conditions. Botany Letters 165(1):67–75. doi:10.1080/23818107.2017.1374209

Nowak P, Schubert H, Schaible R (2016) Molecular evaluation of the validity of the morphological characters of three Swedish *Chara* sections: *Chara*, *Grovesia*, and *Desvauxia* (Charales, Charophyceae). Aquatic Botany 134:113–119. doi:10.1016/j.aquabot.2016.08.001

Oksanen J, Blanchet FG, Friendly M, Kindt R, Legendre P, McGlinn D, Minchin PR, O'Hara RB, Simpson GL, Solymos P, Stevens MHH, Szoecs E, Wagner H (2018) vegan: Community Ecology Package. R package version 2.5-2

Parmar TK, Rawtani D, Agrawal YK (2016) Bioindicators: the natural indicator of environmental pollution. Frontiers in Life Science 9(2):110–118. doi:10.1080/21553769.2016.1162753. `https://doi.org/10.1080/21553769.2016.1162753`

Peters A, Zhang H, Davison W (2003) Performance of the diffusive gradients in thin films technique for measurement of trace metals in low ionic strength freshwaters. Analytica Chimica Acta 478(2):237–244. doi:10.1016/S0003-2670(02)01512-X

Philipps R, Xu X, Mills G, Bringolf R (2018a) Evaluation of diffusive gradients in thin films for prediction of copper bioaccumulation by yellow lampmussel (*Lampsilis cariosa*) and fathead minnow (*Pimephales *promelas*). Environmental Toxicology and Chemistry 37(6):1535–1544. doi:10.1002/etc.4108

Philipps R, Xu X, Mills G, Bringolf R (2018b) Impact of natural organic matter and increased water hardness on DGT prediction of copper bioaccumulation by yellow lampmussel (*Lampsilis cariosa*) and fathead minnow (*Pimephales promelas*). Environmental Pollution 241:451–458. doi:10.1016/j.envpol.2018.05.059

Phillips D, Rainbow P (2013) Biomonitoring of Trace Aquatic Contaminants. Ettore Majorana International Science Series. Springer Netherlands

Pignatti S (1982) Flora d'Italia. Edagricole, Bologna.

Podani J (2005) Multivariate exploratory analysis of ordinal data in ecology: Pitfalls, problems and solutions. Journal of Vegetation Science 16(5):497–510. doi:10.1658/1100-9233

Podani J, Morrison D (2017) Categorizing ideas about systematics: alternative trees of trees, and related representations. Rendiconti Lincei 28(1):191–202. doi:10.1007/s12210-017-0597-z

Puche E, Sánchez-Carrillo S, Álvarez-Cobelas M, Pukacz A, Rodrigo M, Rojo C (2018) Effects of overabundant nitrate and warmer temperatures on charophytes: the roles of plasticity and local adaptation. Aquatic Botany 146:15–22. doi:10.1016/j.aquabot.2018.01.003

Pueyo M, Rauret G, Lück D, Yli-Halla M, Muntau H, Quevauviller P, López-Sánchez J (2001) Certification of the extractable contents of Cd, Cr, Cu, Ni, Pb and Zn in a freshwater sediment following a collaboratively tested and optimised three-step sequential extraction procedure. Journal of Environmental Monitoring 3(2):243–250

QGIS Development Team (2018) QGIS Geographic Information System. Open Source Geospatial Foundation Project. Http://qgis.osgeo.org

R Core Team (2018) R: A Language and Environment for Statistical Computing. R Foundation for Statistical Computing, Vienna, Austria

Rauret G, López-Sánchez J, Sahuquillo A, Rubio R, Davidson C, Ure A, Quevauviller P (1999) Improvement of the BCR three step sequential extraction procedure prior to the certification of new sediment and soil reference materials. Journal of Environmental Monitoring 1(1):57–61. doi:10.1039/a807854h

Ravbar N, Engelhardt I, Goldscheider N (2011) Anomalous behaviour of specific electrical conductivity at a karst spring induced by variable catchment boundaries: The case of the Podstenjşek spring, Slovenia. Hydrological Processes 25(13):2130–2140. doi:10.1002/hyp.7966

Renaudin M, Leblond S, Meyer C, Rose C, Lequy E (2018) The coastal environment affects lead and sodium uptake by the moss hypnum cupressiforme used as an air pollution biomonitor. Chemosphere 193:506 – 513. doi:https://doi.org/10.1016/j.chemosphere.2017.11.045

Romano A, Ventre N, Riso L, Pignataro C, Spilinga C (2013) Amphibians of the "Cilento e Vallo di Diano" National Park (Campania, Southern italy): Updated check list, distribution and conservation notes. Acta Herpetologica 5(2):233–244. doi:10.13128/Acta_Herpetol-9035

Ronse A, Popper Z, Preston J, Watson M (2010) Taxonomic revision of european *Apium* L. sl: *Helosciadium* WDJ Koch restored. Plant systematics and evolution 287(1-2):1–17

Ruzin SE (1999) Plant microtechnique and microscopy. Oxford University Press

Samecka-Cymerman A, Kempers A (1999) Background concentrations of heavy metals in aquatic bryophytes used for biomonitoring in basaltic areas (a case study from central France). Environmental Geology 39(2):117–122. doi:10.1007/s002540050442

Samecka-Cymerman A, Kolon K, Kempers A (2005) A comparison of native and transplanted *Fontinalis antipyretica* Hedw. as biomonitors of water polluted with heavy metals. Science of the Total Environment 341(1-3):97–107. doi:10.1016/j.scitotenv.2004.09.026

Santangelo N, Santo A, Guida D, Lanzara R, Siervo V (2005) The geosites of the Cilento-Vallo di Diano National Park (Campania region, southern Italy). Alpine and Mediterranean Quaternary 18(1):103–114

Schillereff D, Chiverrell R, Macdonald N, Hooke J, Welsh K (2016) Quantifying system disturbance and recovery from historical mining-derived metal contamination at Brotherswater, northwest England. Journal of Paleolimnology 56(2-3):205–221. doi:10.1007/s10933-016-9907-1

Schneider C, Rasband W, Eliceiri K (2012) NIH Image to ImageJ: 25 years of image analysis. Nature Methods 9(7):671–675. doi:10.1038/nmeth.2089

Schneider S, Nowak P, Von Ammon U, Ballot A (2016) Species differentiation in the genus *Chara* (Charophyceae): considerable phenotypic plasticity occurs within homogenous genetic groups. European Journal of Phycology 51(3):282–293. doi:10.1080/09670262.2016.1147085

Schneider S, Rodrigues A, Moe T, Ballot A (2015) DNA barcoding the genus *Chara*: molecular evidence recovers fewer taxa than the classical morphological approach. Journal of Phycology 51(2):367–380. doi:10.1111/jpy.12282

Segan D, Murray K, Watson J (2016) A global assessment of current and future biodiversity vulnerability to habitat loss-climate change interactions. Global Ecology and Conservation 5:12–21. doi:10.1016/j.gecco.2015.11.002

Spencer KL (2017) Estuarine and Coastal Hydrography and Sediment Transport, chap. Estuarine Deposited Sediments: Sampling and Analysis. Cambridge University Press, p. 153–178. doi: 10.1017/9781139644426.007

Srivastava J, Gupta A, Chandra H (2008) Managing water quality with aquatic macrophytes. Reviews in Environmental Science and Bio/Technology 7(3):255–266. doi:10.1007/s11157-008-9135-x

Stark J, Johnstone G, Palmer A, Snape I, Larner B, Riddle M (2006) Monitoring the remediation of a near shore waste disposal site in Antarctica using the amphipod *Paramoera walkeri* and diffusive gradients in thin films (DGTs). Marine Pollution Bulletin 52(12):1595–1610. doi:10.1016/j.marpolbul.2006.05.020

Stoyneva MP, Gärtner G (2004) Taxonomic and ecological notes to the list of green algal species from Bulgarian thermomineral waters. Berichte des Naturwissenschaftlich–Medizinischen Vereins in Innsbruck 91:67–89

Sviben S, Matoničkin Kepčija R, Vidaković-Cifrek v, Sertić Perić M, Kružić P, Popijač A, Primc B (2018) *Chara* spp. exhibit highly heterogeneous light adaptation, calcite encrustation and epiphyton patterns in a marl lake. Aquatic Botany 147:1–10. doi: 10.1016/j.aquabot.2018.01.007

Symoens J (2012) Vegetation of inland waters. Handbook of Vegetation Science. Springer Netherlands

Szczerbińska N, Galczyńska M (2015) Biological methods used to assess surface water quality. Archives of Polish Fisheries 23(4):185–196. doi:10.1515/aopf-2015-0021

Thiombane M, Zuzolo D, Cicchella D, Albanese S, Lima A, Cavaliere M, Vivo BD (2018) Soil geochemical follow-up in the Cilento World Heritage Park (Campania, Italy) through exploratory compositional data analysis and C-A fractal model. Journal of Geochemical Exploration 189:85 – 99. doi:https://doi.org/10.1016/j.gexplo.2017.06.010. Multifractals and singularity analysis in mineral exploration and environmental assessments

Urbaniak J (2011) A SEM and light microscopy study of the oospore wall ornamentation in Polish charophytes (Charales, Charophyceae) - genus *Chara*. Nova Hedwigia 93:1–28. doi:10.1127/0029-5035/2011/0093-0001

Urbaniak J, Sakayama H (2017) Taxonomical analysis of closely related species of *Chara* l. section *Hartmania* (streptophyta: Charales) based on morphological and molecular data. Fottea 17(2):222–239. doi:10.5507/fot.2017.004

Valavanidis A (2018) Ecosystem approach management of environmental resources. an ecological strategy for integrated environmental conservaction. wwwchem-tox-ecotoxorg 1:1–36

van den Boogaart KG, Tolosana-Delgado R, Bren M (2018) compositions: Compositional Data Analysis. R package version 1.40-2

Vázquez-Luis M, Álvarez E, Barrajón A, García-March J, Grau A, Hendriks I, Jiménez S, Kersting D, Moreno D, Pérez M, Ruiz J, Sánchez J, Villalba A, Deudero S (2017) S.O.S. *Pinna nobilis*: A mass mortality event in western Mediterranean Sea. Frontiers in Marine Science 4(JUL). doi:10.3389/fmars.2017.00220

Vlyssides A, Barampouti E, Mai S (2005) Heavy metal removal from water resources using the aquatic plant *Apium nodiflorum*. Communications in Soil Science and Plant Analysis 36(7-8):1075–1081. doi:10.1081/CSS-200050499

Waltham N, Teasdale P, Connolly R (2011) Contaminants in water, sediment and fish biomonitor species from natural and artificial estuarine habitats along the urbanized Gold Coast, Queensland.

Journal of Environmental Monitoring 13(12):3409–3419. doi:10.1039/c1em10664c

Welch W (2014) A Monograph of the Fontinalaceae. Springer Netherlands

Zhang ZY, Abuduwaili J, Jiang FQ (2015) Pollution and potential ecology risk evaluation of heavy metals in river water, top sediments on bed and soils along banks of Bortala River, northwest China. Huan Jing Ke Xue 36:2422–2429

Zoumis T, Schmidt A, Grigorova L, Calmano W (2001) Contaminants in sediments: remobilisation and demobilisation. Science of The Total Environment 266(1):195 – 202. doi:https://doi.org/10.1016/S0048-9697(00)00740-3

Zurayk R, Sukkariyah B, Baalbaki R (2001) Common hydrophytes as bioindicators of nickel, chromium and cadmium pollution. Water Air and Soil Pollution 127:373–388. doi:10.1023/A:1005209823111